The Biogeochemistry and Ecology of Tidal Freshwater Rivers

Scott Howard Ensign

"A dissertation submitted to the faculty of the University of North Carolina at Chapel Hill in partial fulfillment of the requirements for the degree of Doctor of Philosophy in the Curriculum for the Environment and Ecology."

Chapel Hill
2010

Approved by:

Dr. Michael Piehler

Dr. Martin Doyle

Dr. Lawrence Band

Dr. Marc Alperin

Dr. John Bruno

ABSTRACT

SCOTT HOWARD ENSIGN: The Biogeochemistry and Ecology of Tidal Freshwater Rivers
(Under the direction of Michael Piehler and Martin Doyle)

Tides propagate up coastal rivers far upstream from the saline estuary, changing the direction and strength of river flow and the extent of riparian inundation over short time scales. This dissertation explores the effect of tides on river morphology and evolution, nitrogen cycling, and primary production. I examined river hydraulics and channel morphology in the Newport River, N.C. to evaluate how tides change stream power and sediment transport. Tides suppressed stream power in the upper tidal river but enhanced stream power in the lower tidal river. Sediment transport increased from upstream to downstream along the tidal continuum. These patterns suggested the mechanisms by which rivers evolve from non-tidal to tidal during sea level rise. Nitrogen removal in tidal rivers via denitrification is potentially affected by these spatial patterns. Denitrification rates and the lag period prior to the onset of denitrification were measured in riparian habitats of the Newport River. Temporal variation in denitrification over an 11 month period was greater than spatial variation within or between habitat types. A 4.6 hr lag time between floodplain inundation and the onset of denitrification was measured in the field and laboratory experiments. Landscape-scale modeling of these processes indicated that tidal inundation dynamics exerted as strong an influence

on nitrogen attenuation as did rates of denitrification. Tidal hydrology also had a profound influence on primary production. Monitoring and mesocosm experiments showed that phytoplankton growth was enhanced by both the geomorphic influence of tides and the increased residence time in the channel. During spring and summer, nitrogen and phosphorus limit phytoplankton growth in the non-tidal river, and zooplankton grazing may limit phytoplankton growth in the tidal river. Understanding the mechanisms by which tides affect hydrogeomorphology in rivers, and the subsequent impacts on biogeochemical and biological processes is a fundamental step towards conceptual integration of the tidal zone with river networks. Fluvial form and function are essential to applied sciences, such as river restoration and biogeochemical modeling, but are also fundamental for anticipating the future impacts of sea level rise on coastal rivers.

DEDICATION

This research is dedicated to my father, who taught me to be curious and inquisitive about the natural world, and my mother, who taught me the patience and persistence necessary to do scientific research.

ACKNOWLEDGMENTS

I am grateful to the following individuals for providing field and laboratory assistance: Valerie Brock, Karen Fisher, Dr. Ken Fortino, Dr. Todd Jobe, Dr. Dina Leech, Nicholas Politte, Dr. Tony Rodriguez, Ashley Smyth, Laura Stephenson, Suzanne Thompson, and Ben VonKorff. Jeff Muehlbauer provided stastical advice and many hours of constructive discussions. I thank Dr. Hans Paerl and his staff for the use of analytical equipment at UNC-IMS. Herman Godwin and David Wilke provided access to field sites on their property. Stacy Davis, Claude Lewis, and Joe Purifoy at the UNC Chapel Hill Institute of Marine Science provided logistical support. Funding was provided by the Water Resources Research Institute of the University of North Carolina (Project # 70223), NSF Career Award #0441504 (M.W. Doyle), EPA STAR Graduate Fellowship #FP-91686901-0 (S.H. Ensign), and NSF EAR-0815627 (M.F. Piehler), and NOAA Ecological Effects of Sea Level Rise Program grants (M.F. Piehler). The research described in this paper has been funded wholly or in part by the United States Environmental Protection Agency (EPA) under the Science to Achieve Results (STAR) Graduate Fellowship Program. EPA has not officially endorsed this publication and the views expressed herein may not reflect the views of the EPA.

During my Ph.D. education I have been privileged to be mentored by Dr. Mike Piehler and Dr. Martin Doyle. With great patience and generosity, these outstanding faculty taught me how to manage research projects and how to write and communicate the results. I am thankful for the training they have given me on being an academic, a

scientist, a teacher, and a mentor. I am also grateful to Dr. Larry Band, Dr. Marc Alperin, and Dr. John Bruno for their assistance as members of my advisory committee.

TABLE OF CONTENTS

LIST OF TABLES……xii

LIST OF FIGURES……..xiii

LIST OF ABBREVIATIONS AND SYMBOLS……..xv

Chapter

1. INTRODUCTION…….1

1.1. Tidal rivers: What are they and who cares?.....1

1.2. Hydrology and geomorphology……..3

1.3. Biogeochemistry…….7

1.4. Biological production…….9

2. THE EFFECTS OF TIDES ON RIVER HYDRAULICS AND THEIR IMPLICATIONS FOR RIVER GEOMORPHOLOGY……14

2.1. Introduction……14

2.1.1. Tidal river hydrology……...15

2.1.2. Geomorphic adjustment to tidal influence……...17

2.1.3. Objectives……...…….19

2.2. Methods…….….20

2.2.1. Study area……..…20

2.2.2. Discharge……...…..22

2.2.3. Stream power……...…23

2.2.4. Suspended matter transport…….….26

2.2.4.1. Suspended matter concentration……..26

2.2.4.2. Tidal suspended matter flux…….27

2.2.5. Channel morphology……28

2.2.5.1. Observed geomorphology……28

2.2.5.2. Predicted fluvial geomorphology…….29

2.3. Results……29

2.3.1. Discharge…….29

2.3.2. Stream power……...29

2.3.3. Suspended matter transport……..31

2.3.3.1. Suspended matter concentration……..31

2.3.3.2. Tidal suspended matter flux…….……32

2.3.4. Geomorphology……...…32

2.4. Discussion……..33

2.4.1. Tidal influence has counter-veiling effects on river discharge……33

2.4.2. Stream power indicated the effect of tides on river hydrology……35

2.4.3. Suspended matter concentration and transport were functions of tide not watershed runoff……36

2.4.4. Channel geomorphology reflected changes in hydrology and suspended matter…….38

2.4.5. A chronology of tidal river evolution……..40

2.4.6. Conclusions……..……42

3. RIPARIAN ZONE DENITRIFICATION AFFECTS NITROGEN FLUX THROUGH A TIDAL FRESHWATER RIVER…….…..……..57

3.1. Introduction…….……57

3.1.1. Riparian zone denitrification model…….……59

3.1.2. Site description…….61

3.2. Materials and methods…….……62

3.2.1. Riparian zone denitrification…….62

3.2.2. Riparian zone oxidation-reduction potential……..65

3.2.3. Laboratory oxidation-reduction potential experiments……..66

3.2.4. Channel bathymetry and riparian zone topography……67

3.2.5. Tidal freshwater river nitrogen load……...68

3.2.6. Riparian zone denitrification model…….……..69

3.3. Results……..…….70

3.3.1. Riparian zone denitrification……..……70

3.3.2. Riparian zone oxidation-reduction potential……..…….71

3.3.3. Laboratory oxidation-reduction potential experiments……..….72

3.3.4. Channel bathymetry and riparian zone topography…….…...73

3.3.5. Tidal freshwater river nitrogen load…….……..73

3.3.6. Riparian zone denitrification model……...…….74

3.4. Discussion……..……...……74

3.4.1. Denitrification and redox dynamics in tidal freshwater river floodplains……..…..….75

3.4.2. Uncertainties, future development, and application of the floodplain denitrification model……77

3.4.3. How does riparian denitrification compare to in-channel denitrification?.....79

4. LANDSCAPE-SCALE CONTROLS ON DENITRIFICATION IN TIDAL FRESHWATER WETLANDS…….....……93

4.1. Introduction……93

4.2. Methods…….…….95

4.2.1. Study area…….96

4.2.2. Floodplain topography…….96

4.2.3. Water level measurements…….……..97

4.2.4. Wetland inundation……..98

4.2.5. N_2 efflux…….……..99

4.3. Results……..……101

4.3.1. Hydrology and floodplain topography……...……101

4.3.2. Flooplain inundation……..……102

4.3.3. N_2 efflux…….103

4.4. Discussion……104

4.4.1. Two modes of N_2 efflux…….104

4.4.2. Water level governs N_2 efflux in TFW……..106

4.4.3. Modeling denitrification in TFW…….…….107

4.4.4. Shifting landscapes and denitrification during sea level rise……108

4.5. Conclusions……..110

5. THE END OF THE RIVER CONTINUUM: TIDES AND RIVER ECOSYSTEMS……..…….122

5.1. Introduction…….……122

5.2. Methods……..……..124

5.2.1. Study sites……..124

5.2.2. Channel morphology, irradiance, and phytoplankton biomass……..124

5.2.3. Photosynthetic response to irradiance along a tidal gradient…….126

5.2.4. Mesocosm growth experiments in the Newport River……..127

5.3. Results…….….128

5.3.1. Channel morphology, irradiance, and phytoplankton biomass…….128

5.3.2. Photosynthetic response to irradiance……129

5.3.3. Mesocosm growth experiments…….129

5.4. Discussion……130

6. CONCLUSIONS…….…..139

6.1. Hydrology and geomorphology……..…….139

6.2. Biogeochemistry……..……141

6.3. Biological production……..……142

REFERENCES…….....147

LIST OF TABLES

Table

1.1. Length of various tidal rivers……11

2.1. Water flux during tidal cycle experiments in the Newport River…….44

2.2. Hydrologic and geomorphic characteristics of the Newport River……...45

2.3. Generalized river channel and floodplain characteristics of a coastal tidal river….46

3.1. Denitrification rates in the Newport River tidal freshwater zone……..81

3.2. Nitrogen concentrations and sediment organic matter composition……..82

3.3. Nitrate loads, denitrification flux, and nitrate removal in the TFZ Newport River..83

4.1. River characteristics and riparian vegetation type……...112

LIST OF FIGURES

Figure

1.1. Calculation of the rate of upstream advance in tidal regime…….13

2.1. Location of the Newport River and sampling sites……47

2.2. Photos of the upper, middle, and lower Newport tidal river……..48

2.3. Upstream site tidal cycle measurements……49

2.4. Midstream site tidal cycle measurements……..50

2.5. Downstream site tidal cycle measurements……...51

2.6. Observed and predicted energy dissipation……...52

2.7. Fluvial discharge, suspended matter, and turbidity, 2006-2007……53

2.8. Suspended matter flux over a tidal day…….54

2.9. Geomorphic characteristics of the tidal Newport River……55

2.10. Generalized spatial and temporal patterns of tidal hydrology in a tidal river……56

3.1. Map of the Newport River watershed……84

3.2. Water level at three tidal river locations in the Newport River…….85

3.3. Oxidation-reduction potential and soil moisture 2 m from the channel……86

3.4. Oxidation-reduction potential and soil moisture 10 m from the channel……..87

3.5. Oxidation-reduction potential and soil moisture 17 m from the channel……..88

3.6. Laboratory soil core oxidation-reduction potential experiments……...89

3.7. Bathymetry and topography of the Newport River tidal freshwater zone…….90

3.8. Riparian zone topography and resultant denitrification…….91

3.9. Nitrogen concentrations and net downstream discharge in the Newport River……92

4.1. Location of rivers studied in North Carolina……...113

4.2. Water level and hypsometric curves of the tidal riparian zones……..114

4.3. Range in inundation and N_2 efflux in the Newport River……115

4.4. Range in inundation and N_2 efflux in the White Oak River……116

4.5. Range in inundation and N_2 efflux in the New River……..117

4.6. Range in inundation and N_2 efflux in the Northeast Cape Fear River…….118

4.7. Model of the temporal and spatial variation in N_2 efflux in a tidal river…….119

4.8. Predicted N_2 efflux versus mean daily water level……..120

4.9. Frequency-magnitude of water level and N_2 efflux in the Northeast Cape Fear River……...….121

5.1. Hypotheses regarding the influence of tides on phytoplankton biomass…….135

5.2. Tidal amplitude, channel width, irradiance, and phytoplankton in the Newport River……...…….136

5.3. Photosynthesis versus irradiance for Newport and White Oak River phytoplankton……..137

5.4. Chlorophyll *a* biomass and growth rate in mesocosm experiments……138

6.1. Geomorphic, hydrologic, and food web characteristics of tidal rivers relative to other aquatic ecosystems…….145

LIST OF ABBREVIATIONS AND SYMBOLS

Q	river discharge
A	channel cross-sectional area
R_h	hydraulic radius
Ω	cross-sectional stream power
ρ	density of water
g	gravitational acceleration
S	energy grade slope
U	velocity
n	Mannings roughness coefficient
$h_{t,s}$	water level height above mean sea level at any time, t, and location, s
a_s	tidal amplitude
p	tidal period (12.4 hr)
$A_{t,s}$	floodplain area inundated at time t and location s
F_s	polynomial numerical function describing the area inundated at a given water level and location
N_s	denitrification flux within a segment of the tidal river floodplain
R	denitrification rate
q	flow rate of water through the head space of a core
c	surface area of the core
V_f	denitrification mass transfer coefficient
H_L	discharge/(channel width×reach length)
α	TFW area per river length

C	solute concentration
I_x	average water column irradiance
I_o	water surface irradiance
k	water column light attenuation coefficient
z	water depth
P_B	phytoplankton productivity
P^B_S	maximum phytoplankton productivity
I	irradiance
β	slope of the relationship between productivity and irradiance

1. INTRODUCTION

1.1. What are tidal rivers and why should we care?

All freshwater aquatic sciences are premised on the down-hill flow of water. This process defines rivers, fills lakes, and ultimately connects continents with the ocean. Yet there is an freshwater aquatic ecosystem in which this down-slope paradigm must be relaxed, one in which the gravitational force of the moon supersedes the down-slope flow of water across the earth's surface. Here, in tidal rivers, ocean tides propagate upstream, changing the surface elevation of the river and forcing water to flow upstream against the gradient of the river channel. Water, sediment, solutes, and organisms pulse upstream and downstream as the tide ebbs and floods. The tidal wave, born from the sun and moon's gravity, ultimately dissipates into heat and turbulence by the time it reaches the river's head-of-tide. This dissertation is devoted to understanding the physical, biogeochemical, and ecological consequences of the tide's energy dissipation within rivers.

Tidal rivers exist anywhere that tidal amplitude is sufficient to exceed the topographic gradient of a river channel. Low channel gradients allow tides to travel hundreds of kilometers up large rivers (Table 1.1). In smaller rivers crossing low gradient coastal plains, such as the rivers draining eastern North America, tides propagate inland up to half the length of the river (Anderson 1986). Most tidal rivers are sinuous, single thread channels composed of alluvial material (Wells 1995). The upstream boundary of a tidal river is the most landward location at which tides affect water level or

flow velocity, and the downstream boundary is delimited by one of two physical thresholds: a dramatic change in channel width at the bayhead delta, or in the absence of a delta, the boundary between freshwater and the oligohaline zone (saline conditions greater than 0.5).

Tidal rivers are the most under-studied ecosystem along the riverine-estuarine aquatic continuum. One explanation for this is alluded to in the title of the paper "The tidal freshwater reach of the Weser estuary: Riverine or estuarine?", where Schuchardt and colleagues (1993) highlight the hybrid marine-fluvial nature of these ecosystems. The semantics of how tidal rivers are labeled may have deterred researchers because of perceived disciplinary boundaries. Moreover, theory in fluvial geomorphology and stream ecology are based on uni-directional flow and sediment transport, and while the knowledge certainly exists to incorporate tidal processes, the predominant theoretical pursuits of these fields have simply not cast attention towards tidal rivers. On the other side of the disciplinary divide, estuarine scientists have shown little interest in investigating the freshwater end member of estuaries, where the only obvious estuarine process is a reversal in the river's direction of flow, or an even more subtle change in the river's flow velocity.

Tidal rivers have been neglected relative to their purely riverine and marine counterparts, but the literature on tidal rivers is growing. Hydrologists and geomorphologists have quantified tidal influences on sediment transport; ecologists and biogeochemists have investigated vegetation communities and nutrient cycling in tidal freshwater marshes; limnologists have characterized the factors affecting pelagic food webs. However, previous research has not explicitly addressed how tides alter fluvial

processes, but have instead measured the net effect of fluvial discharge and tide together. Upstream-downstream comparisons of process have been performed, but these do not necessarily isolate the influence of tide, nor do inter-site comparisons between tidal and non-tidal rivers. A deeper understanding of tidal rivers requires independent evaluation of how these two components of tidal river flow, watershed discharge and ocean tides, interact.

To understand the hydraulic mechanism by which tides affect a riverine process requires a more explicit approach, one that addresses the question: "How has tidal action affected process 'X' as the river has become tidally-influenced, and how will upstream portions of the river change as sea level rises?" Questions of this nature are the theme of my dissertation. My overall objective was to explore how tides affect the hydrogeomorphology, biogeochemistry, and ecology of tidal rivers.

1.2. Hydrology and geomorphology

The hydrology and geomorphology of tidal rivers began to receive scientific attention during the mid-19th century. As commerce and shipping grew, the demand for river improvements and engineering increased. Engineers in Great Britain recognized that tidal rivers were of particular benefit for transportation because they remained wider and deeper for a longer distance upstream than non-tidal rivers (Wheeler 1893). Not only did these geomorphic attributes make them valuable for shipping, but their high discharge relative to non-tidal rivers was valuable for other industrial purposes (e.g., sewage disposal) (Wheeler 1893). Wheeler's 467 page treatise on tidal rivers provides an

extensive review of early measurements of tide in rivers, but is mostly devoted to educating engineers about the unique challenges of improving tidal rivers for shipping:

> Before, however, such works are undertaken, it is essential for their success, not only that a thorough knowledge of tidal phenomena and of the action of the tides in general should be possessed by the engineer to whose care the river is committed, but also that he should make himself master of all the tidal peculiarities common to the river to be dealt with.

By the mid 19th century, engineers were mastering the idiosyncrasies of tidal rivers by measuring the magnitude, extent, and timing of tides in rivers throughout Europe, Africa and Asia.

Today, engineers continue to study and manipulate tidal rivers for practical purposes of transportation, but in the past decade a new industry has emerged with a quite contrary goal. The applied discipline of river restoration seeks to re-engineer river channels from a previously altered, or degraded, state to a "natural" condition. However, these efforts are hampered by a lack of basic knowledge of how tides affect river morphology, and hence what a natural channel condition is for a tidal river. The long-term viability of these methods for creating stable tidal channels is uncertain. Developing guidelines for tidal river restoration is at the forefront of river restoration activities in North Carolina, which requires basic research understanding the mechanisms by which tides affect river geomorphology.

The disciplines of geomorphology and hydrology have only recently turned attention to tidal rivers. Pioneering research on the geomorphic affect of tides on river hydraulics was performed in a small tidal creek by Langbein (1963) and Myrick and Leopold (1963). The primary contribution of this early research was to highlight that

channel morphology was independent from discharge in tidal creeks, and distinct from upland rivers. Yet the tidal creeks studied by these authors are distinct from tidal rivers. Tidal creeks are predominantly formed by the incision of water into a salt marsh during tidal inundation. In contrast, tidal rivers are initially formed by fluvial, watershed-derived runoff and subsequently exposed to tidal action. The study of tidal creek morphology and hydrology has become a sub-discipline of its own (reviewed by contributors to Perillo et al. 2009), but explicit examination of tidal influence in river channels is a more recent development.

Early study of the effects of tides on water sediment transport in rivers (Ashley 1980; van den Berg 1987; Guézennec et al. 1999) are being followed up with studies applying more advanced technologies (Villard and Church 2003; Wall et al. 2008; Hoitink et al. 2009). General patterns in sediment transport in tidal rivers are emerging (Wells 1995), along with a classification scheme for the longitudinal zones of tidal influence (Gurnell 1997). Outside of the tidal river channel, much attention has been devoted to the hydrology of tidal freshwater marshes that fringe tidal rivers (Pasternack 2009). Study of these wetland processes has contributed substantially to understanding the lateral connectivity between rivers and terrestrial environments, but coupling these lateral processes with the longitudinal exchanges between the rivers and estuaries has not yet occurred.

Tidal influence over time scales of hours (a semi-diurnal sequence) to a year (encompassing the annual range in tides and river discharge) is only one aspect of tidal rivers that requires further research. Another aspect is the long-term evolution of non-tidal to tidal rivers in response to rising sea level. As sea level rises, it extends the

influence of tides further inland and increases the tidal amplitude along the way. For example, in the central eastern portion of N.C. is currently experience sea level rise at a rate of 3 mm yr^{-1} (NOAA 2004), and given the low topographic gradient of the landscape (~0.0001 m m^{-1}), this equates to a upstream migration of tide at 30 m yr^{-1} (without consideration for possible geomorphic adjustments). Figure 1.1 illustrates this simple calculation that is useful for approximating the rate of migration under different scenarios. This relatively rapid conversion of non-tidal to tidal condition should cause observable effects on tidal river hydrology on even annual time scales.

There are three critical questions that will aid our understanding of tides' affect on river geomorphology and tidal river evolution during sea level rise:

1. How do tides affect the capacity of the river to transport sediment along their continuum of activity?
2. How does the combination of tidal energy and sediment transport contribute to channel form?
3. How do these processes occur over time as sea level rises?

Chapter 2 addresses these questions by making a detailed series of hydraulic and geomorphic measurements in a tidal freshwater river. The affects of flow and sediment transport on river geomorphology are inferred from their spatial correlation. This study is the first attempt to explicitly quantify the influence of tide on river hydrology; all previous research has simply measured the net (tidal+fluvial) occurrence in rivers. Chapter 2 reveals previously unknown geomorphic patterns and processes in tidal rivers,

generates hypotheses for future research, and establishes the physical template on which biogeochemical and ecological processes operate in tidal rivers.

1.3. Biogeochemistry

Tidal rivers link the flow of water and materials from river networks with the ocean. In addition to the transport of water and sediment discussed above, tides also affect the transport and fate of dissolved materials. Understanding the processes by which tidal rivers alter the flux of solutes from river basins to coastal ecosystems is critical in determining the fate of anthropogenically-derived pollutants. Nitrogen is one element which is critical for aquatic primary production in rivers and marine environments, but whose excess anthropogenic production and delivery to the ocean have been detrimental to aquatic ecosystems.

Measurement of watershed nitrogen budgets has been a popular topic in ecosystem ecology since the formulation of the watershed ecosystem concept (Likens et al. 1970). Attention to nitrogen transport from watersheds to the ocean grew rapidly as researchers discovered that nitrogen was a culprit in eutrophication of coastal ecosystems (Howarth and Marino 2006) and that humans had more than doubled the loading of labile nitrogen to the earth (Green et al. 2004). There are now legal restrictions on the amount of nitrogen that is allowed to enter some rivers and estuaries, yet knowledge of the transformation and attenuation of nitrogen in tidal rivers is lacking. The quantitative models that are used to trace the source and fate of nitrogen through river networks do not explicitly account for the influence of tidal hydrology because the affect of tides on nitrogen cycling is unknown.

The most critical component of the nitrogen cycle to account for in rivers is denitrification, the microbially-mediated conversion of dissolved, bioavailable nitrogen to relatively inert N_2 gas (Davidson and Seitzinger 2006 and related articles). Quantifying denitrification in tidal rivers could reveal a significant component of the land-to-sea nitrogen flux because of the continual exchange of river water and associated NO_3^- with the floodplain. These riparian wetlands are very dynamic with respect to nitrogen (Megonigal and Neubauer 2009), but knowledge of their influence at the landscape scale is incomplete. Filling this gap in our knowledge requires answers to four questions:

1. What is the rate of denitrification in tidal river wetlands?
2. When does denitrification occur in relation to the semi-diurnal tidal cycle?
3. What is the influence of tides on the surface area over which denitrification occurs?
4. What is the relative importance of denitrification rate versus floodplain inundation on nitrogen removal from tidal rivers?

The first two questions are the focus of Chapter 3, research which involved extensive field work and laboratory experiment. The second two questions are addressed in Chapter 4, research which relied heavily on a topographic and numerical model of floodplain inundation. Together these studies reveal fundamental relationships between nitrogen transport, denitrification, and tidal hydrology that are necessary to account for the flux of nitrogen through tidal rivers to the ocean.

1.4. Biological production

As tides alter the hydrology, geomorphology, and biogeochemistry of tidal rivers they also indirectly influence ecological process. There is a sizable literature indirectly related to tidal river ecology, but as with the topics discussed above, the explicit effect of tides is not considered in these ecological studies. In other words, researchers rarely, if ever, have asked: "How different would this ecosystem process be in the absence of tides?". Sometimes simple comparisons are made between a process in a tidal versus a non-tidal river, but more often tides are merely considered an implicit part of the abiotic environment.

Hydrogeomorphic patterns along the river continuum have provided the framework for developing concepts and theory in stream ecology (Vannote et al. 1980; Thorp et al. 2008). However, tidal rivers have not been included in, or integrated with, any of the formative concepts in stream ecology because hydrogeomorphic patterns in tidal rivers have not yet been described. Previous research has described phytoplankton maxima in the tidal freshwater portion of tidal rivers and corresponding changes in phytoplankton community (reviewed by Van Damme et al. 2009). Yet little attention has been given to quantifying how these tidally-induced changes in hydrogeomorphology explicitly affect ecological processes. Integrating tidal rivers with the rest of the river continuum begins with answering three questions:

1. How do tidally-induced geomorphic patterns affect irradiance, and consequently primary production?
2. How do tidally-induced changes in residence time influence primary production?

3. Are there differences in the growth rate of phytoplankton along the tidal continuum, and if so, what are the causes?

Chapter 5 explores how hydrology and geomorphology indirectly influence the rate of primary production in tidal rivers and the accumulation of phytoplankton biomass. The tidal effects on channel morphology and hydrology identified in Chapter 2 will provide a physical template on which to base predictions of the spatial patterns phytoplankton productivity in tidal rivers. In addition to providing novel analyses on tidal river production, Chapter 5 highlights how the combination of hydrology, geomorphology, and ecology in tidal rivers sets these ecosystems apart from rivers, lakes, and estuaries, opening the door to investigating broader ecological questions in these ecosystems.

Table 1.1 Length of the tidal extent upstream from the ocean in various rivers.

River	Overall tidal extent (km)	Tidal-fresh zone (km)	Head-of-tide landmark	Reference
Tapagos	1448	-	-	Wheeler 1893
Amazon	644[a]	644	Obidos	Wheeler 1893
Gambia	526	276	-	Amphlett and Brabben 1991
Mississippi	495	395[b]	Tarbert Landing	McKee, pers. comm.
Brahmaputra	348	-	Bahadurabad	McKee, pers. comm.
Seine	277	-	-	Wheeler 1893
Ganges	240	-	Nadadwip	Singh 2007
Hudson	240	190	Albany	Lampman et al. 1999
Columbia	235	195[c]	Bonneville Dam	Diefenderfer et al. 2008
Yangze	511	-	Datong	Mckee, pers. comm.
Potomac	187	61	Chain Bridge	Bennett et al. 1986
St. Johns	173	-	Lake George	Phlips et al. 2000
Sheldt	155	60	Ghent	Muylaert et al. 2005
Seine	153	108	Dam of Poses	Guézennec et al. 1999
Severn	108	-	Diglis Weir	Wheeler 1983
Humber	105	-	Naburn	Wheeler 1983
San Joaquin	100	-	Crows Landing	Lehman 2007
Thames	100	-	Teddington Lock	Wheeler 1983
Congo	100	60[c]	Boma	Runge 2007

Table 1.1 continued

Connecticut	97	-	Windsor Locks	Bacon 1906
Fraser	75	65	Mission	Villard and Church 2003
Weser	70	40-70	Bremen	Schuchardt and Schirmer 1991
Loire	64	-	-	Wheeler 1893

[a] Amphlett and Brabben (1991) estimate a tidal length of 735 km from mouth
[b] Amphlett and Brabben (1991) estimate saltwater extends 100 km from mouth
[c] Amphlett and Brabben (1991) estimate saltwater extends 40 km from the mouth

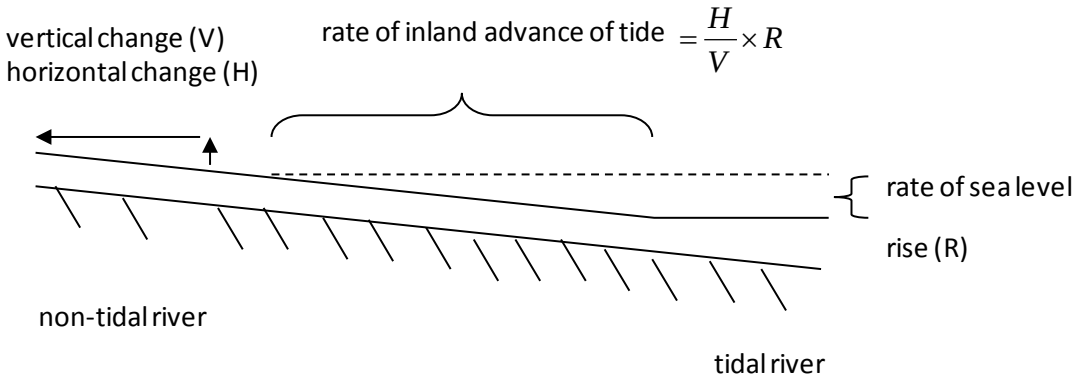

Figure 1.1 General equation for the rate of inland advance of tidal effects.

2. THE EFFECTS OF TIDES ON RIVER HYDRAULICS AND THEIR IMPLICATIONS FOR RIVER GEOMORPHOLOGY

2.1. Introduction

Tidal rivers are a dynamic portion of river networks. Tides travel inland significant distances in large rivers such as the Mississippi (500 km) and Amazon (800 km), and affect half the length of smaller rivers in eastern North America (Anderson, 1986). Moreover, the inland extent of the tide is continually advancing landward as sea level rises over low-gradient coastal plains throughout the world. As tides extend further upstream they alter river geomorphology, although the processes by which this adjustment occurs are poorly understood. These processes ultimately affect the transformation and storage of terrestrial materials transported to the ocean, and therefore understanding how rivers are affected by tidal action over time is a phenomenon central to both fluvial, estuarine and coastal geomorphology.

There is a striking gap in our knowledge of the effects of tides on rivers during rising sea level. Stratigraphic records, facies models, and geochronologic data have provided the foundation for our understanding of how coastal rivers and estuaries responded to fluctuations in sea level over Quaternary and Holocene periods (reviewed by Dalrymple et al. 1992; Schumm, 1993; Blum and Törnqvist, 2000). However, these stratigraphic, conceptual (Dame et al. 1992; Brinson et al. 1995), and numerical (Parker et al. 2008) models of river adjustment assume that river discharge and sediment transport are unaffected by tides (except see Gardner and Bohn 1980). However, tides

affect both discharge and sediment transport in ways which could influence long time-scale coastal evolution through feedbacks between hydrology and geomorphology (e.g., Friedrichs 1995). Bridging the knowledge gap between the geologic patterns in coastal morphology and shorter time-scale hydrologic processes in tidal rivers requires that we link tides with their influence on hydrologic processes and sediment transport.

2.1.1. Tidal river hydrology

The hydrology of tidal rivers is more complex than non-tidal rivers because the water discharge and sediment load are functions of both upstream-derived water and sediment runoff, and downstream-derived tidal water and sediment delivery. Hence, the morphology and hydrology of these rivers is a result of a gradual overlap of tidal influence on fluvial form (Langbein, 1963). This overlap in tidal and fluvial morphology is what distinguishes tidal rivers from tidal creeks: tidal rivers are a variation of a pre-existing fluvial channel, while tidal creeks are formed solely by tides incising into a marsh surface (Fagherazzi et al. 2004). Unlike tidal creeks, which terminate at the landward extent of a tidal marsh, tidal rivers are characterized by a gradient in tidal flow along a non-tidal river to estuary continuum.

The magnitude and direction of river flow along the tidal river continuum can be generalized into 3 zones (modified from Gurnell, 1997). Upstream (zone 1) backwater effects predominate where flow stagnates as water level rises in response to flood tides. At zone 2 tidal amplitude increases relative to zone 1, flow reversal may occur, and discharge will depend on the combination of tide effects and watershed runoff. At zone 3 salinity periodically intrudes from the estuary downstream and there is strong tidal flow

reversal. The flow regime in each of these zones affects floodplain inundation and sediment transport.

In the upper tidal river where velocity does not reverse with tides (zone 1), water level fluctuation alone can influence river geomorphology through a backwater effect (Gurnell, 1997). This backwater is caused by a reduction in surface slope of the river. During flood tide, water surface slope in the channel reaches zero and water ceases to flow downstream; instead, river discharge from upstream fills the channel and depth increases. As water level rises, overbank flow can transport suspended matter laterally into the floodplain where deposition and sediment accretion occur (Darke and Megonigal, 2003; Kroes et al. 2007).

Moving downstream to zones 2 and 3, the direction and velocity of flow vary sinusoidally with tides. The water surface slope reverses between ebb and flood tide (e.g.,, the water surface downstream is higher than upstream) and therefore the direction of river flow reverses. Enhancement of river discharge by tidal flow increases energy flux and resultant sediment transport in tidal rivers (Chen et al. 2005), with a zone of maximum turbidity near the freshwater-saltwater interface (Dyer, 1995). Sediment can be transported upstream over short and long periods of time. In fact, there can be a net, landward transport of sediment (Meade, 1969) as a result of velocity asymmetry between flood and ebb tides (Friedrichs and Aubrey, 1988). For example, net upstream bedload transport in the tidal freshwater Pitt River, British Columbia, resulted in the landward expansion of a delta into a lake upstream (Ashley, 1980). A similar phenomenon was observed in suspended matter in the Seine River, France, where marine-derived material was advected into the freshwater tidal portion of the river (Guézennec et al. 1999).

Demarcating three zones of tidal influence in a tidal river based on its flow regime provides a typology of the relative degree of tidal influence. However, it is unclear where along this gradient tidal influence on water and sediment flux supersedes that of fluvial discharge from the watershed. Furthermore, it is unclear how tides influence the hydrologic and hydraulic mechanisms which drive geomorphic adjustments. More precise understanding of how tides influence channel hydrology and geomorphology requires separating the tidal from fluvial forces occurring simultaneously in the river instead of just measuring their combined effects on river discharge.

2.1.2. Geomorphic adjustment to tidal influence

Tidal rivers and their floodplains exhibit systematic downstream changes in geomorphology. Channel width increases along the length of rivers (Leopold and Mattock, 1953) and estuaries (Langbein, 1963), but the rate of increase is greater in estuarine channels (Leopold Wolman and Miller, 1964). For example, a 10-fold increase in channel cross section area occurred at the transition from non-tidal to tidal river in the Pocomoke River, MD, and the tidal floodplain width increased 3-fold (Kroes et al. 2007). This increase in channel area is presumably accompanied by bank erosion as the channel is forced to accommodate higher tidal discharge as sea level rises (Gardner and Bohn 1980). While mechanistic explanations abound for geomorphic trends along rivers (reviewed by Singh, 2003) and estuaries (Langbein, 1963; Williams et al. 2002), far fewer explanations have been proposed for the geomorphic trends that occur within the tidal freshwater river.

Understanding the mechanisms by which tides influence river geomorphology requires linking the spatial gradients in tidal hydraulics, sediment transport, and channel geomorphology with their chronologic progression during the course of sea level rise. Accounting for a chronology of adjustment in tidal rivers is necessary because the contemporary patterns along a tidal gradient are the result of accumulated changes over time at each zone of tidal influence. For example, the contemporary geomorphology in zone 2 is not just a function of an intermediate tidal regime (e.g.,, regular flow reversal and increased discharge), but is also contingent on geomorphic adjustments that occurred during the prior tidal regime at that location. Therefore, understanding the spatial trends alone does not fully reveal the mechanisms by which tides affect geomorphology; rather we must understand tidal effects and the accumulated landscapes on which they have been acting over time.

The challenge is to couple tides with their influence on hydrology and resultant geomorphic processes over time. Stratigraphic and geochronologic methods by themselves are insufficient because feedbacks between hydrology and sediment transport are not apparent from these data. Likewise, historical records of river channel planform, such as aerial photographs or maps, do not provide information on the hydrologic processes occurring over the intervening time period. An alternative to these methods is location-for-time substitution, where the characteristics of prior landscapes are inferred from contemporary patterns (reviewed by Paine, 1985). In tidal rivers, progressive change over time could be inferred from current spatial patterns in hydrology, sediment transport, and geomorphology. This inferred chronology would be valuable in the

development of hypotheses to explain how river geomorphology adjusts to tidal hydrology as sea level rises.

1.3. Objectives

The objective of this study were to explain: 1) how tides affect river flow and the energy available for geomorphic work, 2) how tides alter a river's sediment transport regime, and 3) how feedbacks may develop between tidal energy, sediment transport, and channel morphology as tidal amplitude increases. The first step was to quantify the hydrologic processes occurring in the three zones of a tidal river and discriminate between the tidal and fluvial contributions to river hydraulics. This required separation of the tidal contribution (that which is solely due to tidally-driven change in flow direction and water level) from fluvial contribution (due solely to watershed-derived runoff) to discharge and stream power. As defined by Rhoads (1987), stream power is a concept that "…refers to the time rate of potential energy expenditure (i.e. conversion of potential energy to kinetic energy that is dissipated in overcoming internal and boundary friction, in transporting sediment and in eroding the channel perimeter) as water travels down slope in a channel.". We relied on cross-sectional stream power to measure how tides affect the energy available to perform geomorphic work (e.g., channel erosion and transport sediment) in tidal rivers.

The second step was to measure the spatial and temporal patterns in suspended matter concentration and transport, and relate them to tidal and fluvial discharge regimes. We focused on suspended matter instead of bedload because floodplain accretion and levee formation result from settling of suspended matter during overbank flow.

Suspended sediment concentration in river water is strongly related to vertical accretion rate in tidal freshwater ecosystems (Darke and Megonigal 2003). Therefore, we inferred the potential for vertical accretion of the floodplain and channel banks from suspended sediment concentration, susceptibility of the floodplain to inundation, and the direction of net sediment flux.

The third step was to explain how river channel geomorphology was affected by tidal influence over the course of sea level rise; a critical component of this step was comparing observed data with predictions of channel area in the absence of tides. We conclude with a hypothesized chronology of tidal river evolution inferred using location-for-time substitution and our observations of tidal hydrology, sediment transport, and geomorphology.

2.2 Methods

2.2.1 Study area

The Newport River is a third-order, blackwater river in eastern North Carolina, U.S.A. The 310 km^2 watershed drains to the Atlantic Ocean at Beaufort Inlet (Figure 2.1). Two headwater tributaries drain the 86 km^2 atidal upper watershed and form the Newport River at their confluence at the head-of-tide. The main channel drains a further 128 km^2 before entering a large polyhaline estuary with a mixed semi-diurnal tide with a 1 m amplitude. Four sites were studied, beginning just upstream from the head-of-tide at the Atidal site. Three sites along the tidal river, Upstream (Figure 2.2A), Midstream (Figure 2.2B), and Downstream (Figure 2.2C), were located 2.5 km, 5 km, and 9 km from the head-of-tide, respectively. These sites have drainage areas of 100 km^2, 116 km^2, and

162 km^2, respectively. The 9 km reach of river we studied is 7 km upstream from the bayhead delta near the estuary. The river is a meandering, single thread channel; cut banks and depositional bars at meander bends are only found between the Atidal and Upstream sites. Downstream of the Atidal site, the riparian floodplain rarely exceeds 1 m in elevation (NAVD88) and is uninterrupted by geologic or topographic features except for two highway bridge abutments and one railroad trestle.

The Newport River is typical of the blackwater rivers that drain coastal plain watersheds in the southeastern US. Extensive alluvial riparian floodplains and low channel gradients result in a high concentration of dissolved organic material and a low concentration of upstream-derived sediment (Meyer, 1990; Hupp, 2000). Riparian vegetation transitions from bottomland hardwood forest (*Taxodium, Nyssa, Acer*), to freshwater emergent (*Pontedaria, Peltandra*), and finally to estuarine marsh (*Juncus, Phragmites, Spartina*) in the lower tidal river. While sediment yield from the Newport River watershed is generally low, erosion and subsequent colluvial storage in the post-colonial era were 100 times higher than the pre-colonial period (Phillips, 1997a and 1997b).

Sea level rose in the Newport River estuary at a rate of 3.2 mm yr^{-1} between 1973 and 2002 (NOAA 2004), and this region of North Carolina experienced sea level rise of 0.8 mm yr^{-1} through the late-Holocene (Horton et al. 2009). Despite rising sea level, the bayhead delta has prograded into the estuary 1 km over the past 50 years and accreted vertically 5 mm yr^{-1}, largely due to a pulse of sediment from land clearing activity in the lower watershed (Mattheus et al. 2009); this material entered the river through a tributary downstream from the river reach we studied. Accretion rates in the tidal river riparian

zone are unknown, although similar settings in other eastern U.S. rivers have positive accretion rates. The median accretion rate for tidal freshwater marshes in the U.S. is 8 mm yr^{-1} (Neubauer 2008) and up to 20 mm yr^{-1} in tidal riparian forests (Baldwin 2007).

2.2.2. Discharge

Discharge at the Atidal site was measured monthly from May 2007 through May 2008, and again in February 2009. A Sontek Flowtracker acoustic Doppler velocimeter (SonTek/YSI, San Diego, CA, USA) was used to measure velocity at 0.6×depth at 0.5 m intervals across the channel, and discharge was calculated using standard procedures (Gordon et al. 2004). Channel cross-section area, A, and hydraulic radius, R_h, were also calculated.

Observations of Q were made at the Upstream, Midstream, and Downstream sites over 2 semi-diurnal tidal cycles (24.8 hr, hereafter referred to as a tidal day) once in June 2008 and once in February 2009. River discharge was calculated from current velocities measured using a Nortek 2 mHz Aquadopp (NortekUSA, Annapolis, MD) current profiler at 1 min intervals. The profiler was deployed horizontally on the side of the channel such that cross-channel profiles of velocity were measured at 1 m intervals; the Aquadopp allowed for a maximum profiled channel width of 10 m. Cross-channel depth was measured at 1 m intervals, and water level change was recorded every minute using Intech TruTrak (Intech Instruments LTD, New Zealand) capacitance rods. Depth at each channel station (corrected for tidal water level change every minute) was multiplied by its corresponding velocity and summed across the channel to calculate Q at 1 min intervals.

Fluvial discharge from the watershed at the tidal sites was measured as the net downstream water flux over a 24.8 hr period.

The current profiler had to be mounted below the low tide water level, therefore discharge occurring within the intertidal portion of the channel at high tide could not be directly measured. To correct for this omission, velocity measurements were linearly extrapolated from the end of the measured transect to the channel bank at high tide where velocity was assumed to be zero. Relative to the other studies of tidal river discharge, which have mostly been conducted in large rivers, the small width of the Newport River was a distinct advantage in that it allowed for velocity measurement across the entire channel at low tide. This precluded the need for more complex methods developed for large rivers (Simpson and Bland, 2000; Chen and Chiu, 2002; Hoitink et al. 2009).

Current profiler data were not always reliable because of signal interference from the channel bottom; measurements whose range in signal-to-noise ratio included background levels were not used for further analysis. This was a problem at Midstream (2008 and 2009) and Upstream (2009) when only a portion of the channel was properly profiled. Subsequently, synoptic surveys of velocity were made at these sites during ebb and flood tide using a Sontek Flowtracker. The cross-channel ratios of velocity from synoptic surveys were used to extrapolate the AquaDopp profiler data to the portions of the channel where signal-to-noise ratios were unreliable.

2.2.3 Stream power

While discharge is the predominant variable affecting sediment flux, it is not a measure of the power available to perform geomorphic work of moving sediment. To

better understand the processes by which discharge affects sediment movement and hence geomorphology, we calculated cross-sectional stream power:

$$\Omega = \rho g S Q \tag{2.1}$$

where ρ is the density of water, g is gravitational acceleration, S is the energy grade slope (hereafter called energy slope and sometimes approximated as water surface slope), and Q is discharge (Rhoads, 1987). When integrated over time, stream power (J s^{-1} m^{-1}) is equivalent to energy dissipation (J m^{-1}), a common metric in fluvial research (e.g.,, Molnár and Ramírez, 1998), estuarine research (e.g.,, van der Wegen et al. 2008), and stratigraphic models (Dalrymple et al. 1992) because it couples the force of moving water with the potential for geomorphic work.

Stream power at the Atidal site was calculated using equation 2.1. Energy slope was calculated using a standard formulation for steady flow:

$$S = \frac{U^2}{\left(\frac{R_h^{1/6}}{n}\right)^2 \times R_h} \tag{2.2}$$

where U is velocity (Q/A), R_h is the hydraulic radius of the channel, and n is the Manning's friction term. A Manning's n of 0.06±0.01 was used, representing the mean and standard deviation from 12 coastal plain streams in North Carolina (Geratz, personal communication, see Sweet and Geratz 2003 for methodology). Stream power was multiplied by 24.8 hr to calculate the energy dissipation that occurred over a tidal day.

Calculating stream power and energy slope at the tidal sites required considering contributions of unsteady flow to energy slope and Q. The energy slope was calculated using a standard formulation for unsteady flow in rivers:

$$S = \frac{U|U|}{\left(\frac{R_h^{1/6}}{n}\right)^2 \times R_h} - \left(\frac{1}{g} \times \frac{\partial U}{\partial t}\right) \quad (2.3)$$

where t is time; upstream flow during flood tide results in a negative value of energy slope. A Manning's n of 0.06±0.01 was used based on the assumption that flow resistance in the tidal river was similar to the non-tidal river. Using this calculated value for S, stream power was calculated every minute using equation 2.1. Several criteria were applied to this calculation due to the rapidly varying velocity and direction of flow. First, if flow deceleration resulted in a negative result from equation 2.3 stream power was assumed to be zero for that 1 min period. Second, transient reversals of flow direction that lasted for only 1 min were considered to have a stream power of zero for that minute. Finally, total energy over each flood and ebb period was calculated by integrating the absolute values of the calculated stream power. The density of water used in equation 2.1 is salinity-dependent, therefore salinity was measured and recorded at 5 min intervals using a YSI 6560 conductivity and salinity probe in conjunction with the 6600 sonde and 650 data logger (Yellow Springs Instruments, Yellow Springs, OH, USA).

Calculation of energy slope in rivers usually depends on the use of a friction factor, often either Manning's n or a Chézy coefficient. Our application of a Manning's n value of 0.06 corresponded with a Chézy coefficient of 16-18 $m^{1/2}$ s^{-1} given the R_h of the Newport River. For comparison, the measured Chézy coefficient in large tidal river in Indonesia ranged from 40-56 $m^{1/2}$ s^{-1} during ebb tide and 45-70 $m^{1/2}$ s^{-1} during flood tide (Buschman et al. 2009), indicating less friction and lower energy slope than the Newport River. We attempted to measure vertical velocity profiles with which to quantify the

change in Manning's *n* over a tidal cycle, but were unable to obtain usable measurements due to the rapid fluctuations in velocity. Despite this limitation, we believe our calculations of stream power using equations 2.2 and 2.3 are more accurate than if water surface slope (a commonly used substitute for energy slope) was used.

The contribution of fluvial discharge to stream power was determined using equations 2.1 and 2.2. Net downstream discharge (fluvial discharge) was divided by an estimate of *A* to calculated *U* in equation 2.2. To estimate *A*, we developed a power function relationship between the observed *A* and *Q* at the Atidal site during low-flow conditions, and applied this equation to the net daily downstream discharge at each tidal site (the at-a-station hydraulic geometry approach of Leopold and Mattock, 1953). The mean R_h observed during low-flow conditions at the Atidal site was used in equation 2.1, with ±1 standard deviation of this mean applied to represent the uncertainty in this assumption. We used two combinations of R_h and Manning's *n* to calculate a lower and upper bound on the predicted stream power. A lower bound was calculated by combining a low Manning's *n* (0.05) with a high R_h (mean Atidal value + 1 standard deviation). An upper bound was calculated using a high Manning's *n* (0.07) and low R_h (mean Atidal value – 1 standard deviation). The resultant stream power was integrated over a tidal day to calculate the energy dissipation that occurred due to fluvial discharge alone.

2.2.4. Suspended matter transport

2.2.4.1. Suspended matter concentration

Suspended matter concentration was measured over an annual period along the tidal gradient to characterize spatial trends and their response to changes in Atidal river discharge. All sites were sampled twice-monthly from May 2006 through May 2007. The concentration was determined by filtering up to 1 L of water through a 2.7 μm glass fiber filter (Whatman GF/D), drying at 105^{o}C for >1 hr, and weighing. This filter pore size (2.7 μm) was larger than the standard 0.2 μm pore size used for suspended matter analysis, therefore ours is a conservative measure of suspended matter concentration. Both the organic and inorganic fractions contributing to suspended matter were measured since these fractions contribute differently to rates of wetland sediment accretion (Neubauer, 2008). The organic matter fraction was calculated by mass loss after combustion at 550^{o}C for 4 hr . In addition, turbidity was measured using a YSI 6136 probe attached to a 6600 sonde and 650 data logger and calibrated using a formazin standard per manufacturer's protocol. Sampling was conducted during ebb tide on most occasions. Differences in suspended matter and turbidity between sites were tested using an ANOVA at the 0.05 significance level.

2.2.4.2. Tidal suspended matter flux

Turbidity and an estimate of suspended matter flux were made during a tidal day to characterize spatial trends in the direction of net sediment transport. Turbidity was measured using the YSI 6136 probe described above and values were recorded at 10 min intervals (although turbidity sensors were not available for the Upstream and Downstream experiments in 2008). Suspended matter flux was estimated using a relationship between turbidity and suspended matter generated for each site from the

yearly data described above. Linear regressions and their 95% confidence interval were calculated for each site and applied to each turbidity measurement following the procedures of Wright and Schoellhamer (2005). Estimates of suspended matter flux were numerically integrated over a tidal day.

2.2.5. Channel geomorphology

2.2.5.1. Observed geomorphology

Measurements of channel cross-section area at bankfull flow and high tide were made along the tidal river. Channel cross-sectional area was measured every 500 m along the 9 km tidal river. At each cross-section, depth was measured at 1 m intervals across the channel. These transects only extended to the boundary between the open channel and riparian zone. Floodplain topography adjacent to surveyed channel cross-sections was determined from digital LIDAR (Light Image Detection and Ranging) data. Bare-earth LIDAR points were obtained from the North Carolina Floodplain Mapping Agency (www.ncfloodmaps.com), and ArcGIS (ESRI, Redlands, CA, USA) software was used to construct a triangulated irregular network from the LIDAR data. This elevation model was used to extract the elevation profile of the riparian floodplain for the 50 m adjacent to each in-channel transect. Extracted elevations (NAVD 88 datum) were corrected to mean sea level by adding 9 cm (determined using Vdatum software, http://vdatum.noaa.gov/). Cross-sectional area at bankfull discharge was determined from cross-section profiles using the bench index metric of Riley (1972); high tide channel area was observed in the field during surveys.

2.2.5.2. Predicted Fluvial Geomorphology

A hydraulic geometry relationship developed for coastal plain streams in North Carolina was used to predict how channel cross-sectional area would increase in the downstream direction in the absence of tides. The expected bankfull channel cross-sectional area (A_{bkf}, m^2) for each site in the absence of tidal flow was estimated as $9.43 \times A_w^{0.74} \times 0.0929$, where A_w is watershed area (mi^2) and the regression $r^2=0.96$ (Sweet and Geratz, 2003). The difference between these predictions and the observed channel cross-sectional area was attributed to tidal influence.

2.3. Results

2.3.1. Discharge

Semi-diurnal *Q* at all sites showed an oscillating pattern indicative of tidal influence, with peak *Q* much larger than predicted fluvial *Q* (Figures 2.3-2.5). Net downstream (fluvial) discharge decreased between the Atidal and Upstream sites, with the more dramatic reduction occurring in June than February (Table 2.1). *Q* and fluvial discharge increased from Upstream to Downstream, but flood *Q* increased more than ebb *Q* (Figures 2.3-2.5, Table 2.1). Unlike the Upstream and Midstream sites where highest *Q* occurred during ebb tide, highest *Q* occurred during flood tide at the Downstream site (Figures 2.3-2.5). The prominence of flood tide over ebb tide Downstream is also reflected in the velocity data: higher mean and peak velocities occurred during flood than ebb tide (Table 2.2).

2.3.2. Stream power

Stream power was calculated as a function of *Q* and *S* (equation 2.1). Salinity was generally less than 0.5 which indicated fresh, non-brackish water at all sites (Table 2.2), and therefore a constant water density was used in equation 2.1 (1000 kg m^{-3}). Energy slope displayed the same sinusoidal trend as *Q* over a semi-diurnal tidal cycle, but was generally less than predicted for fluvial discharge alone (Figures 2.2-2.5). Observed *S* was lower than predicted for a purely fluvial condition because predicted velocities were higher (0.19 to 0.29 m s^{-1}) and R_h were lower (0.25 to 0.49) than observed values (Table 2.2; equations 2.2 and 2.3).

Stream power increased along the tidal continuum, with peak values occurring during ebb tide Upstream and Midstream but during flood tide Downstream (Figures 2.3-2.5). Stream power was generally lower than predicted Upstream, but much greater than predicted Midstream and Downstream (Figures 2.3-2.5). At the Midstream and Downstream sites, tidally-enhanced *Q* over-compensated for the suppressed *S* and resulted in higher stream power than was predicted based on fluvial discharge alone (Figures 2.3-2.5, Tables 2.1 and 2.2).

To more effectively compare the energy regime between sites and to distinguish the tidal from fluvial components, we integrated stream power over a tidal day. This total energy dissipation averaged 58 kJ, 424 kJ, and 2529 kJ at the Upstream, Midstream, and Downstream sites (Figure 2.6). The predicted fluvial energy dissipation in the absence of tidal influence also increased from Upstream to Downstream, but at a rate much lower than what was observed (Figure 2.6). Energy dissipation during the two years of observation averaged 19%, 186%, and 368% of that predicted for the fluvial condition alone (Figure 2.6). The difference between the observed and predicted fluvial energy

dissipation was significant Upstream in both years and Downstream in 2008, as indicated by non-overlapping error bars in Figure 2.6. However, the choice of Manning's n and R_h had a relatively large affect on the differences observed during the other periods and at the Midstream site (Figure 2.6).

2.3.3. Suspended matter transport

2.3.3.1. Suspended Matter Concentration

Over an annual period, there was an increase in suspended matter concentration along the tidal continuum (Figure 2.7). Mean suspended matter was 2.7 mg L^{-1}, 5.9 mg L^{-1}, and 11.4 mg L^{-1}, Upstream, Midstream and Downstream, respectively. These means were statistically different from one another (one-way ANOVA $P<0.001$, $F_{2,66}=10$). The organic and inorganic fractions also differed statistically between sites: organic matter averaged 2.1 mg L^{-1}, 3.0 mg L^{-1}, and 4.4 mg L^{-1} Upstream, Midstream, and Downstream, respectively (one-way ANOVA $P<0.0001$, $F_{2,66}=67$). Inorganic matter averaged 0.6 mg L^{-1}, 2.9 mg L^{-1}, and 7.0 mg L^{-1} at Upstream, Midstream, and Downstream, respectively, and were again significantly different (one-way ANOVA $P<0.0001$, $F_{2,66}=24$). The inorganic fraction increased relative to the organic fraction along the river continuum (Figure 2.7). Overall, suspended matter concentration was low during high discharge events but highest during the spring and summer when watershed runoff was low (Figure 2.7). Turbidity increased along the river, with means of 1 NTU, 5 NTU, and 9 NTU at Upstream, Midstream, and Downstream, respectively; means were statistically different from one another (one-way ANOVA $P<0.001$, $F_{2,66}=10$). The r^2 values of the turbidity

versus suspended matter regressions were 0.47, 0.68, and 0.88 at Upstream, Midstream, and Downstream, respectively.

2.3.3.2. Tidal Suspended Matter Flux

During tidal cycle observations, mean and maximum turbidity (our proxy for suspended matter) increased along the river (Table 2.2). Highest turbidity occurred during flood tide at the Midstream and Downstream sites (Table 2.2). Net suspended matter flux at the Upstream site was predicted to be 9 kg day^{-1} with a ±5 kg day^{-1} uncertainty from the regression's 95% confidence interval (Figure 2.8). In 2008, suspended matter flux Midstream was estimated to be 2883±1103 kg day^{-1} during ebb tide and -3493±1336 kg day^{-1} during flood tide, with a net landward directed flux of -610 kg day^{-1} (uncertainty estimated to range from -3049 to 1829 kg day^{-1}) (Figure 2.8). In 2009, the flux Midstream was 639±395 kg day^{-1} during ebb tide and -695±429 kg day^{-1} during flood tide, again producing a net landward flux of -56 kg day^{-1} (uncertainty estimated to range from -880 to 768 kg day^{-1}) (Figure 2.8). Suspended matter flux Downstream during ebb tide was 21,221±4282 kg day^{-1} and -27,707±5592 kg day^{-1} during flood tide, with a net landward flux of -6486 kg day^{-1} (uncertainty estimated to range from -16,360 to 3388 kg day^{-1}) (Figure 2.8).

2.3.4. Geomorphology

Bankfull cross-sectional area exceeded high tide area in the upper 2.6 km of the tidal river, was over-topped by high tide in the middle portion of the river, and again exceeded high tide cross-sectional area in the lower 1 km (Figure 2.9). From Upstream

to Downstream, channel width increased proportionally more than channel depth (Table 2.2). The lateral change in open channel width from low tide to high tide increased from 0.5 m Upstream to 7 m Downstream (Table 2.2).

Based on watershed area and a hydraulic geometry relationship for coastal plain, non-tidal rivers in this region, the Newport River would be expected to have a bankfull cross-sectional area increasing from 11 m^2 to 18 m^2 from the Atidal site to the Downstream site (Figure 2.9). This predicted fluvial cross-sectional area was similar to that observed in the upper tidal river, but was only a third of the observed area in the lower tidal river (Figure 2.9).

2.4. DISCUSSION

2.4.1. Tidal Influence has Counter-veiling Effects on River Discharge

Discharge data indicated that our Upstream, Midstream, and Downstream sites were representative of zones 1, 2, and 3 of a tidal river. The Upstream site (zone 1) exhibited both flow reversal (2008) and a backwater effect with no reversal (2009). The Midstream site was consistent with the flow reversal and increased *Q* as expected in zone 2. The Downstream site showed even stronger flow reversal and higher *Q*, and received brackish water (0.6 salinity) at peak flood tide, as expected in zone 3.

This delineation of zones 1 through 3 is based on the *Q* observed over the course of a tidal day. A surprising result emerged when these values were integrated over a tidal day: fluvial discharge (net downstream discharge) decreased between the Atidal site and the Upstream (2008 and 2009) and Midstream (2009) sites. Net daily discharge at all tidal sites during summer (June 2008) was much lower than winter (February 2009), a

difference too large to be explained by the modest 7% increase in Atidal discharge (Table 2.1). Two process may account for the net reduction in discharge: evapotranspiration and groundwater recharge. The strong seasonal difference suggests that evapotranspiration may play an important role in decreasing watershed discharge; tidal flow forces water onto riparian floodplains where evapotranspiration occurs rapidly. The NC State Climate Office (www.nc-climate.ncsu.edu) reported an average reference crop evapotranspiration rate of 5.6 mm day^{-1} and 2.3 mm day^{-1} for the June 2008 and February 2009 measurement periods, respectively, at the Croatan Remote Automated Weather Station (located in the Newport River watershed). When this rate is applied over the 426,000 m^2 riparian zone (Ensign et al. 2008) evapotranspiration would be 2412 m^3 day^{-1} and 989 m^3 day^{-1} during June and February, respectively, a relatively small component of the net discharge. Seepage to shallow groundwater could also be a net loss from the channel if subsurface return flow was low. Counter-acting these loss mechanisms are tributary inflows, and it is this combination of sources and sinks that are reflected in the hydrologic fluxes in Table 2.1. In summary, *Q* was clearly augmented by tides, but the overall effect of tidal influence was to reduce the net daily discharge of watershed-derived water, presumably through evaporative loss (Figure 2.10A, Table 2.3).

The combination of discharge magnitude and frequency dictate fluvial landform morphology in rivers (Wolman and Miller 1960), but it is unknown how tides modulate either the magnitude or frequency of the hydrologic forces acting in tidal rivers. Our measurements were constrained to relatively low flow periods of the year, and we do not know the relative importance of large river discharge events on the patterns we observed. However, water level (depth) in the Newport River (Ensign, unpublished data) and other

tidal rivers (Kroes et al. 2007; Light et al. 2007) is affected more by tides than upstream river discharge. If channel width and velocity are also more influenced by tides than river discharge, then the frequency and magnitude of forces acting in tidal channels may be only weakly related to river discharge. In which case, our measurements during baseflow would represent the dominant hydrologic forces acting in the Newport River. The frequency-magnitude of tidal versus fluvial forces is a critical topic for further research in tidal rivers.

2.4.2. Stream Power Indicated the Effect of Tides on River Hydrology

Stream power represents the energy lost through friction and turbulence, a portion of which is expended to erode and transport sediment, and thus shape channel geometry (Rhoads, 1987). We relied on stream power as a measure of the hydraulic influence on channel morphology, as have previous studies of non-tidal (e.g., Knighton, 1999; Reinfields et al. 2004) and tidal (Phillips and Slattery 2007) rivers. Our study built on these previous studies in two ways. First, we separated the tidal and fluvial components of stream power, and second we quantified the fluctuation in stream power over a tidal cycle.

Maximum stream power increased along the Newport River, and greatly exceeded the predicted fluvial condition Midstream and Downstream (Figures 2.2-2.4). This trend was not unexpected since stream power was calculated as a function of Q (equation 2.1), and Q during peak ebb and flood tides were much greater than the predicted fluvial condition. Counter-acting Q's influence on stream power was a decrease in S relative to the fluvial condition. Energy slope is inversely related to R_h (equation 2.2), and R_h

increased along the tidal continuum. If we assume that this trend in R_h was caused by tidal influence, then tide has two counter-veiling affects on stream power. Tidal flow increases the peak *Q* during a tidal cycle and thereby increases stream power, but also increases R_h which reduces *S* and thereby reduces stream power (Figure 2.10). In the Newport River, the increase in peak *Q* during maximum ebb and flood tide over-compensated for reduced *S*, resulting in an increase in stream power from Upstream to Downstream (Figure 2.10).

Since stream power fluctuates over a tidal cycle, a better measure of the force exerted in the river channel is energy dissipation (temporally integrated stream power) (Figures 2.5 and 2.9). Energy dissipation decreased between the Atidal and Upstream tidal site because net daily discharge and *U* decreased while R_h increased (Table 2.1 and 2.2). Apparently the small tidal amplitude in zone 1 (Upstream) suppressed energy dissipation (Figure 2.6). Increased tidal amplitude and discharge in zone 2 (Midstream) increased energy dissipation, but only enough to equal the energy dissipation that would occur from fluvial discharge alone. Not until zone 3 was the observed energy dissipation significantly higher than would have occurred without tides (Figure 2.6). The important conclusion to be drawn from these data is that energy dissipation does not increase as a simple function of tidal amplitude. Instead, tides affect channel morphology (R_h) and discharge (both tidal and fluvial components) in ways which result in a non-linear change in energy dissipation through a tidal river (Figure 2.10).

2.4.3. Suspended Matter Concentration and Transport were Functions of Tide not Watershed Runoff

Suspended matter concentration increased along the tidal river continuum (Figure 2.7). The low concentration Upstream is consistent with previous measurements in the Newport River (Simmons, 1988; Phillips, 1997b) and is typical of coastal plain rivers in general (Hupp, 2000). The higher concentrations Midstream and Downstream did not correspond with increases in *Q* (Figure 2.7); in fact, the highest concentrations were observed during low watershed runoff in early summer (April-May). We are not aware of tributary inputs to the lower Newport River that would contribute a higher concentration of suspended material to the mainstem. Therefore, the longitudinal gradient in concentration, combined with a lack of correspondence between fluvial discharge and concentration, indicate that tidal influence was a more important factor affecting suspended matter than precipitation and watershed runoff. High concentrations Downstream were presumably the result of in-channel mobilization by erosion, flocculation, and delivery from the zone of turbidity maximum downstream (Eisma, 1986; Dyer, 1995; Chen et al. 2005).

Suspended matter became increasingly dominated by inorganic material along the tidal river continuum, indicating either a change in source or in-situ transformation (Figure 2.7). The predominantly organic suspended matter at the Upstream site is indicative of the high concentration of amorphous particulate seston typical of a blackwater river (Carlough, 1994). Downstream, however, inorganic material was the dominant fraction of the suspended load, likely due to higher flow velocities that were able to suspend heavier, inorganic particles.

Flux of suspended matter over a tidal cycle at each location increased as a function of both higher concentrations and higher *Q*. Interestingly, there was a net

upstream flux of material over a tidal cycle at the Midstream and Downstream sites, implying short-term storage in the river channel or on the floodplain. While there was uncertainty in these measurements due to the error associated with the turbidity-suspended matter regression, it is conceivable that a net upstream flux could occur based on the differences in flood and ebb velocity. Downstream, highest mean and maximum velocity occurred during flood tide of both years, and maximum stream power occurred during flood tide. Since erosion, suspension, and transport of material are functions of velocity, higher flood than ebb velocity can lead to "flood-tide dominant" transport where net upstream sediment flux exceeds downstream flux (Friedrichs and Aubrey, 1988; Fry and Aubrey, 1990). Numerical modeling of currents in the upper Newport River estuary (10 km from our Downstream site) indicated that net upstream transport of suspended matter can occur (Chen et al. 1997). In fact, net landward (i.e. upstream) sediment transport occurs in many estuaries and tidal rivers (Meade, 1969; Ashley 1980; Wells 1995; Guézennec et al. 1999; Phillips and Slattery, 2006).

As a final note on suspended matter, it is important to clarify that the occurrence of flood-tide dominant transport does not preclude watershed-derived sediment pulses from being exported to the estuary during large runoff events (as was reported by Mattheus et al. (2009) in the Newport River). Both mechanisms are responsible for distributing sediment along the tidal river continuum under different hydrologic conditions and time scales; it is the relative magnitude and frequency of these processes over long time scales that remains unknown.

2.4.4. Channel geomorphology reflected changes in hydrology and suspended matter

Channel cross-sectional area (both bankfull and high tide) increased greatly along the tidal Newport River, exceeding the fluvial prediction by 3-fold at the Downstream site (Figure 2.9). The divergence from predicted fluvial conditions began near the Upstream site, corresponding with the region where energy dissipation was lowest (Figure 2.6). This paradoxical increase in channel area despite a reduced capacity of river flow to erode the channel suggests that the increase in channel area is simply a result of the channel accommodating a larger volume of water during flood tide. Channel area (both bankfull and high tide) plateaued near the end of the study reach (Figure 2.9). The enlarged channel area Downstream corresponded with the location of the river where energy dissipation exceeded the predicted fluvial condition (Figure 2.6). We attribute the larger than predicted channel area to the additional energy dissipation and erosion caused by tidal flow.

The relationship between high tide channel area and the bankfull channel area along the tidal gradient indicates the potential for channel bank and riparian sediment accretion to occur. The low concentration of suspended matter Upstream and Midstream suggests that even when overbank flow occurs during high tide, deposition will be minimal. In contrast, high suspended matter concentration and flux Downstream suggest that overbank deposition will be large when overbank flow occurs (Figure 2.10). Other tidal rivers exhibit a similar gradient in which upstream levees disappear in the middle tidal zone where floodplain extent and inundation are greater than the upstream or downstream zones (Baldwin 2007; Kroes et al. 2007; Light et al. 2007). The rate of riparian sediment accretion is directly related to riverine sediment concentration and frequency of inundation (Darke and Megonigal 2003). In the absence of other factors

that affect sediment deposition (e.g., riparian vegetation; Neubauer et al. 2002; Pasternack and Brush, 2002), we expect that maximum riparian sediment accretion should occur where riverine sediment concentration and the frequency of inundation are highest.

2.4.5. A chronology of tidal river evolution

Discharge, stream power, and sediment transport change dramatically due to tides; our goal now is to relate these spatial patterns to their chronologic progression as sea level rises. Location-for-time reasoning is commonly used to infer prior geomorphic form from contemporary spatial patterns (reviewed by Paine, 1985). By applying location-for-time reasoning to our observations of the Newport River, we can develop a conceptual model of how the river has evolved over time as sea level has risen. In doing so, we assume that sea level is the only variable which has changed over time, and that topography and surficial geology of this 9 km reach of the Newport River were homogenous prior to tidal influence. This assumption is justified by the riparian zone's nearly level topography of (<1 m), lack of broader-scale topographic features, and uniform soil type and depth (>2 m; SCS, 1987). A potential confounding factor is substantial upland erosion during the pre-colonial era that may have changed suspended sediment load to the river (Phillips 1997b). While this sediment load may have influenced channel morphology, it is unknown what the deposition rates were along this section of the Newport River. Therefore, we will proceed with the caveat that future research on historical sedimentation rates in this river may require us to modify the conceptual model we propose or to suggest alternatives to the hypotheses that follow.

The chronologic stages of riverine adjustment that have occurred during sea level rise can be inferred from the contemporary zones of hydrology and stream power. Stage 1 of this chronology represents the initial changes of river evolution and corresponds with the characteristics of zone 1. Stage 3 representing the effects of the longest period of tidal influence, and correspond with the characteristics of zone 3. The changes involved in river adjustment from stage 1 through stage 3 are inferred from the contemporary differences in hydrology and sediment transport between zones 1 through zone 3.

The initial effect of tides was to reduce stream power due to a decrease in fluvial discharge and U, and an increase R_h. A backwater effect increased channel area, but not enough to exceed bankfull capacity of the channel. The concentration and transport of suspended matter are limited by a low upstream supply at this stage. As the river transitions over time to stage 2, the increased Q during peak ebb and flood tides returns stream power to its pre-tidal condition, despite further increase in R_h and decrease in fluvial discharge. Channel area and floodplain inundation increases dramatically due to the increased volume of tidal exchange. Stronger velocity is capable of entraining more sediment, a portion of which may be derived from downstream sources and delivered during flood tide. Deposition on levees may increase as this material is dispersed across the floodplain during high tide. Finally, in stage 3, stream power increases above its pre-tidal condition, despite the reduction in fluvial discharge. High suspended matter concentration and deposition ultimately reduce the extent of overbank inundation as the floodplain accretes. Flood-tide dominant transport in zone 3 transports suspended matter upstream to zone 2.

The establishment of flood-tide dominant transport is a pivotal process in tidal river evolution. In coastal rivers with low watershed-derived sediment load, the upstream transport of suspended matter provides an important sediment source for riparian accretion. However, accretion of the river bank levees becomes self-limiting when the tidal range can not overtop the levee. The subsequent decrease in overbank flooding results in less tidal energy being lost during intertidal inundation and enhancement of flood-tide dominant transport (Friedrichs and Aubrey, 1988). In this positive feedback, flood-tide dominant flow accelerates the rate at which the river progresses from stage 2 to stage 3. A similar feedback between channel area and flood-dominant transport was proposed as the mechanism that maintains estuarine channels in morphodynamic equilibrium (Friedrichs 1995).

Our conceptual framework of tidal river evolution offers hypotheses for further testing. First, we predict that the current rate riparian sediment accretion will be highest in zone 2 of a tidal river. Lower rates would be expected in zones 1 and 3 because of low suspended matter concentration in the former and less frequent over-bank inundation in the latter. Second, we predict that geochronologic dating should reveal that peak sediment accretion rates occur during stage 2 of tidal river adjustment. We anticipate that future research will modify (or reject) our conceptual model and hypotheses as the challenge of explaining how tides influence coastal river evolution continues.

2.4.6. Conclusions

This study found that tides greatly affected the discharge, stream power, and sediment transport in a tidal freshwater river. Tides enhanced river discharge during peak

ebb and flood flow, but their overall effect was to decrease the volume of watershed-derived discharge during a low-flow periods of the year. Stream power, an indication of the potential for geomorphic work, was suppressed by tides upstream, but enhanced by tides downstream. Enhanced stream power throughout the tidal river was reflected in a 3-fold increase in channel area. Tidally-enhanced stream power also increased suspended matter concentration and flux; we predict that deposition of this material in the floodplain caused accretion of the channel bank and limited overbank flooding in the lower tidal river. We hypothesize that rivers respond to tidal influence in a predictable sequence of adjustment that parallels the contemporary spatial patterns we observed along the tidal gradient. This conceptual model provides a mechanistic explanation for the geomorphic patterns in channel size and floodplain morphology observed along tidal rivers and suggests how coastal river geomorphology and concomitant ecosystem processes will change with future sea level rise (Craft et al. 2009). Further research is needed to test these predictions, but we believe our observations of the tidal effects on hydrology, sediment transport, and channel morphology will contribute to a better understanding of how tides affect river geomorphology.

Table 2.1 Water flux (m^3) during tidal cycle experiments lasting 24.8hr.

Year	Tide	Non-tidal	Upstream	Midstream	Downstream
2008	ebb		43,359	212,365	555,687
	flood*		-15,302	-185,428	-491,182
	net daily discharge	61,588	28,057	26,937	64,505
2009	ebb		58,831	220,488	485,229
	flood*		-596	-125,215	-383,312
	net daily discharge	66,058	58,236	95,273	101,917

* negative values denote downstream-to-upstream flow

Table 2.2 Hydrologic and geomorphic characteristics of Newport River during monitoring at the Atidal site (2006-2007, n=15) and tidal sites in June 2008 and February 2009 at the tidal sites. Data presented as: mean (minimum, maximum). Channel depth (m), width (m), and velocity (m s^{-1}) are the average of all cross-channel measurements. Units of R_h and turbidity are m and nephelometric turbidity units, respectively.

Year	Tide	Parameter	Non-Tidal	Upstream	Midstream	Downstream
2006-2009	none	depth	0.5 (0.3, 1.0)			
		width	6.4 (4, 9.5)			
		velocity	0.21 (0.10, 0.28)			
		R_h	0.5 (0.2, 0.9)			
2008	ebb	depth		1.2 (1.0, 1.5)	1.1 (0.9, 1.6)	1.4 (1.2, 1.8)
		width		6.8 (6.5, 7.0)	22 (18, 24)	22.7 (20.0, 27.0)
		velocity		0.10 (0, 0.18)	0.16 (0, 0.30)	0.31 (0, 0.433)
		R_h		0.9 (0.8, 1.1)	1.1 (0.8, 1.4)	1.3 (1.1, 1.7)
		salinity		0.05 (0.05, 0.07)	0.14 (0.07, 0.30)	0.12 (0.07, 0.56)
		turbidity		no data	13 (10, 19)	no data
	flood	depth		1.3 (1.0, 1.5)	1.3 (0.9, 1.6)	1.7 (1.2, 1.8)
		width		7.0 (6.5, 7.0)	23 (18, 24)	25.0 (21.0, 27.0)
		velocity		-0.07 (0, -0.12)	-0.15 (0, -0.27)	-0.33 (0, -0.53)
		R_h		1.0 (0.8, 1.1)	1.2 (1.5, 0.8)	1.6 (1.1, 1.8)
		salinity		0.05 (0.05, 0.05)	0.09 (0.02, 0.30)	0.15 (0.07, 0.56)
		turbidity		no data	17 (11, 28)	no data
2009	ebb	depth		0.9 (0.7, 1.2)	1.1 (0.8, 1.6)	1.4 (1.2, 1.8)
		width		7.0 (7.0, 7.0)	23 (22, 25)	23.6 (22.0, 28.0)
		velocity		0.13 (0, 0.24)	0.15 (0, 0.37)	0.24 (0, 0.40)
		R_h		0.7 (0.6, 0.9)	1.0 (0.8, 1.4)	1.3 (1.1, 1.7)
		salinity		0.07 (0.06, 0.07)	0.16 (0.08, 0.31)	0.12 (0.09, 0.20)
		turbidity		0.1 (0, 4.5)	2 (0, 8)	30 (11, 48)
	flood	depth		1.1 (1.0, 1.2)	1.2 (0.8, 1.6)	1.6 (1.3, 1.8)
		width		7.0 (7.0, 7.0)	24 (22, 25)	25.9 (22.0, 28.0)
		velocity		-0.03 (0, -0.10)	-0.12 (0, 0.26)	-0.30 (0, -0.45)
		R_h		0.8 (0.8, 0.9)	1.1 (0.8, 1.4)	1.5 (1.2, 1.7)
		salinity		0.07 (0.06, 0.07)	0.12 (0.07, 0.31)	0.14 (0.09, 0.20)
		turbidity		0 (0,0)	3 (0, 12)	49 (16, 77)

* negative values denote upstream flow during flood tide

Table 2.3 River channel and floodplain characteristics along the non-tidal to tidal continuum of a coastal plain river with low watershed sediment yield.

Stage	Tidal influence	Hydraulic geometry	Sediment transport/geomorphic process	Riparian characteristics
0	• no tidal influence • hydrograph dictated by precipitation	• slope set by topography • basic hydraulic geometry holds (channel area=A×drainage area$^{0.7}$)	• sediment transport primarily during spates • morphology set by dominant (effective) discharge (~annual flood)	• natural levees • bottomland mixed hardwood forest • inundated ~30 days/yr
1	• small tidal amplitude • negligable upstream flow	• bankfull depth > high tide depth • width increases rapidly downstream • reduced slope by tidal influence, but predominantly >0	• low sediment transport • predominantly organic sediment	• natural levees • bottomland mixed hardwood forest • tidal flooding contained in channel • inundated ~30 days/yr
2	• large tidal amplitude • peak ebb flow ≈ peak flood flow	• bankfull depth < high tide depth • increasing width • large slope variations from positive to negative	• increased sediment transport • alternating organic-inorganic dominant fractions • upstream flux = downstream flux	• no levees • mixed bottomland forest with fringing emergent macrophytes • inundated daily
3	• large tidal amplitude • tidal influence dominates hydrograph • peak flood flow < peak ebb flow	• bankfull depth ≥ high tide depth • width constrained by natural levees • large slope variation from positive to negative	• high, predominantly inorganic sediment transport • upstream flux > downstream flux	• re-establishment of levees • inundation during spring tides • emergent macrophyte vegetation

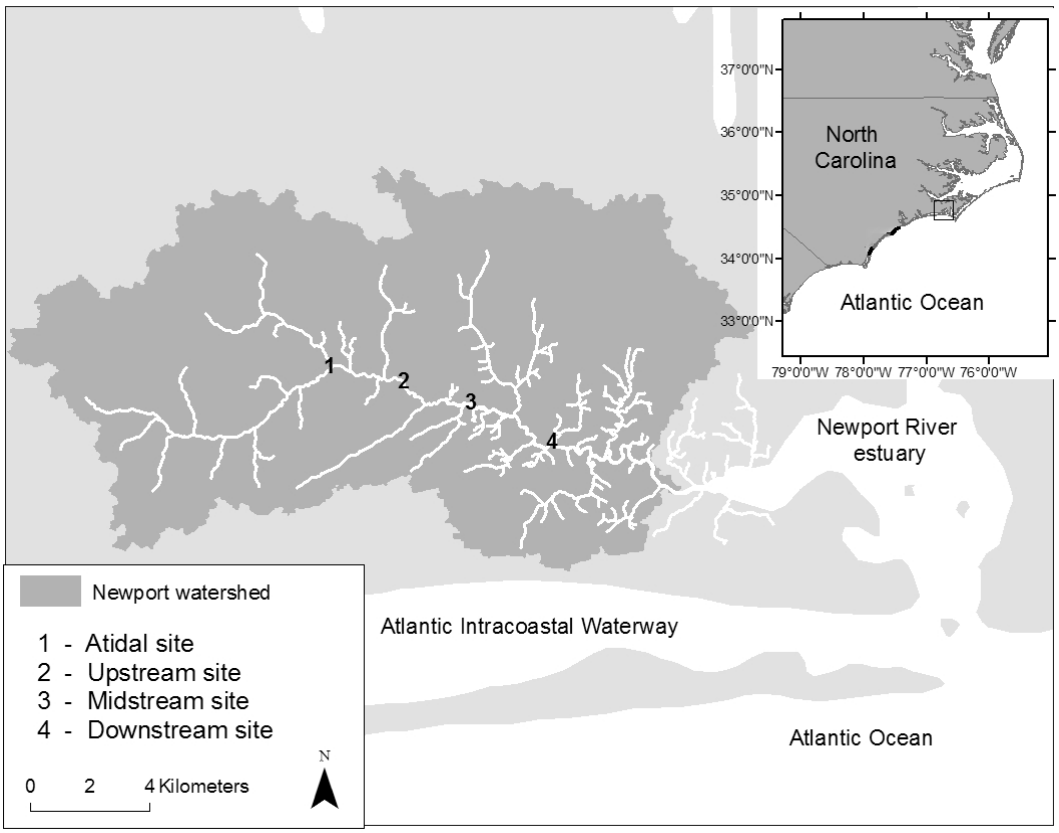

Figure 2.1 Location of the Newport River in North Carolina and the location of 4 sampling sites within the Newport River stream network.

Figure 2.2 The upper (A), middle (B), and lower (C) portions of the tidal Newport River.

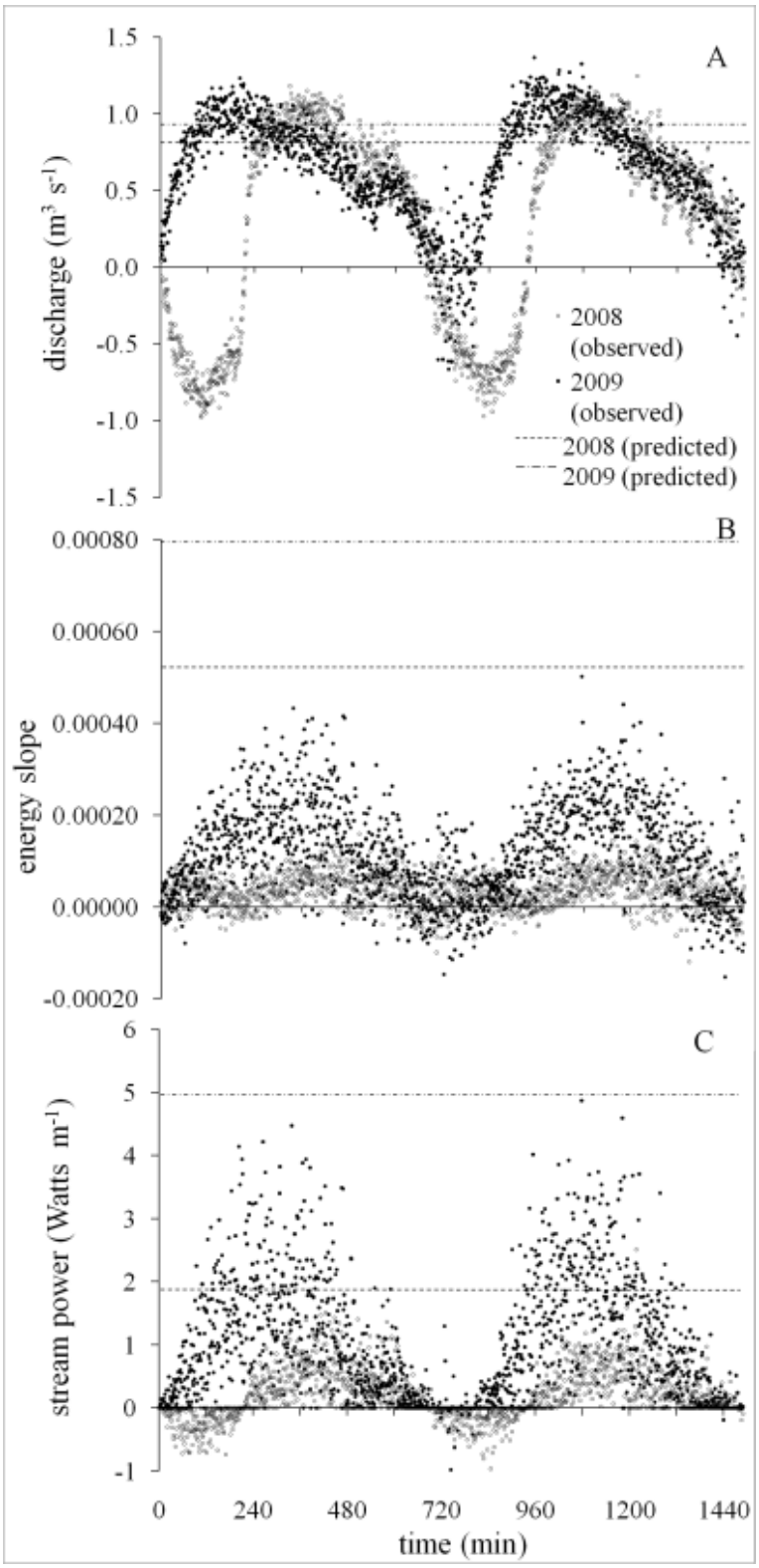

Figure 2.3 Upstream site tidal cycle measurements of discharge (A), energy slope (B), and stream power (C).

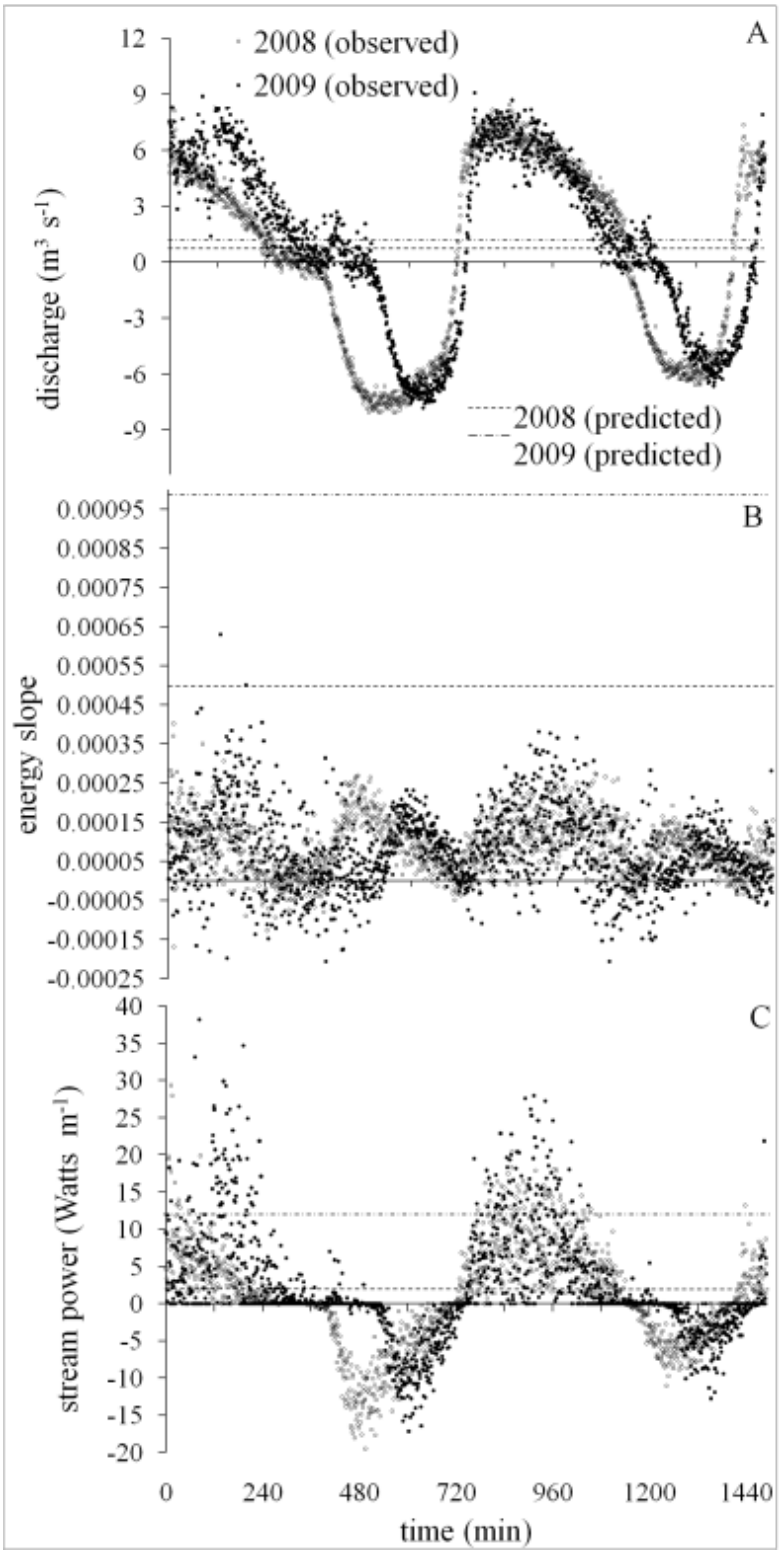

Figure 2.4 Midstream site tidal cycle measurements of discharge (A), energy slope (B), and stream power (C).

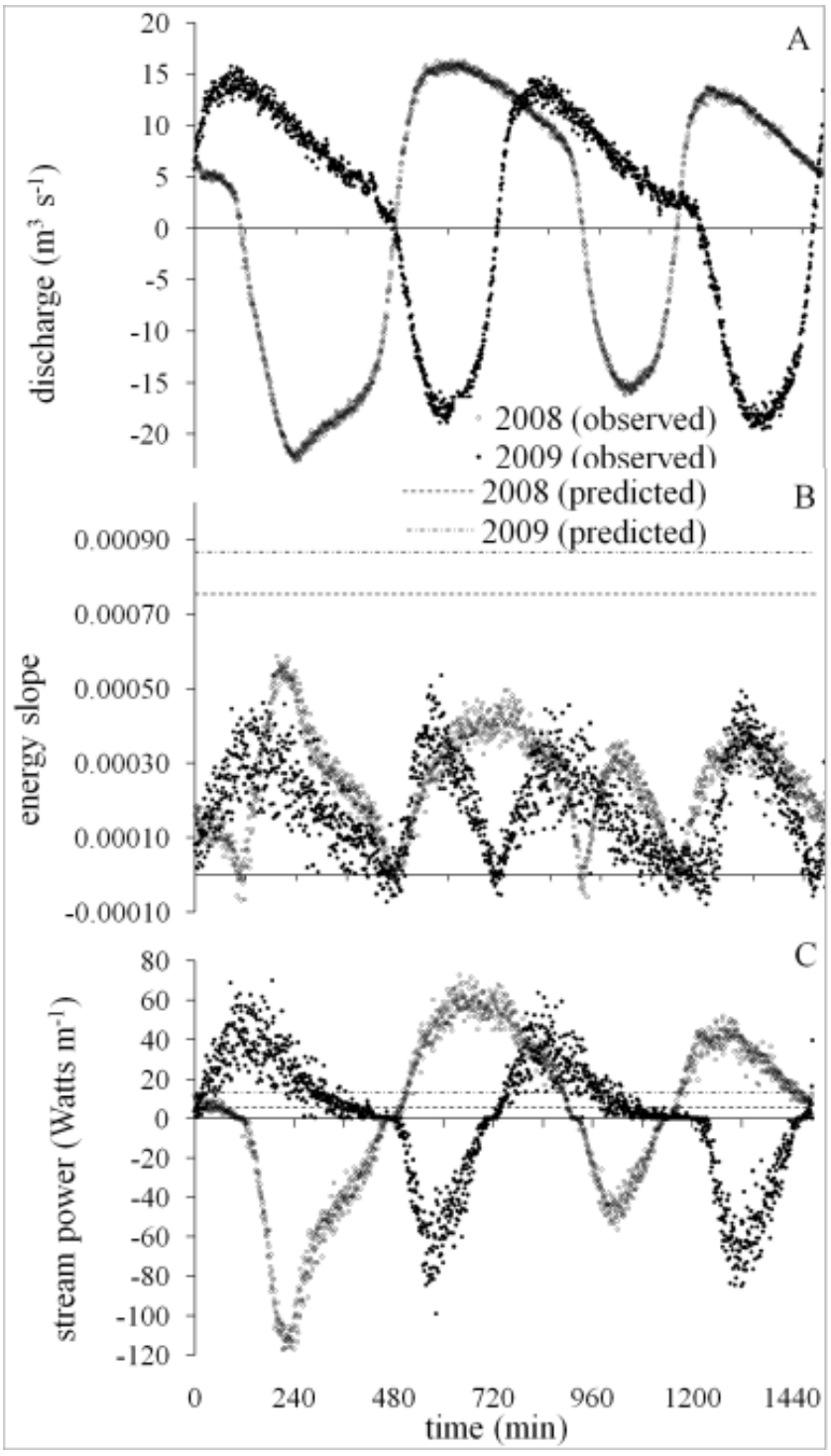

Figure 2.5 Downstream site tidal cycle experiments of discharge (A), energy slope (B), and stream power (C).

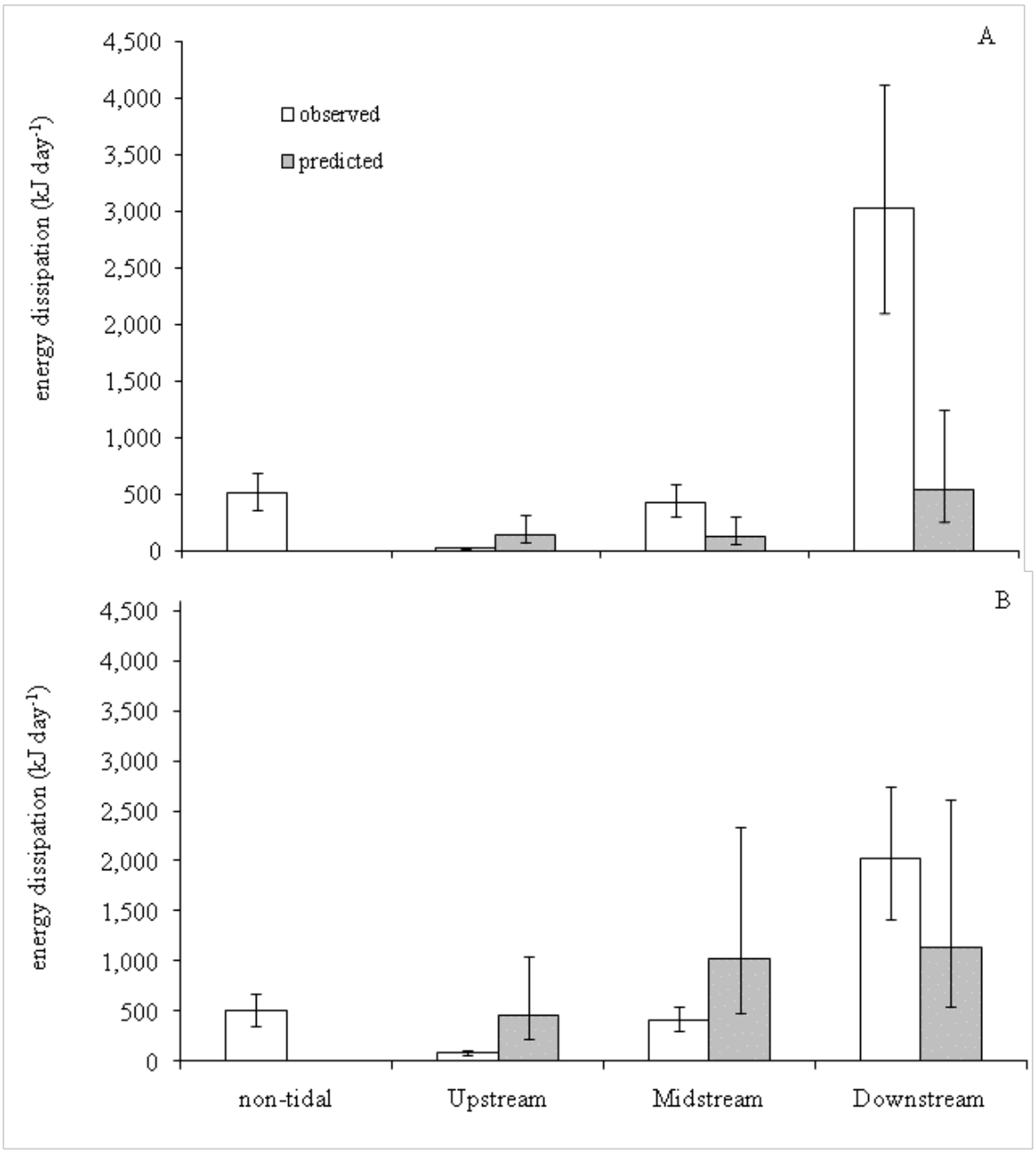

Figure 2.6 Observed (tidal+fluvial) and predicted (fluvial) energy dissipation in 2008 (A) and 2009 (B). Error bars represent the influence of a 0.01 difference in Mannings *n* combined with a 0.12 difference in hydraulic radius.

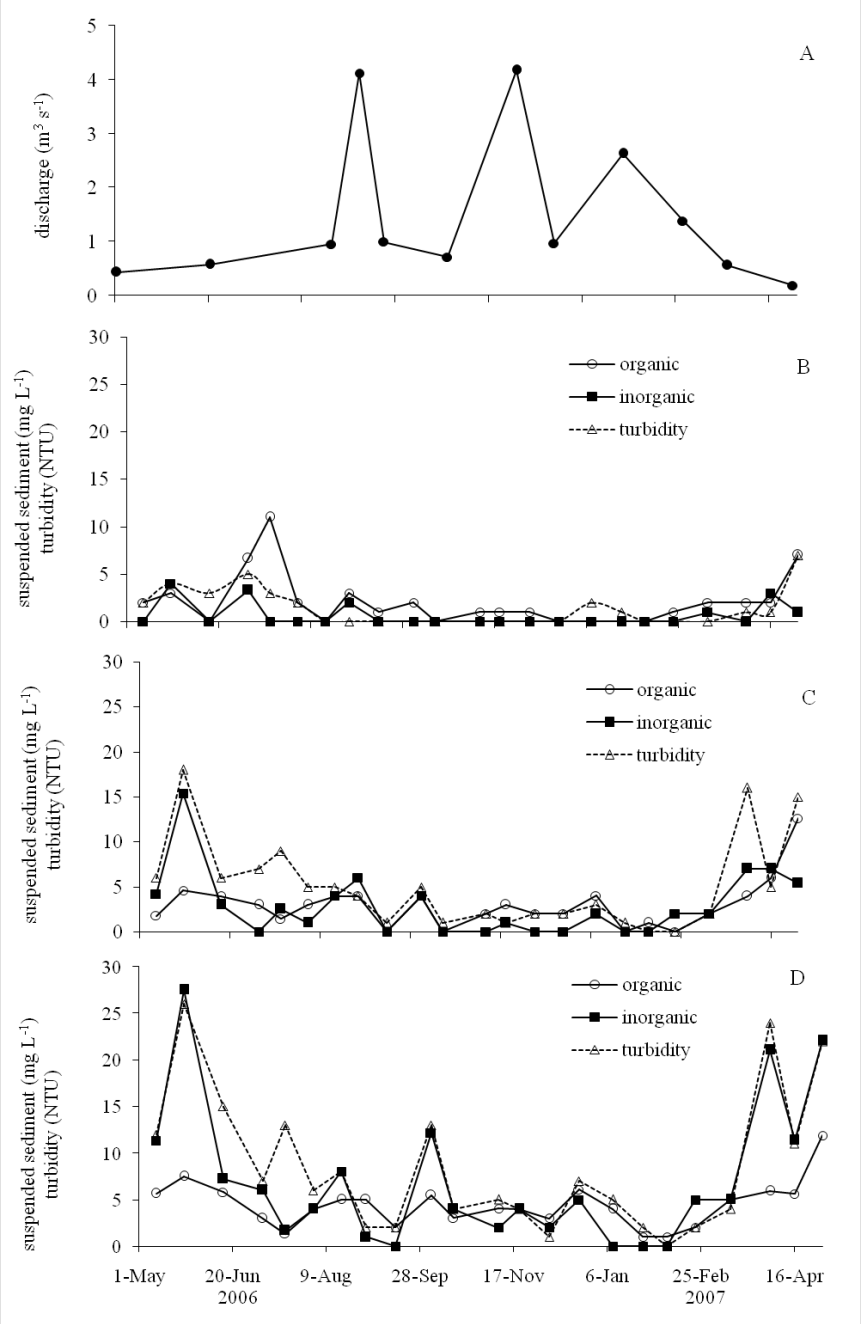

Figure 2.7 Fluvial discharge at the Atidal site (A), organic and inorganic fractions of total suspended matter and turbidity at Upstream (B), Midstream (C), and Downstream (D) from May 2006 to May 2007.

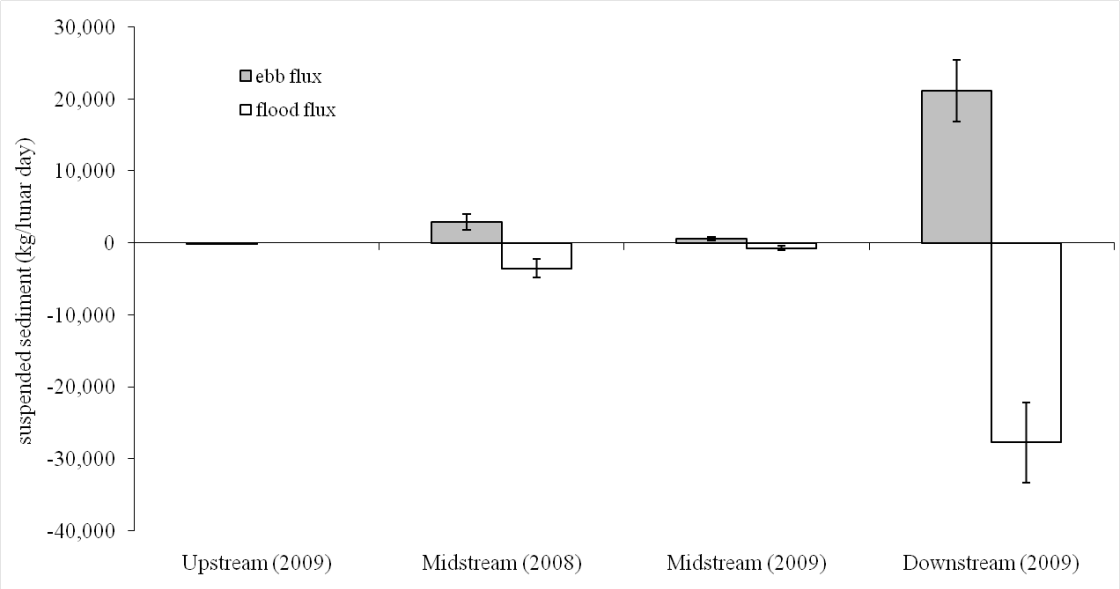

Figure 2.8 Suspended matter flux over tidal days. Error bars represent the 95% confidence interval of the turbidity versus suspended matter regressions.

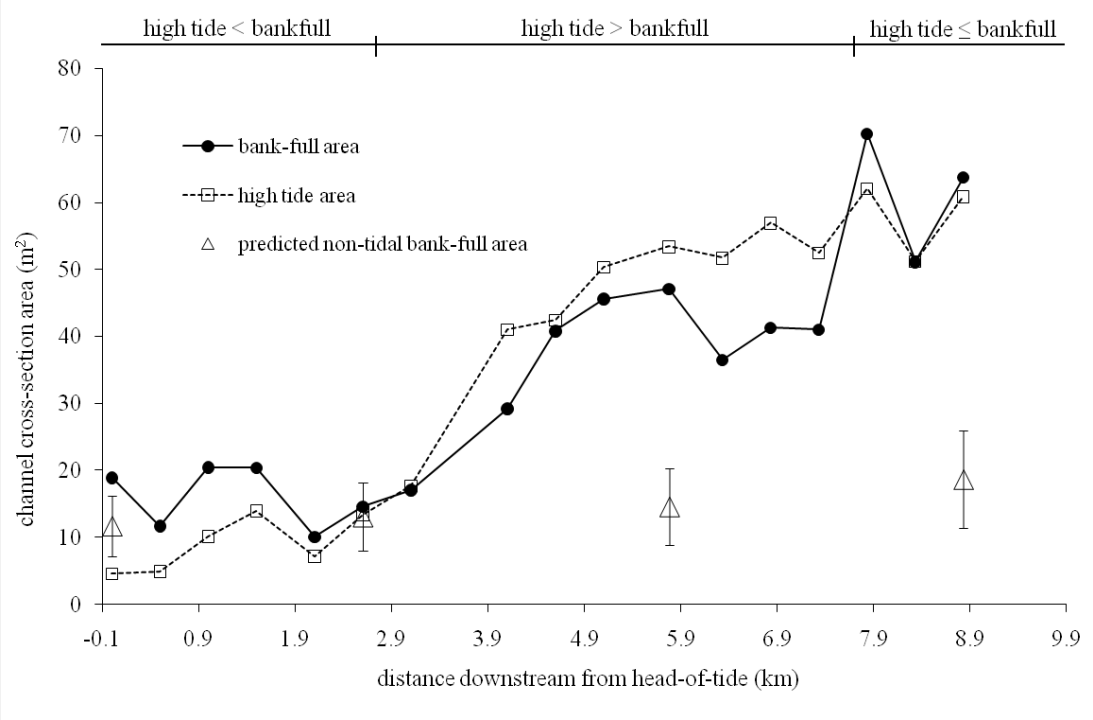

Figure 2.9 Geomorphic characteristics of the tidal Newport River and the predicted channel area from a hydraulic geometry equation developed for coastal plain streams in North Carolina.

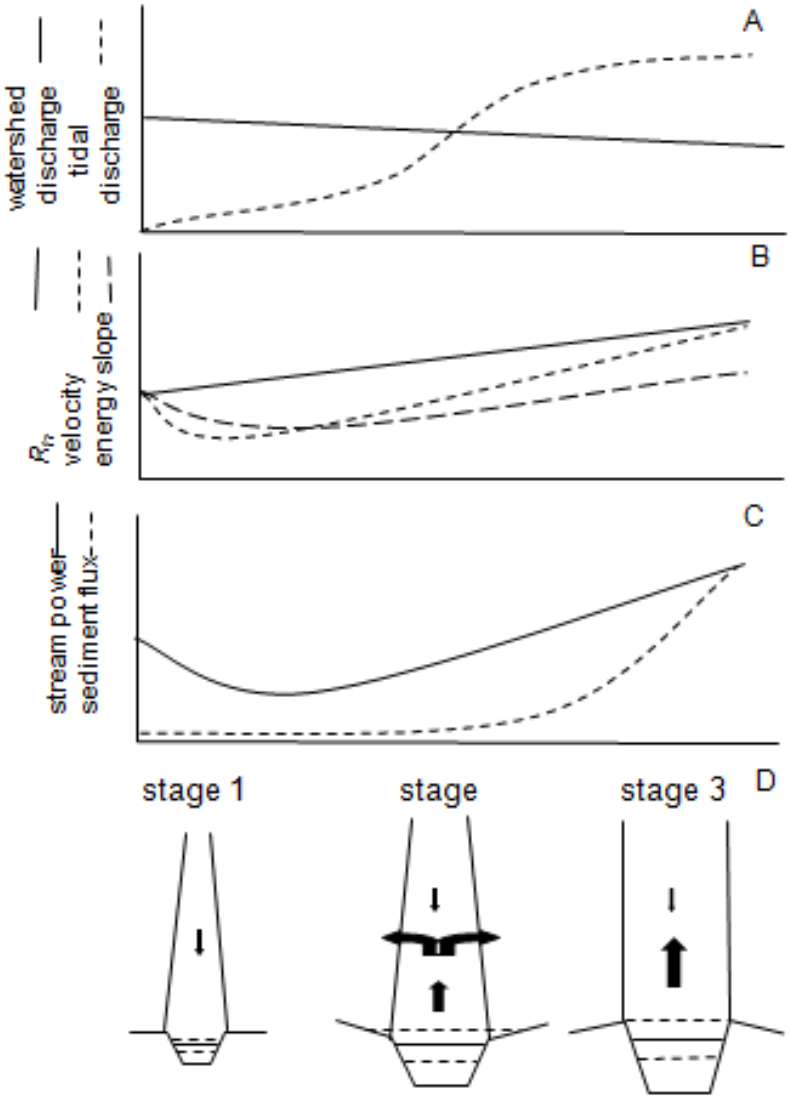

Figure 2.10 Generalized spatial trends (zones 1-3) in watershed (fluvial) and tidal discharge (A), hydraulic radius, velocity, and energy slope (B), and stream power and suspended matter (C). Panel D presents the chronology (stages 1-3) of adjustments in channel area, sediment transport (arrows), and riparian topography at a location over a time as tidal amplitude increases

3. RIPARIAN ZONE DENITRIFICATION AFFECTS NITROGEN FLUX THROUGH A TIDAL FRESHWATER RIVER[1]

3.1 Introduction

Along the hydrologic continuum between streams and oceans lies a unique ecotone where river meets estuary. In this tidal freshwater zone (TFZ) river flow is tidally-influenced but is upstream of saltwater intrusion. This hydrologic variability affects river geomorphology, river discharge, and biogeochemistry, making the TFZ ecologically distinct from non-tidal rivers (Schuchardt et al. 1993). These differences between tidal and non-tidal rivers pose a challenge to watershed-scale biogeochemical research for two reasons. First, measurement of downstream elemental flux in TFZ rivers is obscured by constantly changing discharge over hourly timescales due to varying water level and velocity. Consequently, riverine fluxes of environmentally important elements are commonly measured upstream of the TFZ, thereby omitting a sizable portion of the lower watershed (Destouni et al. 2008). Second, the unique geomorphology and hydrology of the TFZ make it difficult to apply riverine biogeochemical models to this portion of the river continuum. Fundamental information on how TFZ geomorphology and hydrology influence biogeochemical processes is needed to properly include this ecotone in river and watershed elemental budgets.

Nitrogen budgets for watersheds, regions, and the globe are continually being refined due to the importance of this element for biological production and also because

of its role as a pollutant that has caused environmental degradation of freshwater and marine ecosystems (Vitousek et al. 1997; Smith et al. 1999; Green et al. 2004). River networks and associated lakes and reservoirs are highly reactive with respect to nitrogen and remove 53% of their terrestrially-derived nitrogen load prior to reaching the oceans (Wollheim et al. 2008), principally through the microbially-mediated process of denitrification (Seitzinger et al. 2006). However, regional and global models of riverine nitrogen attenuation (See Boyer et al. 2006 and Wollheim et al. 2006 for review) have not accounted for TFZ biogeochemistry differently from the rest of the river network, and it is unknown what affect this may have on model accuracy.

One unique characteristic of the TFZ that may have a large effect on riverine nitrogen flux is their expansive riparian floodplains. Denitrification in floodplain soils can substantially decrease the nitrate concentration of floodwaters and thereby reduce the nitrate load of adjacent rivers (Lindau et al. 1994; Tockner et al. 1999; Forshay and Stanley, 2005). In contrast with non-tidal riparian floodplains where the duration of flooding ranges from 12 to 69 days per year (Tockner et al. 1999; Valett et al. 2005), TFZ floodplains are inundated twice-daily by tidal river flow. During these short duration (<6 hr), high frequency (12-24 hour) flooding events, TFZ floodplains also exchange all of their surface water with the river channel when water level recedes during low tide. These two characteristics of TFZs, high frequency inundation and complete hydrologic connectivity with the river, set these floodplains apart from others along the spectrum of river-floodplain interaction and may optimize conditions for nitrogen removal from TFZ rivers.

The goal of this study was to quantify denitrification flux from the TFZ riparian floodplain of a coastal river. This denitrification flux was compared with the riverine nitrate load to evaluate the potential importance of the floodplain in attenuating this load. We begin by presenting an empirical model that addresses the primary biogeochemical and geomorphic factors affecting floodplain denitrification.

3.1.1. Riparian zone denitrification model

Denitrification flux from TFZ riparian floodplain is a function of three elements: 1) the spatial and temporal extent of inundation, 2) denitrification rate, and 3) the lag time between inundation of the riparian sediments and the onset of denitrification. The first of these elements (the extent and duration of flooding) is a function of water level height and floodplain topography. Water level height, h, above mean sea level at any time, t, of the tidal cycle and location, s, along the TFZ is calculated as:

$$h_{t,s} = a_s \times \sin(\frac{2 \times \pi \times t}{p}) \quad (3.1)$$

were a_s is tidal amplitude specific to a location along the TFZ and p is the tidal period of 12.4 hours. Floodplain topography determines the area inundated at any time (t) and location (s), $A_{t,s}$, such that:

$$A_{t,s} = h_{t,s} \times F_s \quad (3.2)$$

where F_s is a numerical function describing the area inundated at a given water level height for a particular location along the TFZ.

The second element that determines denitrification flux from the TFZ riparian floodplain is the area-specific denitrification rate (mass length^{-2} time^{-1}). The

denitrification flux, N (mass time^{-1}) is the product of the area-specific denitrification rate, R, and the area inundated (A). The final element controlling denitrification is the lag time, L, between the time that water inundates the riparian sediment and the initiation of denitrification. This lag time is due to the preferential use of O_2 over NO_3^- during microbial respiration; denitrification does not begin until O_2 is depleted in sediment porewater. After the lag time L expires, denitrification occurs on the portion of the floodplain that has been inundated for a period of time greater than L. The area of the floodplain in which anaerobic respiration occurs, and subsequent denitrification flux, continue to increase until the receding tide limits the denitrifying area. Assuming that the floodplain is inundated and drained in 6.2 hr (half of the 12.4 hour tidal period), then the period of denitrification (6.2-L) is divided equally between two phases of the flood tide period. The first phase occurs between t_0 of the flood tide and t_1 (t_1=(6.2-L)/2) when denitrification flux increases in proportion to the area inundated for greater than L. The second phase occurs between t_2 (t_2=t_1+L) and 6.2 hr when the denitrification flux is limited by the receding tide. Denitrification flux within a segment of the TFZ floodplain is calculated as:

$$N_s = \int_{t_0}^{t_1} A_{t,s} \times R + \int_{t_2}^{6.2} A_{t,s} \times R \qquad (3.3)$$

where $A_{t,s}$ is calculated at each time step using equation 3.2 with the $h_{t,s}$ and F_s specific for that location. The denitrification flux from the entire TFZ over the 6.2 hr high tide is the summation of all N_s comprising the TFZ. Equation 3.3 incorporates all three of the principal controls on denitrification flux: topography, denitrification rate, and temporal lag in the onset of denitrification after tidal inundation.

This model is relevant to the surficial sediments where denitrification is interrupted by aerobic conditions during low tide. Denitrification in these surficial sediments during inundation directly affects the nitrogen concentration in the overlying floodplain water, and subsequently affects the nitrogen load of the river when this water drains back into the channel. While denitrification occurs in deeper sediment strata of the floodplain where reduced conditions occur continually, the influence of this process requires information on subsurface hydrology that was beyond the scope of this study.

3.1.2. Site description

The Newport River is a third-order blackwater stream in eastern North Carolina, U.S.A. that enters the Atlantic Ocean at Beaufort Inlet (Figure 3.1). The 310 km^2 watershed drains unconsolidated late Cretaceous to Holocene sandy sediments (Phillips, 1997); overall channel gradient from headwaters to estuary is 0.4 m km^{-1}. The 34 km^2 non-tidal upper watershed has predominantly agricultural and silvicultural land use. The TFZ drains an additional 128 km^2 of agricultural and light urban development. The TFZ is characterized by a semi-diurnal tide that propagates 8 km upstream from the oligohaline estuary (Figure 3.1). The meandering, sand-bed channel is bordered by a wide riparian zone consisting of hardwoods (*Taxodium* spp, *Nyssa* spp, *Acer rubrum*, *Pinus* spp). Small pockets of tidal freshwater emergent marsh (*Peltandra virginica*, *Pontederia cordata*) are common along the entire length of the TFZ and grow on the muddy channel margin exposed at low tide. The riparian zone is inundated daily during the two high tides even during periods of low discharge (Figure 3.2). Denitrification measurements were conducted approximately equidistant between the upper and lower

bounds of the TFZ (Figure 3.1). The average annual salinity was 0.07 in the vicinity of denitrification measurements and 0.25 at the downstream boundary of the tidal freshwater zone where the oligohaline river begins.

3.2. Materials and methods

3.2.1. Riparian zone denitrification

Denitrification rate of riparian zone sediments was measured to parameterize *R* in equation 3.3. Sediment cores were collected monthly from 3 intertidal habitats along the TFZ of the Newport River (Figure 3.1). The three sample collection sites were located within 500 m of each other and included a hardwood riparian forest, an emergent freshwater marsh, and an unvegetated mudflat. Triplicate cores from each site were collected in clear polycarbonate tubes (6.4 × 40 cm). The sediment cores and 50 L of river water were returned to a temperature controlled room at the University of North Carolina's Institute of Marine Sciences (UNC-IMS) maintained at the temperature of the river. Next, cores were filled with approximately 350 mL of river water and capped with air-tight lids containing two sampling ports. Cores were pre-incubated for >18 hr prior to gas measurements to allow equilibration of dissolved gases within all materials (Eyre et al. 2002). For samples collected between August and November 2006 cores were incubated with a static volume of overlying water for 6 hours and N_2 was measured in the overlying water every 2 hours (Fear et al. 2005). A linear regression between N_2 concentration and incubation time was used to derive the rate of N_2 production (denitrification) within the core. From December 2006 through August 2007 cores were plumbed to a multi-channel peristaltic pump that circulated river water through the

headspace of the core at a known rate between 1-2 mL min^{-1} (McCarthy et al. 2007). Water samples for dissolved gas analysis were collected in 5 mL glass tubes from the inflow and outflow of the cores.

Dissolved gas analysis was measured using a Balzers Prisma QME 200 quadropole mass spectrometer (Pfeiffer Vacuum, Nashua, NH, USA) coupled to a silicon, gas-permeable, flow-through membrane inlet as described by Kana et al. (1994). The mass spectrometer was tuned to monitor the ratio of N_2:Ar instead of N_2 alone because the N_2:Ar signal is relatively unaffected by oxygen concentrations above 50% saturation (Kana and Weiss 2004; Fear et al. 2005). A continually-mixed water bath containing tap water at 16°C was maintained as an atmospheric gas-saturated standard for calibration of the mass spectrometer, where the [N_2]:[Ar] ratio of this water bath was 37.9266 (Lide 2004). This signal ratio ($(N_2:Ar)_{standard\ signal}$) was used to determine the N_2 concentration of the sample using the following formula:

$$\left[N_2\right]_{sample} = \left(N_2 : Ar\right)_{sample\ signal} \times \frac{37.9266}{\left(N_2 : Ar\right)_{standard\ signal}} \times \left[Ar\right]_{sample} \qquad (3.4)$$

Since Ar is conservative and assumed to maintain a saturated concentration in water, standard gas saturation tables for a range of temperature in freshwater were used to obtain the $[Ar]_{sample}$ at the temperature of the incubation (Lide 2004). The precision of the N_2 concentration measurement was 0.5% and the minimum detectable concentration of N_2 was 183 μM (A. Smyth, personal communication).

Next, the denitrification rate (R, mass N $area^{-1}$ $time^{-1}$) occurring within the sediment core was calculated as:

$$R = 2 \times \left(\left[N_{2\,outflow}\right] - \left[N_{2\,inflow}\right]\right) \times \frac{q}{c} \qquad (3.5)$$

where [$N_{2\ outflow}$] and [$N_{2\ inflow}$] are the [N_2] measured leaving and entering the core, respectively, q is the flow rate through the head space of the core, and c is the surface area of the core. Differences between sites during each experiment and overall during the period of study were examined using an ANOVA and Tukey post-hoc analysis ($p<0.05$) with SPSS software (SPSS, Inc., Chicago, IL).

Calculation of denitrification from N_2 fluxes within sediment cores has a number of advantages over the more commonly used acetylene block method (Cornwell et al. 1999; Groffman et al. 2006). Most importantly, direct measurement of N_2 fluxes using a mass spectrometer does not interfere with coupled nitrification-denitrification as the acetylene block method does, thereby making denitrification rate measurements derived from N_2 fluxes more accurate. The resultant denitrification rates thus reflect both the benthic mineralization-nitrification-denitrification pathway and the denitrification of nitrate from the water column, but our methodology did not allow us to resolve the proportion of the total denitrification occurring by these pathways.

One drawback of the laboratory-based sediment core incubations performed in this study is that they reflect denitrification rates occurring when sediments are continually saturated and the sediment porewater O_2 has been depleted. In order to extrapolate the laboratory denitrification rates across the TFZ using equation 3.3, it was necessary to determine the lag time between inundation and the onset of denitrifying conditions. A combination of in-situ and laboratory measurements of oxidation-reduction potential (an indicator of O_2 availability and hence propensity of a sediment bacteria to denitrify NO_3^-) were performed to measure this lag time.

3.2.2. Riparian zone oxidation-reduction potential

Oxidation-reduction potential was measured as a proxy for O_2 concentration within surficial sediments where denitrification of water-column NO_3^- could occur. Oxidation-reduction potential of 300 mV was considered the threshold below which O_2 concentration would be low enough for facultative aerobic bacteria to use preferentially use NO_3^- instead of O_2 in the oxidation of organic matter (Faulkner and Patrick, 1992). In-situ measurements of oxidation-reduction potential in the TFZ riparian floodplain were conducted during winter (7 February to 7 March 2007) and summer (27 July to 13 August 2007) to measure the fluctuation between oxidized (>300 mV) and reduced (<300 mV) conditions.

In-situ oxidation-reduction measurements were made during February and August 2007 at the TFZ riparian location where denitrification cores were collected. Platinum tipped probes (purchased from Dr. Wayne Hudnall at Texas Tech University) were deployed from a 17 m wooden boardwalk constructed perpendicular to the river. Two oxidation-reduction potential probes (5 and 10 cm below the sediment/water interface) and one soil moisture probe (5 cm deep) were deployed at 2 m, 10 m, and 17 m from the low tide channel margin. Sensor depths and distances from the channel were chosen based upon observations reported in other TFZs (Kerner et al. 1990; Seybold et al. 2002). To minimize soil disturbance during deployment, a 15 cm deep hole was dug, oxidation-reduction potential and soil moisture probes were inserted laterally into the wall of the hole, and the hole was back-filled with the excavated soil.

Oxidation reduction robes were wired to a Campbell Scientific CR1000 data logger and measurements were recorded every 5 minutes. A Ag/AgCl reference

electrode (Accumet 13-620-53) was connected to the sediment using a salt bridge (2 cm diameter PVC pipe filled with a gelled solution of agar and KCl) to provide an electrical ground for the oxidation-reduction potential measurements. Measured oxidation-reduction potential values were converted to Eh by adding 200 mV (per manufacturer's instructions); no temperature or pH corrections were made. Electrode calibration was verified by measuring a 220 mV oxidation-reduction potential solution: following the February deployment all probes read 220±10 mV. Prior to and following the August deployments all probes read 261±1 mV and 263±2 mV, respectively. While the maximum stabilization period allowed by the data logger was used for voltage measurements (3000 ms), it may not have been long enough to allow the voltage to stabilize in strongly reduced sediments (0-200 mV) (van Bochove et al. 2002). Values in this range may be an underestimate of oxidation reduction potential by up to 140 mV (van Bochove et al. 2002).

Soil moisture was measured as an indicator of the tidal inundation of the sediment that could be compared against the oxidation-reduction potential data. Furthermore, soil moisture indicates the propensity for denitrification to occur and the extent of nitrate reduction (N_20 versus N_2) (Machefert and Dise 2004). Soil moisture probes (model CS616, Campbell Scientific, Incorporated, Logan, UT, USA) were calibrated according to the manufacturer's instructions and installed at 5 cm depth at each of the three distances from the river channel. Probes were wired to the data logger and volumetric soil moisture was recorded every 5 minutes.

3.2.3. Laboratory oxidation-reduction potential experiments

As a compliment to the in-situ measurements described above, a laboratory experiment was conducted in January 2008 to assess the time required for oxidized (drained) sediments to become reduced after inundation (lag time parameter, *L*, in equation 3.3). The experimental design was based on the observation from in-situ monitoring that large oxidation-reduction potential fluctuation only occurred within the upper 5 cm of the sediment profile. Accordingly, soil cores 6 cm in depth were collected from the boardwalk described above and returned to the UNC-IMS. Oxidation-reduction potential probes were inserted into the cores through holes at 1, 2, 3, and 5 cm, while a second hole at each depth allowed lateral water infiltration. Oxidation-reduction potential was measured and logged as described for the in-situ measurements. In a series of experiments, the instrumented sediment cores were incubated at 10 and 25 ^{o}C in a temperature controlled room and were initially allowed to drain until a constant oxidation-reduction potential condition was observed. Cores were then submerged in river water equilibrated to the temperature of the experiment and the time required for oxidation-reduction potential to drop below 300 mV (reducing conditions amenable for denitrification; Faulkner and Patrick 1992) was measured.

3.2.4. Channel bathymetry and riparian zone topography

Channel width and cross-section area were measured from a boat along the TFZ during high tide at 28 locations. These surveys only spanned the channel between vegetated banks, so digital elevation data was used to develop a topographic surface of the riparian zone beyond the banks of the channel. Topographic Light Image Detection and Ranging (LIDAR) data were obtained for the Newport River watershed from the

North Carolina Floodplain Mapping Agency (www.ncfloodmaps.com). These elevation data have a vertical root mean square error of 20 cm and the NAVD 88 vertical datum on which the data are based is 9 cm below mean sea level for the Newport River (as determined using Vdatum software, http://vdatum.noaa.gov/). ArcGIS (ESRI, Redlands, CA, USA) software was used to construct a triangulated irregular network (TIN) from the LIDAR data within 50 m of the river channel (tributaries were not included in this analysis). A zero elevation hard break line was forced along the river channel to represent the river surface at mean sea level and a soft break line was enforced at 50 m from the channel. The surface area of this TIN at 0.03 m intervals between mean sea level and 0.45 m in elevation was calculated for 9, 1 km reaches of the TFZ using ArcGIS.

The change in inundated surface area with elevation above mean sea level (F_s, equation 3.2) was represented by fitting a polynomial regression to the modeled points for each river reach; r^2 values for all regressions were >0.999. This topographic model was used to generate a relationship between water level height ($h_{t,s}$, equation 3.1) and the area ($A_{t,s}$, equation 3.2) of floodplain inundated within 50 m of the river channel. Inundation may occur beyond 50 m, but we choose this conservative boundary for two reasons. First, lateral flow velocity of water from the channel into the riparian zone will limit the extent of inundation, but was not measured in this study. Second, we wanted to minimize consideration of ponds in the outer floodplain that would not be expected to exchange water with the river channel.

3.2.5. Tidal freshwater river nitrogen load

Nitrate, ammonium, and total nitrogen concentration were measured twice-monthly from river water collected during the ebb tide in the upper TFZ (Figure 3.1). Water samples were filtered through a 2.7 mm glass fiber filter and frozen until analyzed on a Lachat QuikChem 8000 autoanalyzer with method detection limits of 0.6 mg L-1, 2.55 mg L-1, and 35.4 mg L-1 for nitrate, ammonium, and total nitrogen, respectively (Lachat Instruments, Milwaukee, WI, USA) at the UNC-IMS. Total nitrogen was measured as nitrate after in-line alkaline-persulfate and ultra-violet oxidiation. River discharge was measured monthly 100 m upstream of the TFZ using a Sontek handheld acoustic doppler velocimeter (SonTek/YSI, San Diego, CA, USA) to measure velocity at 1 m intervals across the channel. An area-specific discharge was calculated for the watershed at this non-tidal location and used to estimate discharge downstream at the location where river nitrogen was measured (Leopold et al. 1964). River nitrogen load in the upper TFZ was calculated as the product of discharge and river water nitrogen concentration measured on the date closest to when discharge was measured.

3.2.6. Riparian zone denitrification model

The total denitrification flux of nitrogen from the riparian TFZ (kg N day^{-1}) was calculated using equation 3.3 on a monthly basis, resulting in 11 estimates of denitrification flux over the year of study. For each month, the average denitrification rate of the three intertidal habitats was used to extrapolate across the entire TFZ riparian area. Equation 3.3 was implemented at a 0.1 hr time step for each of the 9 reaches of the TFZ using water level height-inundated area relationships (F_s) specific to that reach. Denitrification flux (N_s, equation 3.3) over the 6.2 hr period was numerically integrated

for each reach, and N_s for all 9 reaches was summed to obtain N for the entire TFZ. These flux estimates only account for denitrification occurring above mean sea level and therefore do not include denitrification occurring in the portion of the channel inundated continuously throughout the tidal cycle.

3.3. Results

3.3.1. Riparian zone denitrification

Denitrification rates ranged from 233 μg m^{-2} hr^{-1} (mud flat in September 2006) to 4418 μg m^{-2} hr^{-1} (riparian forest in October 2006) (Table 3.1). There was a significant difference (p<0.05) between habitat types during September and October 2006, with rates from the forest higher than rates at the mudflat; no other significant differences were found between habitats during the same month. Denitrification over the 11 months of study averaged 2018 μg m^{-2} hr^{-1}, 1832 μg m^{-2} hr^{-1}, and 1956 μg m^{-2} hr^{-1} at the forest, marsh, and mud flat, respectively, and these differences were not statistically significant ($F_{2,30}$=0.057, p=0.944) (Table 3.1). No significant difference was found between the monthly averages of the three habitats over the year of study ($F_{10,22}$=2.21, p=0.058).

Ambient water temperatures and subsequent incubation temperatures of denitrification experiments ranged from 9.7 to 25.5 ^{o}C (Table 3.2). The ranges in dissolved nitrogen concentrations were 93-450 μg N-NO_3^- L^{-1}, 12-58 μg N-NH_4^+ L^{-1}, and 140-982 μg N-dissolved organic L^{-1} (Table 2). Organic matter in the top 5 cm of sediment of incubated cores was highest in the forest (19%), followed by the marsh (11%), and mudflat (10%) (Table 3.2).

3.3.2. Riparian zone oxidation-reduction potential

The channel bank (2 m from the low tide channel) during winter had dramatic oxidation-reduction potential fluctuations at 5 cm soil depth between oxidized (>300 mV) and reduced (<300 mV) conditions that were inversely related to changes in soil moisture (Figure 3.3A). During 25 Feb through 2 Mar, reduction of sediments from an oxidized condition to <300 mV required 4 hr 40 min. Sediments at 10 cm depth were continually reduced and showed little fluctuation during winter. Oxidation-reduction potential decreased with distance from the channel during winter and oxidation-reduction potential values at 5 and 10 cm were similar to one another (Figure 3.4A and 3.5A). At 10 m from the channel, oxidation-reduction potential at both 5 and 10 cm showed small semi-diurnal fluctuations that were inversely related to soil moisture fluctuations (Figure 3.4A). This pattern was dampened even further at 17 m from the channel except during the final 4 days of this period when a rain event on 1-3 March coincided with rapid semi-diurnal changes in oxidation-reduction potential at 5 cm (Figure 3.5A).

Oxidation-reduction potential was generally lower in summer than winter. Nearest the channel, oxidation-reduction potential at 5 cm fell rapidly following rain events on 30-31 July and 2 August (Figure 3.3B). These upper sediments remained highly reduced (<0 mV) except during 3 instances of low soil moisture when oxidation-reduction potential temporarily spiked to ~150 mV. Sediments at 10 cm during summer fell from ~200 mV to ~ -50 mV following rain events on 2 and 6 August (Figure 3.3B). Oxidation-reduction potential 10 m from the low tide channel decreased over time, with significant changes coinciding with rain events on 30-31 July and 2 August (Figure 3.4B). The 2 August rain event corresponded with a large decrease in oxidation-

reduction potential at the site farthest from the channel (Figure 3.5B). By the end of August both riparian sites showed similar oxidation-reduction potential conditions without large vertical gradients (Figure 3.4B and 3.5B). Given the highly reduced conditions during August, the oxidation-reduction potential measurements may under-represent true conditions (van Bochove et al. 2002). However, since values were mostly below 150 mV, under-estimation by 140 mV would not interfere with the detection of oxidized (>300 mV) to reduced (<300 mV) fluctuations.

Volumetric soil moisture was generally higher during winter than summer and showed a semi-diurnal pattern at all sites and seasons that reflected the tidal influence (Figures 3.3, 3.4, and 3.5). Soil moisture changed by <1% v/v over a tidal cycle at all sites and seasons, indicating that the soils were poorly drained during low tide. Rain events were not reflected in the soil moisture data presumably because the soils maintained a near-saturated condition continuously due to tidal inundation. Throughout the study period volumetric soil moisture was >50%, corresponding with the highest denitrification rates in a wide variety of ecosystems and the maximum N_2 versus N_20 production (Machefert and Dise 2004).

3.3.3. Laboratory oxidation-reduction potential experiments

Manipulation of water level in sediment cores in the laboratory revealed time lags between oxidized and reduced conditions consistent with those observed in-situ. The laboratory experiment conducted at 10 ^oC did not show a dramatic response in oxidation-reduction at 1-2 cm in depth. However, at 3 cm, the sediment took 4 hours and 40 min to become reduced from an oxidized condition (Figure 3.6A). This lag period between

inundation and denitrifying conditions is the same as that observed in-situ during 25 Feb-2 Mar (Figure 3.3A). At 25 ^{o}C, 5 hr 10 min was required for the sediments at 1 cm to become reduced from a fully oxidized condition; sediments below that depth were never fully oxidized (Figure 3.6B). Given the agreement between field and laboratory measurements in lag time of 4 hr 40 min, this value was used to parameterize *L* in equation 3.3.

3.3.4. Channel bathymetry and riparian zone topography

The aerial extent of the TFZ river channel at low tide was 149,360 m^2, while the maximum inundated area at high tide was 426,627 m^2. The surface area of riparian floodplain inundated during the flood tide was greatest in the middle and upper portion of the TFZ, between 3 and 7 kilometers from the oligohaline estuary (Figure 3.7, 3.8A).

3.3.5. Tidal freshwater river nitrogen load

In the upper TFZ, low river discharges <1 $m^3 s^{-1}$ occurred during April—June of 2006 and 2007; peak discharges of 4.8 $m^3 s^{-1}$ occurred in September 2006 following Hurricane Ernesto and 4.9 $m^3 s^{-1}$ in December 2006 (Figure 3.9). Nitrate, ammonium, and organic nitrogen in the upper portion of the TFZ averaged 53 μg L^{-1}, 46 μg L^{-1}, and 399 μg L^{-1}, respectively during the study period (Figure 9). Average nitrate concentration in the middle TFZ where denitrification rates were measured (see Figure 3.1) was 203 μg L^{-1} (Table 3.1), 4-fold higher than the average in the upper TFZ (53 μg L^{-1}). A sewage treatment plant outfall near the study site may be partly responsible for the increased nitrate concentration; total nitrogen load from the treatment plant was

similar to the riverine total nitrogen load during low flow periods (Ensign, unpublished data).

3.3.6. Riparian zone denitrification model

Denitrification flux was greatest in this middle and upper portion of the TFZ where inundated area was greatest (Figure 3.8B is representative of the trend in denitrification over time and space, although the magnitude of this flux changed from month to month). The peaked pattern shown in Figure 3.8B is a consequence of the lag time (4.6 hr) implemented in equation 3.3, the increase in wetted surface after this lag time, and the subsequent decrease in wetted surface area and denitrification as the water level receded. Denitrification flux from the TFZ riparian area ranged from 0.200 kg N per lunar day (24.8 hr) in August 2007 to 0.589 kg N per lunar day in October 2006 (Table 3.3). As a proportion of the daily riverine nitrate load entering the upper portion of the TFZ, these denitrification fluxes ranged from 2% in September 2006 to 262% in May 2007 (Table 3.3). The high removal capacity predicted in May 2007 was a result of extremely low river discharge and thus low riverine nitrogen load (Figure 3.9).

3.4. Discussion

Semi-diurnal changes in water level in a tidal freshwater river in coastal North Carolina resulted in a 3-fold expansion in riverine surface area from low tide to high tide. Denitrification within three intertidal habitats of the river's riparian zone occurred at similar rates, which varied 3-fold over an annual period. The onset of denitrification in surficial sediments occurred 4-5 hr after inundation by the flood tide. Denitrification flux

from the floodplain was estimated to constitute between 2% and 15% of the daily in-channel riverine nitrate load during most of the year, and >100% during periods of low river discharge. Since these floodplains are inundated twice daily by river water from the channel, they are unique relative to non-tidal floodplains that flood only seasonally. This regularly occurring, direct hydrologic exchange between river channel and floodplain results in a continuous, year-round loss of nitrogen from the tidal freshwater portion of this coastal river.

3.4.1. Denitrification and redox dynamics in tidal freshwater river floodplains

The current study is the first to quantify the effect of denitrification occurring across an entire tidal freshwater riparian zone on the nitrogen budget of a tidal freshwater river. Most previous research on TFZ environments has been done on nitrogen cycling within emergent freshwater marshes. For example, the annual net flux of nitrate to the riparian zone of a Massachusetts coastal river was 5% of riverine load, although the portion of this flux that was denitrified was not well constrained in the budget (Bowden et al. 1991). A TFZ marsh in Virginia was also an annual net sink for riverine nitrate where denitrification (42%) and burial (52%) accounted for permanent nitrogen loss; however, the net affect of this on riverine load was not calculated (Neubauer et al. 2005). Other TFZ studies have carefully analyzed nitrogen uptake and transformations within a TFZ marsh, but did not assess denitrification (Gribsholt et al. 2005; Gribsholt et al. 2006; Gribsholt et al. 2007). Our intention was not to disregard the complexity of nitrogen transformations documented in these earlier studies, but to focus on the net effect of the TFZ on nitrogen cycling within the river continuum.

The denitrification rates measured in the Newport River TFZ are similar to those reported in a Virginia TFZ marsh (Neubauer et al. 2005), slightly higher than those reported in some European TFZ floodplain environments (Verhoeven et al. 2001), but lower than those reported in a Belgium TFZ marsh (Gribsholt et al. 2006). Floodplains can have high spatial and temporal heterogeneity in denitrification rates (Orr et al. 2007) as a result of variable soil characteristics and geomorphology (Pinay et al. 1995; Pinay et al. 2000), soil moisture (Machefert and Dise 2004; Pinay et al. 2007), temperature, and nitrate concentration (Pinay et al. 2007). Rates in this study were usually similar between habitats due to the identical water column nitrate concentration and incubation temperature during experiments. The two occasions during which rates were significantly higher in the forest than the mudflat (September and October 2006) could have been due to higher organic matter in the forest site. Relative to non-tidal floodplains, tidal freshwater floodplains may have relatively homogenous denitrification rates as a result of similar soils, soil moisture regimes, and flooding.

Oxidation-reduction potential was used as an indicator of when denitrification would likely occur in the tidal freshwater riparian zone. In-situ measurements showed that the upper 5 cm of sediment was predominantly oxic during winter along the channel edge, likely due to cooler temperatures than summer. Sites farther from the channel never showed oxidized conditions during winter or summer, perhaps due to low topographic relief and subsequently slow local groundwater movement. Laboratory experiments examined finer-scale responses within the upper 5 cm of sediment, showing that between 4.3 and 5.2 hr were required for the oxic-to-reduced transition. Contrary to expectations, this longer transition period occurred at 10^{o}C instead of 25^{o}C. We expected

temperature would decrease this lag time for two reasons. First, higher metabolism at higher temperature would increase the rate at which sediments become reduced. Second, higher temperature should lower the peak sediment porewater oxygen concentration attained after flooding and facilitate a faster reduction period.

With respect to the oxidation-reduction dynamics considered in our model, we assumed that exposed surficial sediments in this active zone equilibrated to 350 mV as indicated by our in-situ monitoring (Figure 3.4A), laboratory based oxidation-reduction potential experiments (Figure 3.7), and other studies (Kerner et al. 1990). Other sediment types may achieve a higher oxidation-reduction potential during exposure to air, thereby increasing the lag time (*L*, equation 3.3) prior to the onset of denitrification. For example, the lag period of 7 days was reported for a Mississippi wetland (Lindau et al. 1994). Longer lag time would decrease the denitrification flux from the TFZ floodplain, while shorter lag time would increase denitrification flux.

3.4.2. Uncertainties, future development, and application of the floodplain denitrification model

There are several uncertainties in our parameterization of the denitrification model which may have resulted in either under- or over-estimating denitrification. Our model estimates may be under-estimates of denitrification flux for three reasons. First, nitrification occurs during the oxidized phase of the tidal cycle as found in other TFZ studies (Gribsholt et al. 2006), and this nitrate is subsequently denitrified when sediments are inundated. While our denitrification measurements included coupled nitrification-denitrification occurring in the cores, our experimental approach did not replicate the pulse of nitrate that occurs under field conditions during low tide. This additional nitrate

would increase the denitrification rate and consequently the N_2 flux from the riparian zone. Second, the inundated riparian zone may be wider than the 50 m width we accounted for with the digital topographic model. Third, the lag time that was implemented in the model was based upon oxidation-reduction measurements in the upper 5 cm of sediment, although oxidation-reduction data suggest denitrification occurred in deeper sediments, as well. Since the intention of the model was to estimate nitrate removal from the overlying water column, we focused on the upper 5 cm of the sediment profile whose oxidation-reduction potential responded quickest following inundation. Consideration of denitrification occurring in the continuously reduced sediments below 5 cm would increase the expected nitrate removal in the TFZ floodplain, but we do not currently have data on riparian groundwater dynamics to evaluate this process. Lastly, the model may have over-estimated denitrification in the TFZ since the denitrification rates used for extrapolation were based on water column nitrate concentrations that were higher than elsewhere along the river; lower water column nitrate concentrations would result in lower denitrification rates (Garcia-Ruiz et al. 1998).

Future development of our model would involve research to address the uncertainties identified above and implementation of more spatially-explicit information from the riparian zone. First, spatial delineation of the floodplain into habitat types would allow explicit consideration of denitrification rates and oxidation-reduction dynamics within habitats in the proportion and configuration that they occur across the floodplain. Second, data on the relationship between river discharge and the extent of overbank flooding in the TFZ would improve estimates of inundated area during seasonal cycles of discharge regime.

The denitrification flux modeling framework presented here can be widely applied to generate estimates of nitrogen loss from coastal rivers worldwide. This exercise would serve two purposes. First, it would provide data on nitrogen attenuation rates along a missing link in the river continuum which is not currently accounted for in river network nitrogen models (see comparison of riparian versus in-channel denitrification below). Second, it would enable analysis of the effects of floodplain topography and river geomorphology on nitrogen dynamics in rivers. The current model could be useful in addressing many critical questions regarding nitrogen flux through tidal freshwater rivers, such as: Does inundated surface area (and subsequent denitrification flux) scale proportionally to river size? What is the relative importance of denitrification rate versus floodplain area in affecting riverine nitrogen loads? The denitrification model presented here provides a tool to efficiently pursue these questions and advance our understanding nitrogen flux through tidal freshwater rivers.

3.4.3. How does riparian denitrification compare to in-channel denitrification?

Nitrogen uptake within river networks does not normally include riparian zone processes since over-bank flooding in non-tidal rivers is a periodic event on annual time-scales. The current study indicates that exclusion of riparian zone denitrification in a riverine nitrogen uptake model of the Newport River would underestimate nitrate uptake, but to what extent? As a first approximation, an empirical model of river nitrogen attenuation (Wollheim et al. 2006; Wollheim et al. 2008) can be applied to the TFZ of the Newport River. This model predicts that benthic in-channel denitrification occurring throughout the tidal cycle removed 4-94% of the daily riverine nitrate load over the

course of this study (Table 3.3). Our estimates of riparian zone denitrification ranged from 27% to 278% of this in-channel denitrification, reflecting the importance of the riparian zone to overall nitrogen attenuation. On average, calculation of riverine nitrate attenuation without consideration for riparian denitrification would under-estimate nitrate attenuation in the TFZ by 38%.

Future efforts to model river network nitrogen attenuation can be improved by consideration of the additional nitrogen attenuation that occurs in the TFZ of coastal rivers, and the model presented here may provide a starting point for this research. Ultimately, the goal of this research should be the development of generalized empirical relationships between tidal freshwater river geomorphology and nitrogen attenuation similar to those developed for non-tidal rivers (see footnote of Table 3.3 for discussion of existing methodology). These data will fill a missing biogeochemical link along the riverine continuum and lead to improved accuracy of nitrogen budgets at the regional and global scale.

Table 3.1 Nitrogen generation (μg N m^{-2} hr^{-1}) from intertidal sediments in three riparian habitats of the Newport River, NC; values are mean ± 1 standard deviation. Letters indicate homogenous subsets of treatments during each month found to differ by ANOVA and Tukey post-hoc analysis ($p<0.05$).

Date	Forest	Vegetated wetland	Mud flat	Habitat average
31 Aug 2006	-	1669 ± 1592	2731 ± 552	2200 ± 751
14 Sep 2006	1535 ± 588^{A}	1428 ± 210^{AB}	233 ± 359^{C}	1065 ± 722
24 Oct 2006	4418 ± 45^{A}	3250 ± 1267^{AB}	1626 ± 525^{C}	3098 ± 1402
21 Nov 2006	4177 ± 1952	2517 ± 420	1796 ± 608	2830 ± 1221
14 Dec 2006	675 ± 645	957 ± 743	2108 ± 526	1247 ± 759
18 Jan 2007	1226 ± 159	2261 ± 1040	2925 ± 629	2137 ± 857
14 Feb 2007	883 ± 1464	2006 ± 1503	3753 ± 533	2214 ± 1446
7 Mar 2007	1750 ± 292	1508 ± 323	1315 ± 134	1524 ± 218
16 May 2007	1998 ± 1232	732 ± 473	1310 ± 199	1347 ± 634
31 Jun 2007	2784 ± 977	2806 ± 1156	2683 ± 1415	2758 ± 65
8 Aug 2007	735 ± 566	1379 ± 285	1039 ± 208	1051 ± 322
annual average	2018 ± 1361	1865 ± 781	1956 ± 1005	-

Table 3.2 Water column nitrogen concentrations and sediment organic matter composition during denitrification experiments.

Date	Habitat	Temperature (^oC)	NO_3 ($\mu g\ N\ L^{-1}$)	NH_4 ($\mu g\ N\ L^{-1}$)	Organic N ($\mu g\ N\ L^{-1}$)	% organic matter
31 Aug 2006	marsh	25.0	369	45	140	10.8
	mudflat					10.8
	forest					no data
14 Sep 2006	marsh	22.0	93	37	no data	8.7
	mudflat					7.7
	forest					14.3
24 Oct 2006	marsh	15.5	220	21	no data	8.1
	mudflat					6.7
	forest					15.9
21 Nov 2006	marsh	14.0	178	30	982	no data
	mudflat					no data
	forest					no data
14 Dec 2006	marsh	9.7	175	28	348	14.9
	mudflat					9.8
	forest					19.8
18 Jan 2007	marsh	12.2	124	24	323	17.9
	mudflat					21.1
	forest					25.9
14 Feb 2007	marsh	10.0	144	58	318	10.6
	mudflat					10.4
	forest					32.4
7 Mar 2007	marsh	11.9	450	23	326	12.9
	mudflat					4.1
	forest					8.0
16 May 2007	marsh	19.8	161	12	424	7.0
	mudflat					8.6
	forest					15.4
31 Jun 2007	marsh	25.5	294	19	415	8.2
	mudflat					11.9
	forest					24.1
8 Aug 2007	marsh	28.0	29	21	558	7.1
	mudflat					9.2
	forest					28.5

Table 3.3 Nitrate loads, denitrification flux, and nitrate removal in the TFZ Newport River, N.C. Nitrate loads were calculated from discharge and concentration in the upper TFZ. A lunar day lasts 24.8 hr.

riverine nitrate load		riparian denitrification flux		proportion of riverine nitrate denitrified in riparian zone	proportion of riverine nitrate denitrified in-channel[1]
date	kg lunar day^{-1}	date	kg lunar day^{-1}	%	%
25 Aug 2006	7.706	31 Aug 2006	0.418	5	13
9 Sep 2006	15.024	14 Sep 2006	0.203	2	8
22 Sep 2006	3.613				
26 Oct 2006	3.969	24 Oct 2006	0.589	15	21
2 Dec 2006	10.734	21 Nov 2006	0.538	5	4
22 Dec 2006	4.053	14 Dec 2006	0.237	6	19
28 Jan 2007	11.436	18 Jan 2007	0.406	4	7
1 Mar 2007	7.435	14 Feb 2007	0.421	6	9
		7 Mar 2007	0.290	4	12
29 Apr 2007	0.098	16 May 2007	0.256	262	94
no data	no data	30 Jun 2007	0.524	no data	no data
no data	no data	8 Aug 2007	0.200	no data	no data

[1]The proportion of riverine nitrate load denitrified in-channel (R) was estimated as: R=1-exp(V_f/H_L), where H_L=discharge/(channel width × reach length) (Wollheim et al. 2006). Channel width was assumed to be 16 m and reach length was 8000 m. The denitrification mass transfer coefficient, V_f, was estimated from river NO_3^- concentration using the formula $V_f = -0.493 \times \log[NO_3^-] - 2.975$ (Mulholland et al. 2008). V_f values ranged from 1.2×10^{-4} to 4.8×10^{-4} cm s^{-1}.

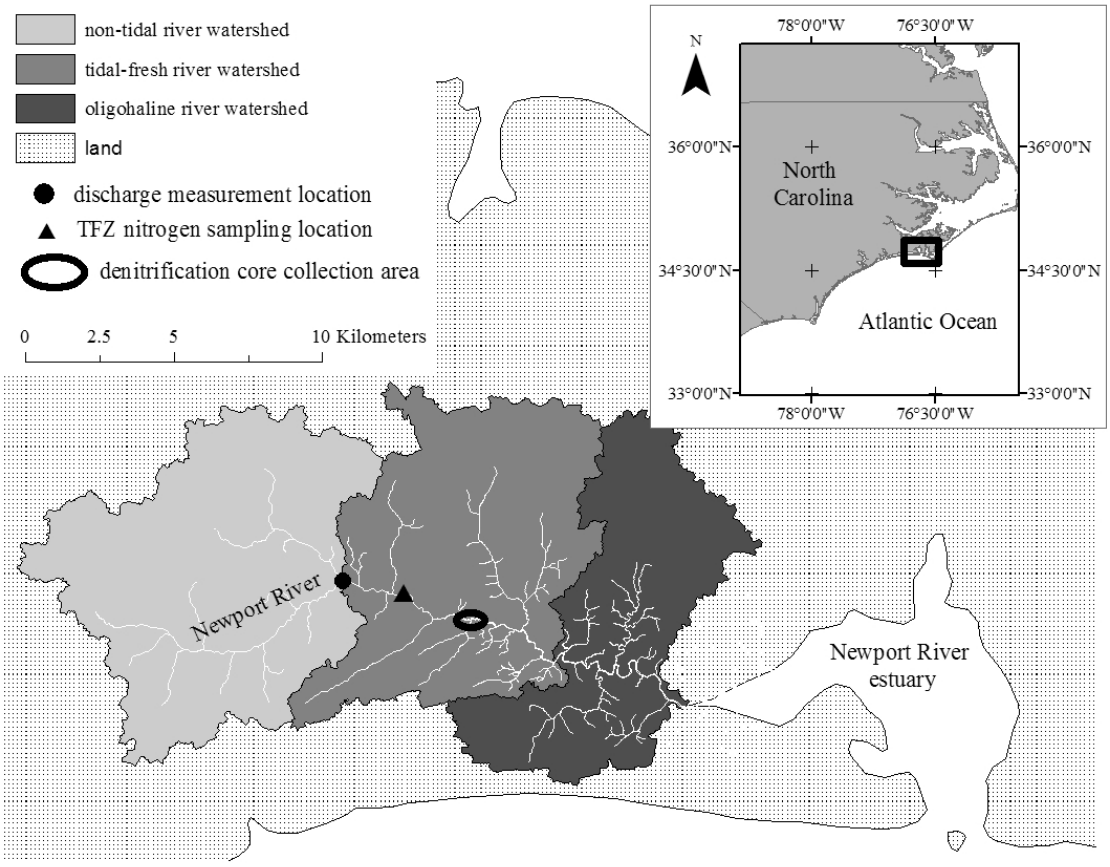

Figure 3.1 Map of the Newport River watershed delineating the drainage areas of the non-tidal river, tidal freshwater river, and oligohaline estuary. Inset map shows the location of the Newport River in eastern North Carolina, USA.

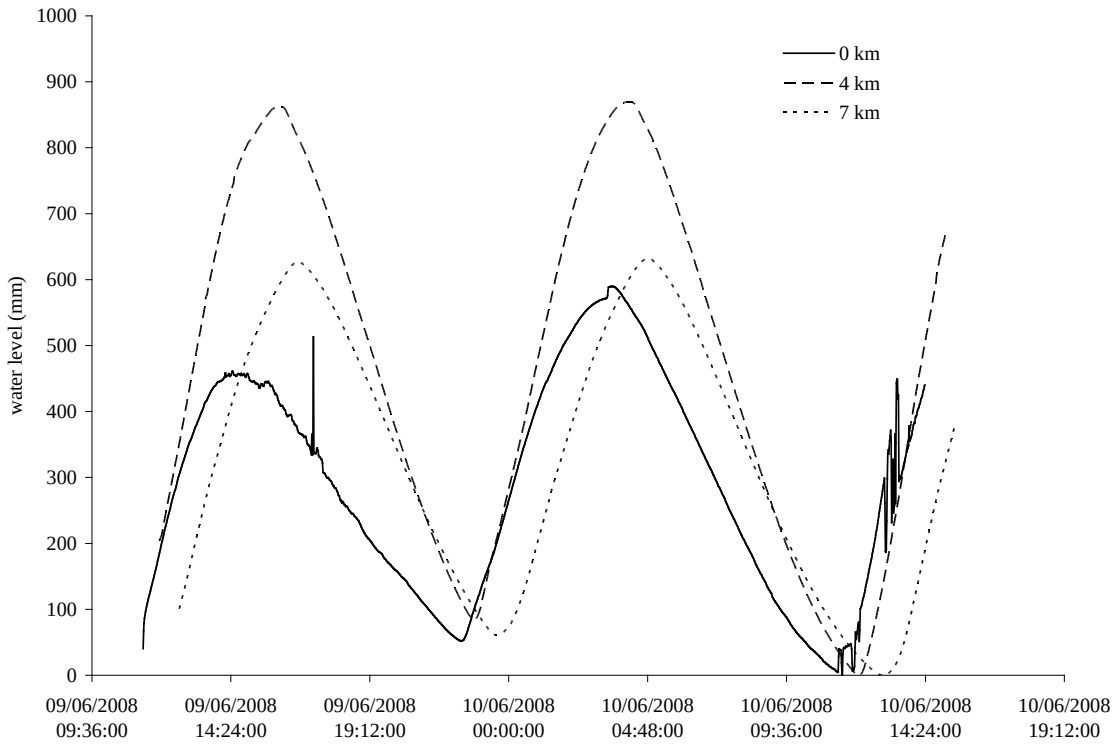

Figure 3.2 Water level at three TFZ locations upstream from the oligohaline estuary of the Newport River, 9 June 2008 – 10 June 2008. Values are relative to the lowest water level observed during the 1.2 day period at each location. Overbank flooding into the riparian zone was observed throughout the TFZ during this period despite the relatively low river discharge (0.780 $m^3 s^{-1}$). Water level was recorded at 5 min intervals using Intech WT-HR water height probe (Intech Instruments LTD, Christchurch, NZ).

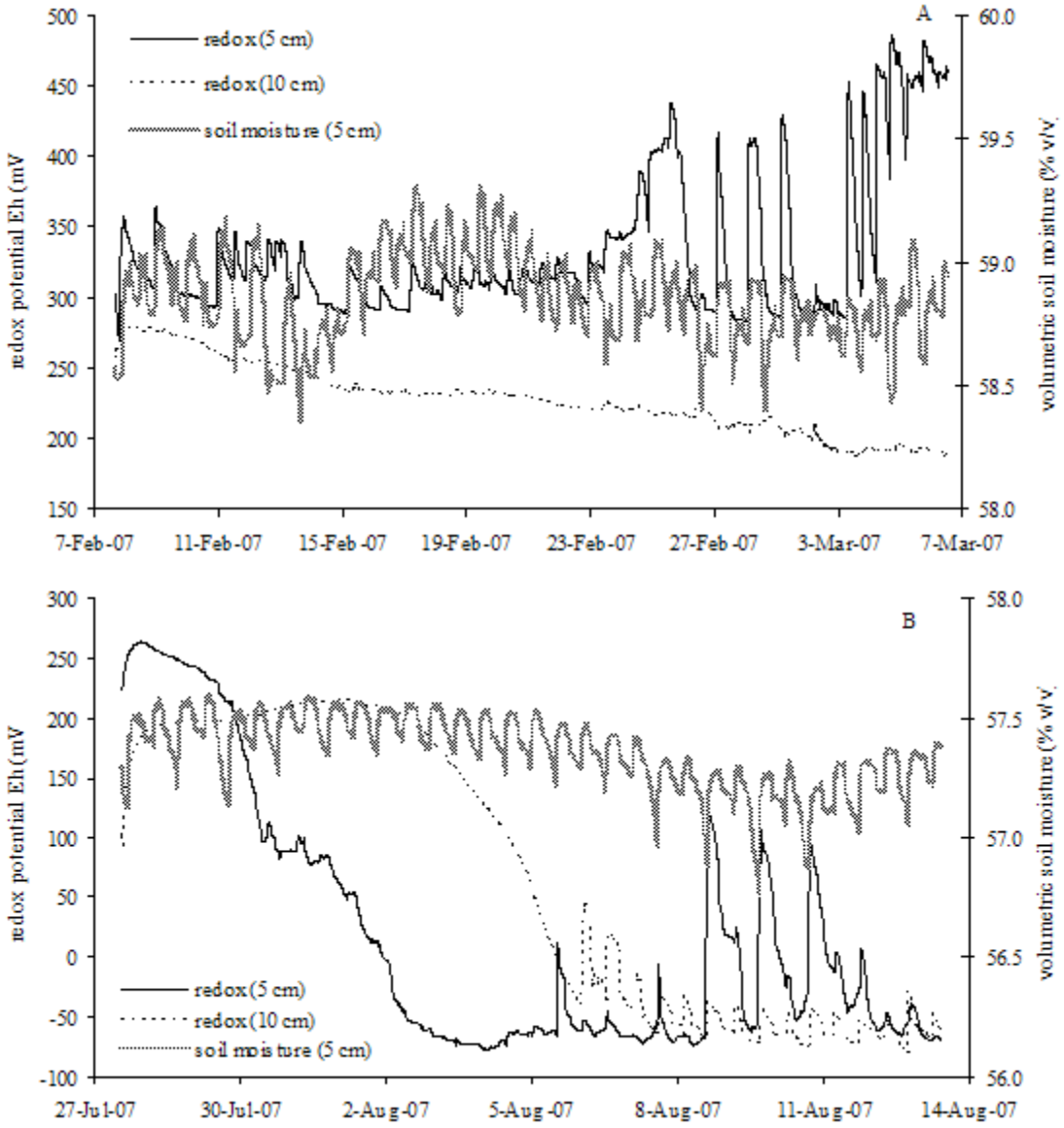

Figure 3.3 Oxidation-reduction potential and soil moisture 2 m from the channel of the Newport River near Old Highway 70 during A) February-March 2007 and B) July-August 2007.

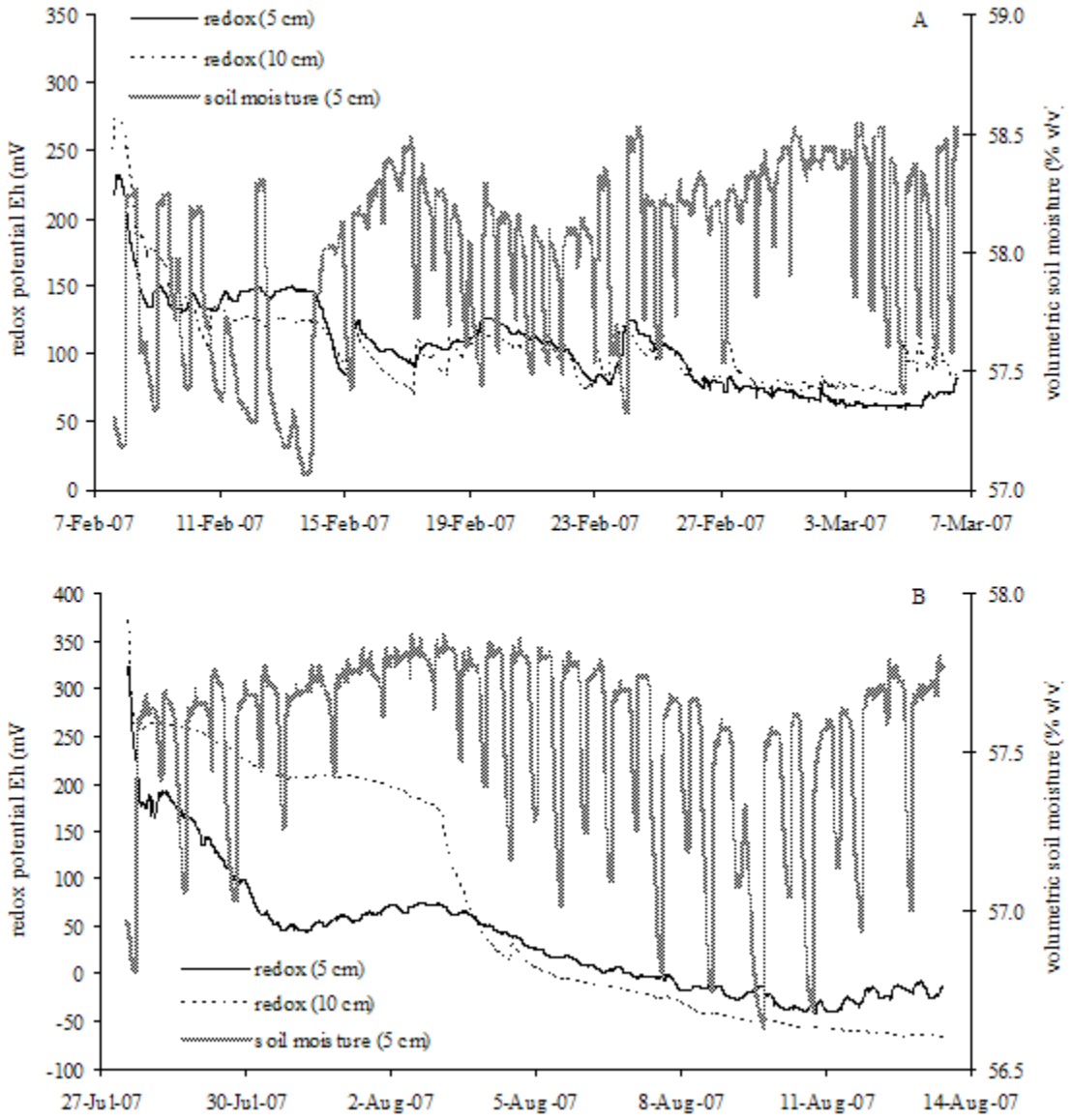

Figure 3.4 Oxidation-reduction potential and soil moisture 10 m from the channel of the Newport River near Old Highway 70 during A) February-March 2007 and B) July-August 2007.

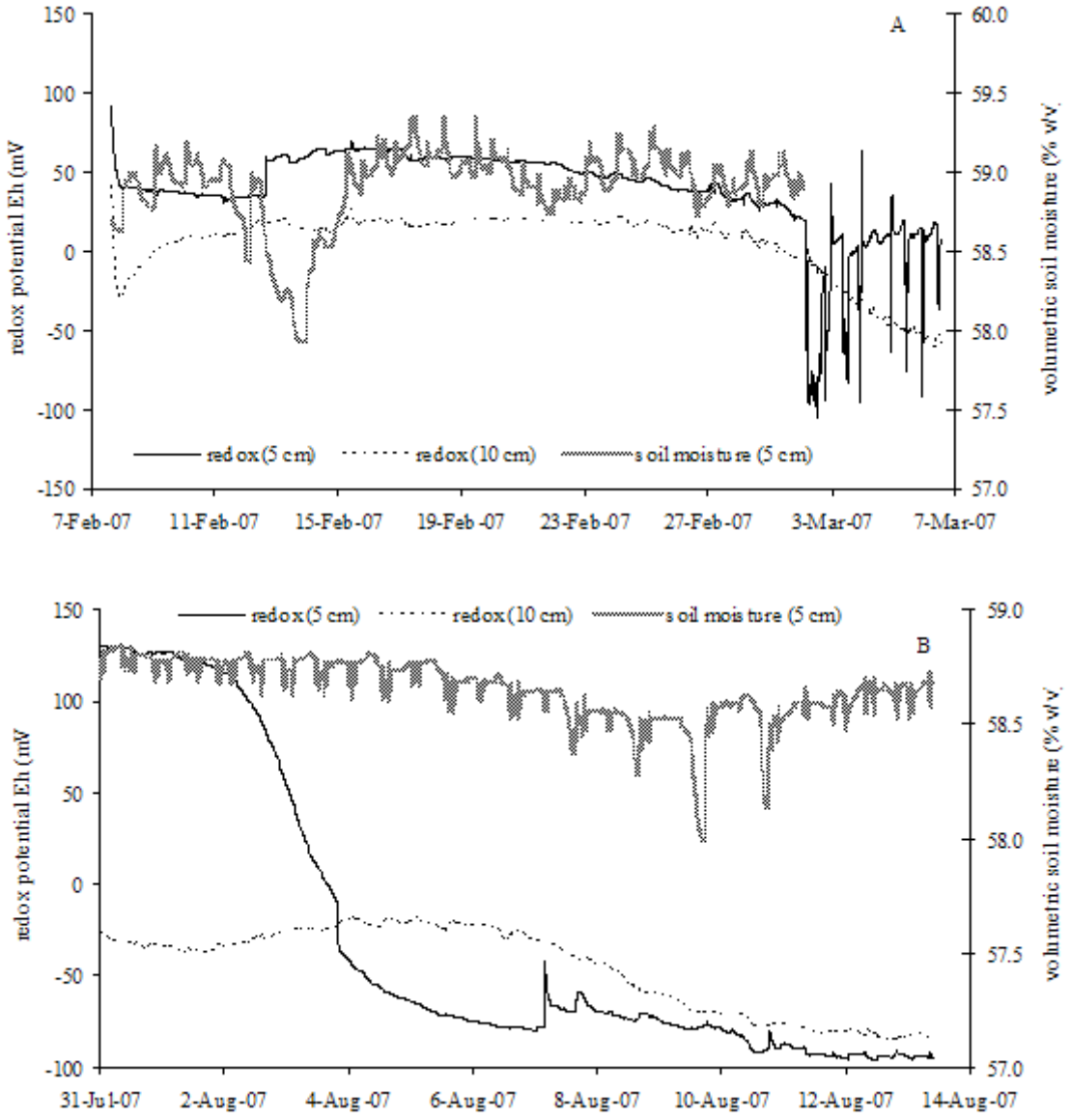

Figure 3.5 Oxidation-reduction potential and soil moisture 17 m from the channel of the Newport River near Old Highway 70 during A) February-March 2007 and B) July-August 2007.

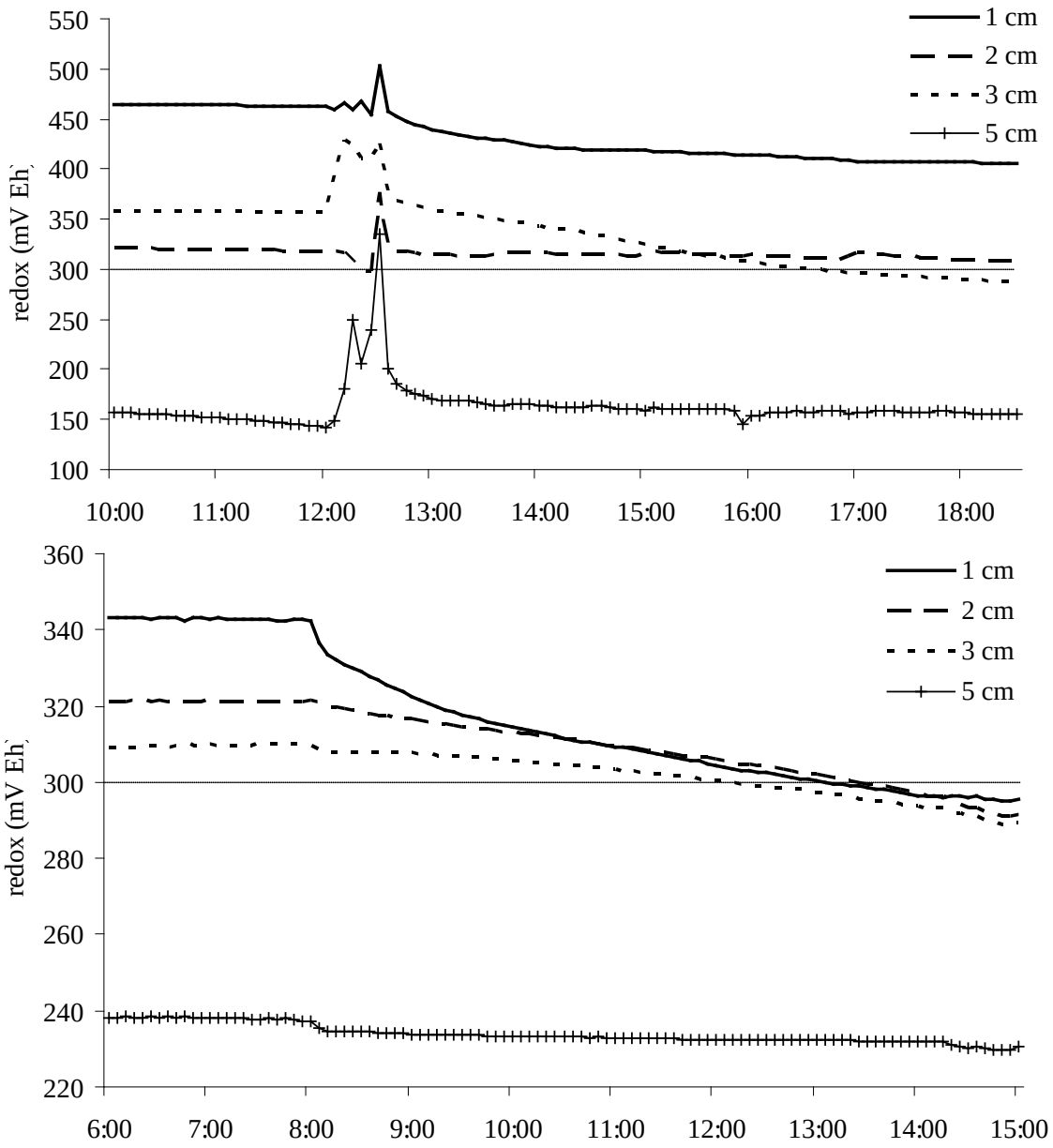

Figure 3.6 A) Laboratory soil core oxidation-reduction potential experiment at 10 ^{o}C; core was submerged at 12:00, and B) laboratory soil core oxidation-reduction potential experiment at 25 ^{o}C; core was submerged at 08:00. The gray line marks the transition between oxic and reduced conditions.

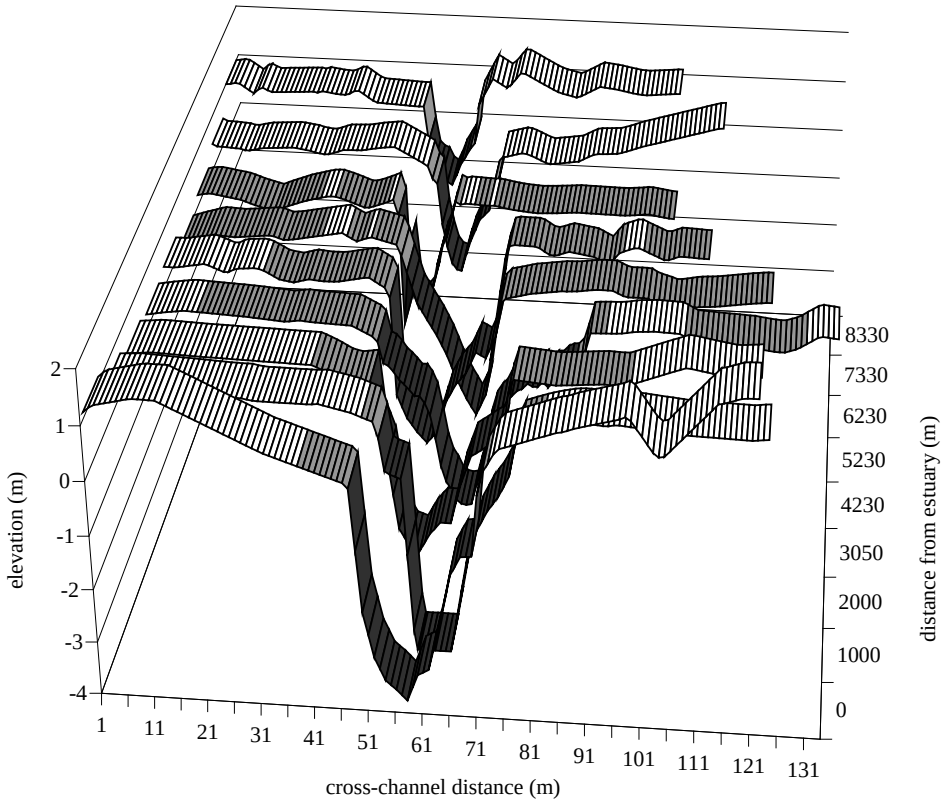

Figure 3.7 Bathymetry and topography of the Newport River tidal freshwater zone from merged LIDAR and cross-section survey data. Dark gray represents low-tide wetted channel, light gray represents high tide wetted riparian zone, and white represents upland non-inundated area.

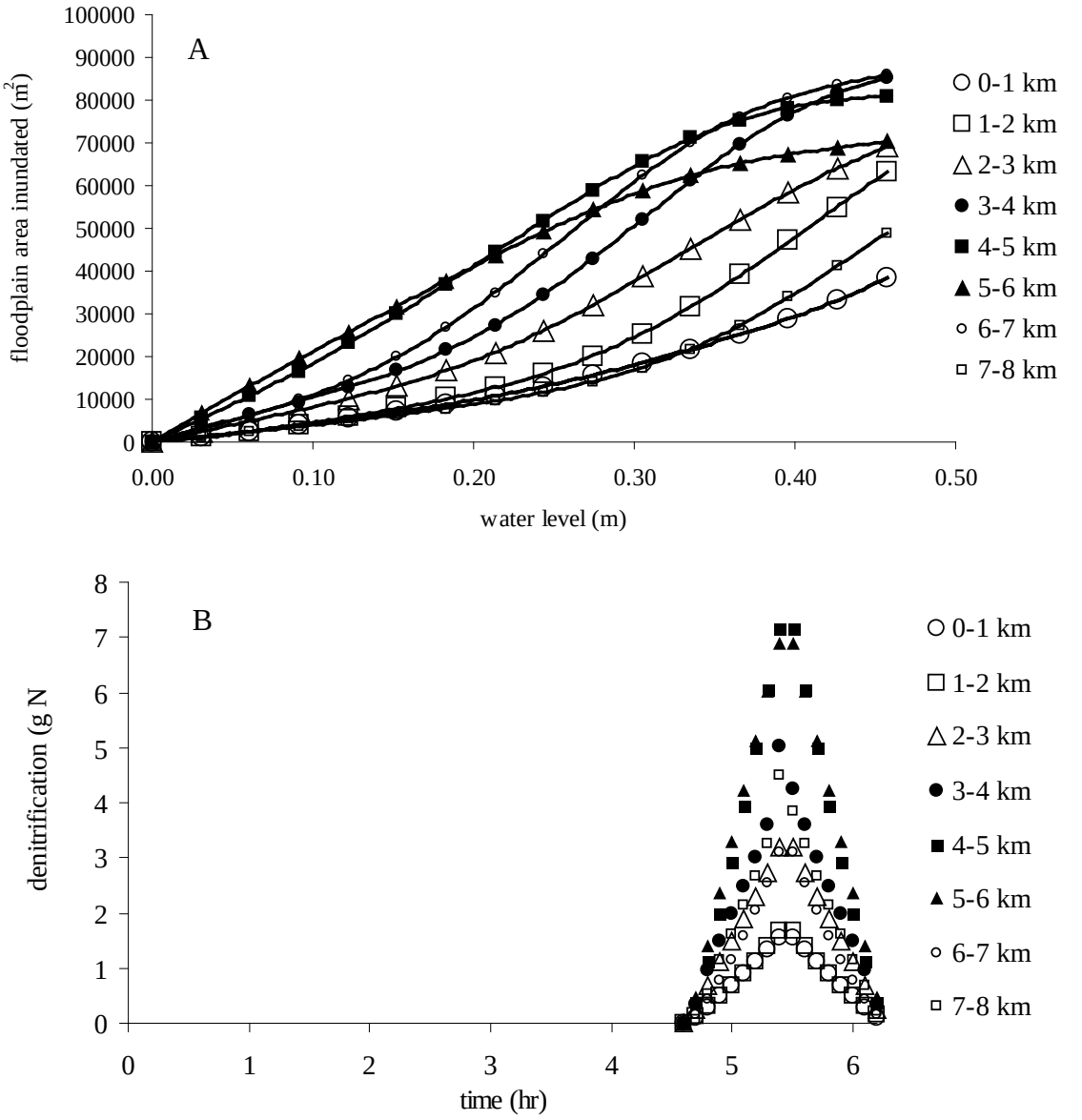

Figure 3.8 A) Results of the GIS topographic analysis of river floodplain morphology along nine 1-km river segments of the Newport River extending from the oligohaline estuary to the top of the TFZ, and B) denitrification within the Newport River TFZ during June 2007 estimated using equation 3.3.

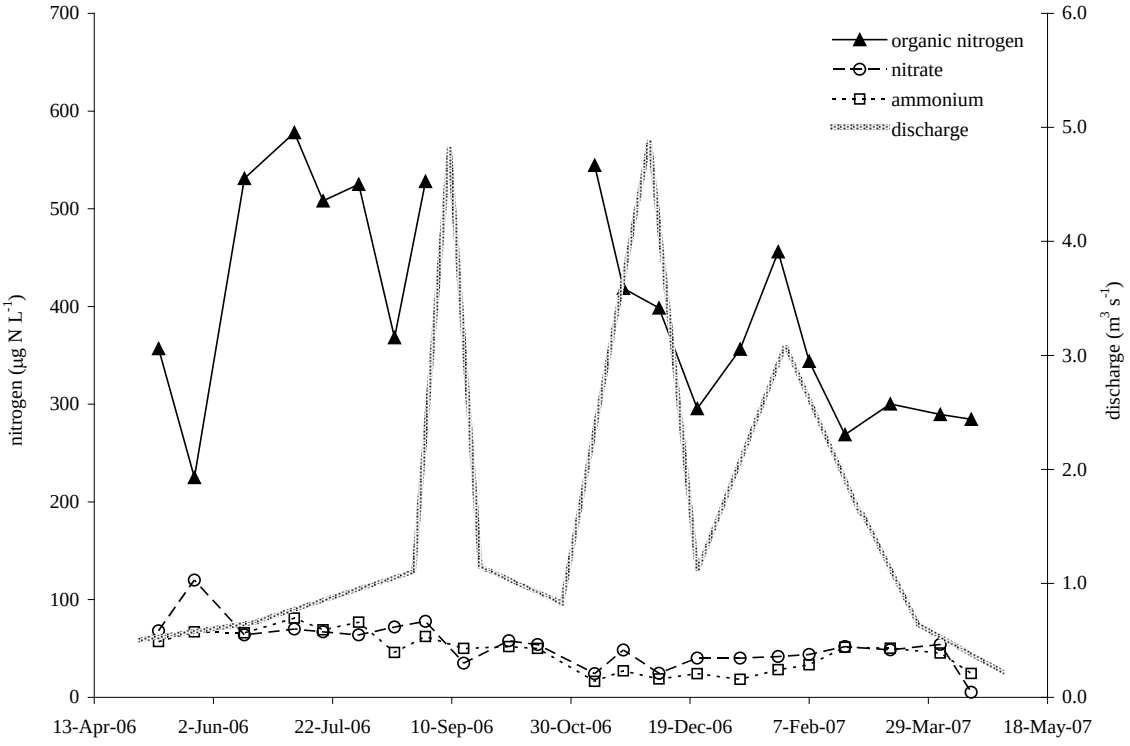

Figure 3.9 Nitrogen concentrations and net downstream discharge in the upper TFZ Newport River, NC, April 2006 – April 2007.

4. LANDSCAPE-SCALE CONTROLS ON DENITRIFICATION IN TIDAL FRESHWATER WETLANDS

4.1. Introduction

The tidal exchange of water and solutes between tidal freshwater wetlands (TFW) and rivers affects solute concentrations in the river, which in turn affects broader-scale solute flux from watersheds to the coastal ocean. While TFW constitute a small part of the landscape, they play a disproportionately large role in biogeochemical cycling because of their high degree of hydrologic connectivity with their adjoining rivers. Nitrogen is particularly reactive in TFW, and the downstream flux of river-borne nitrogen can be reduced 20-35% by TFW processes in large rivers (Seitzinger 1988), and about 1% per river km in smaller rivers (Bowden et al. 1991).

Daily inundation of TFW by tides is necessary for the two processes to occur which permanently sequester river-borne nitrogen: denitrification and long-term burial. We focused this study on the process of denitrification: the microbial reduction of NO_3^- to N_2 (a non-reactive gas that is emitted to the atmosphere) that occurs in the reducing conditions when O_2 is eliminated from riparian sediment. Total N_2 efflux at the scale of an entire tidal river is the product of the rate of denitrification, the area over which it occurs, and the duration of denitrifying conditions. Ultimately, it is this landscape-scale N_2 efflux which is necessary for predicting the delivery of terrestrially-derived nitrogen to the ocean (Davidson and Seitzinger 2006, Seitzinger et al. 2006, and accompanying articles).

Efforts to extrapolate landscape-scale N_2 efflux are plagued by the spatial and temporal variability in denitrification rate (Cornwell et al. 1999; Kulkarni et al. 2008), which has garnered much attention in the biogeochemical 'hot spots' literature (Groffman et al. 2009). Adding to the high variability in denitrification rate is the variability in inundation across a landscape, particularly in TFW where inundation changes continually due to tidal influence. While the spatial and temporal variation in denitrification rate has been studied extensively in TFW to improve the accuracy of landscape-scale extrapolations (Neubauer et al. 2005; Gribsholt et al. 2006 and 2007; Ensign et al. 2008; Hopfensperger et al. 2009), less attention has been given to how the variability in inundation affects these extrapolations. With two sources of variation affecting the calculation of N_2 efflux, denitrification rate and inundated area, a fundamental question remains: Is N_2 efflux more sensitive to the temporal and spatial variation in microbial processing or hydrologic variation in inundation? How do broad-scale patterns in TFW topography and hydrology affect where, when, and how much N_2 efflux occur along a tidal river? Moreover, is there a predominant driver that can be used to scale N_2 efflux occurring in TFW over broad spatial and temporal scale as there are in other ecosystems? Answers to these questions are necessary for the development of empirical models of denitrification in TFW.

The temporal and spatial patterns in N_2 efflux from TFW have implications beyond the challenges they pose to landscape-scale models of nitrogen cycling. TFW are advancing inland as sea level rises, thus changing the spatial configuration of the landscape itself. A rough approximation of this rate of tidal migration highlights the importance of this process over contemporary timescales: the quotient of coastal river

slope in NC (0.0009 on average, Sweet and Geratz 2003) and the current rate of sea level rise in NC (0.003 m yr^{-1}, NOAA 2004) results in a landward migration of 3.3 m yr^{-1} (depending on rates of channel aggradation). Over the coming decade, the spatial patterns we observe in N_2 efflux today will shift inland 33 m, thereby changing broader-scale patterns in TFW nitrogen cycling (Craft et al. 2009). Predicting how this process will affect nitrogen cycling over the coming decades requires knowledge of the contemporary temporal and spatial patterns in N_2 efflux and their landscape-scale controls in TFW.

This study investigated the dynamics of TFW inundation and their potential influence on N_2 efflux. Our objective was to identify the relative importance of the two components of N_2 efflux: inundation extent and denitrification rate. We used a modeling approach wherein field observations of water level were merged with digital topographic data to predict inundation along the entire length of tidal rivers of widely varying size; N_2 efflux was calculated using rate measurements previously reported for one of these rivers. The model allowed examination of the influence of the spatial variation in denitrification rates relative to the spatial variation in inundation on N_2 efflux. Temporal changes in N_2 efflux over time due to water level variation were compared with the temporal variability in denitrification rates. Our analysis is similar to a previous study of tidal amplitude and nutrient cycling in tidal marshes (Vörösmarty and Loder 1994), except that we were able to incorporate recently available remote sensing data to investigate landscape-scale patterns at a resolution not previously available.

4.2. Methods

4.2.1. Study area

Our study investigated the tidal freshwater and oligohaline portion of four coastal plain rivers in North Carolina of varying lengths and watershed areas (Figure 4.1, Table 4.1). The low topographic relief of these watersheds results in the propagation of tides >100 km upstream from the ocean. The National Wetlands Inventory (NWI, U.S. Fish and Wildlife Service 2010) categorizes the predominant riparian vegetation community type as freshwater forested/shrub wetland, followed by estuarine and marine wetland in the Newport and White Oak rivers (Table 4.1). Emergent freshwater wetlands were only reported by the NWI as occurring in Newport River (Table 4.1), but small areas (100-1000 m^2) of emergent freshwater wetlands do occur along the margins of the White Oak and Northeast Cape Fear Rivers, as well.

4.2.2. Floodplain topography

A digital topographic model of the tidal river's riparian zone was developed using geographic information software (ArcGIS, ESRI, Redlands, CA) and Light Image Detection and Ranging Data (LIDAR). Comparison of these topographic models with other digital data sources is described in Rayberg et al. (2009), and a similar topographic analysis of floodplain inundation was performed by Diefenderfer et al. (2008). The LIDAR data were obtained from the North Carolina Floodplain Mapping Program (NCFMP); the data have a vertical accuracy of ≤0.2 m RMS (NCDEM 2002, 2004a and 2004b). The location and shape of river channels was represented using digital line and polygon files of surface hydrology distributed by the NCFMP. LIDAR data within 60 m of the channels was extracted for analysis, and a triangulated irregular network (TIN) was

created to provide a continuous representation of topography (based on the NAVD88 datum) across the floodplain. Only a 50 m width of the original 60 m-wide TIN was analyzed to eliminate edge artifacts from the topographic modeling process. This 50 m floodplain width was chosen based on personal observation that inundation can extend at least this far into the floodplain. Elevation of the TIN was summarized in segments (1 river km in the Newport, New, and White Oak Rivers and 3 river km in the NECF River) using a function within ArcGIS which computes the 3-D area inundated at a given water level. A series of elevations between 0 and 1.5 m were used to generate hypsometric curves for the floodplain area inundated within each river segment.

4.2.3. Water level measurements

Water level was measured in the three rivers over a 29.5 day period (one lunar month) to encompass one spring-neap tidal sequence. The Newport River was monitored from December 2009 through January 2010, a winter period when high river discharge is common. Three HOBO water level loggers (Onset Computer Corporation, Pocasset, MA) were installed in the subtidal river bed at 6 km, 11 km, and 19 km from the mesohaline estuary, and measurements were logged every 5 min. These measurements, with an accuracy of 0.003 m, were corrected to NAVD88 datum using elevation benchmarks measured with a Trimble RTK-GPS (Trimble Navigation Limited, Sunnyvale, CA).

The White Oak River was monitored from June through July 2009, a period when river discharge is typically low. Four HOBO water level loggers were installed in the subtidal river bed at locations 8 km, 12 km, 15 km, and 17 km upstream from the

mesohaline estuary; water level was logged every 5 min. River discharge during this period was near baseflow, so we assumed that the average water level at each of the four sites was mean local sea level. This average was subtracted from each water level measurement to calculate the water elevation relative to local mean sea level (LMSL), and LMSL was converted to NAVD88 by subtracting 0.134 m (the offset determined using NOAA's Vdatum model (http://vdatum.noaa.gov/) at the mouth of the White Oak River, 34.6379N, 77.1037W).

The New River was monitored from May 2010 through June 2010. Water level data (NAVD88) at 15 min intervals was obtained from the USGS gages at Jacksonville (#0209303205) and Gum Branch (#02093000).

The Northeast Cape Fear River water level was monitored from March through April 2010. Water level, measured at 15 min intervals, in the upper portion of the Northeast Cape Fear River was obtained from the USGS gage at Burgaw (#02108566), located 73 km from the mesohaline estuary. These measurements were converted from NGVD29 datum to NAVD88 using the NOAA VERTCON model, which resulted in subtracting 0.293 m from the NGVD29 values (http://www.ngs.noaa.gov/cgi-bin/VERTCON/vert_con.prl). Water level in the lower Northeast Cape Fear River was measured at NAVD88 every 6 min at gages 4 km and 15 km from the mesohaline estuary (data provided courtesy of Dr. Lynn Leonard, University of North Carolina at Wilmington).

4.2.4. Wetland inundation

Inundation in each river segment (1 km in the Newport and White Oak Rivers, 3 km in the Northeast Cape Fear River) was calculated from hypsometric curves and the water level measured closest to that segment. Water levels less than 0 m (NAVD88) were assumed to equate to zero inundated floodplain area. All calculations of inundation and denitrification that follow were conducted in the R software program (R Development Core Team 2009).

4.2.5. N_2 efflux

We examined the effect of spatial and temporal variation in denitrification rate and inundation on N_2 efflux calculated during each lunar day (2 semi-diurnal tidal cycles lasting 24.8 hr) over a lunar month (2 spring-neap tidal cycles lasting 29.5 days). Spatial variability in denitrification rates were compared against the spatial variation in inundation along the tidal river, and temporal variation in rates were compared against the temporal variation in inundation over a lunar month in the upper and lower half of the tidal river. Overlap in monthly N_2 efflux at intervals along the length of the river, or at daily intervals within one section of the river, indicated that N_2 efflux was more sensitive to variation in denitrification rate. In contrast, if the range in N_2 efflux did not overlap, either between intervals along the river or over time in one section, than the variability in inundation was interpreted to be a more significant factor than denitrification rate.

This comparison required a spatial and temporal range of denitrification rates and a central rate estimate. In a previous study, we measured denitrification rates in three riparian zone habitat types (hardwood forest, emergent marsh, and mudflat) over a 11 month period in the Newport River (Ensign et al. 2008); the TFW habitats in the Newport

River are very similar to the other rivers studied (Table 4.1). For the current study we estimated the spatial variation in denitrification as the mean of the monthly range in rates between the three habitats, which was 12 μg m^{-2} min^{-1}. The temporal variation was estimated as the range in mean values for each habitat over an annual period, which was 17 μg m^{-2} min^{-1}. The mean denitrification rate of all measurements made in all habitats and all months in the Newport River was 29 μg m^{-2} min^{-1}, and therefore our spatial variation in rate was 23 to 35 μg m^{-2} min^{-1}, and the temporal variation was 21 to 38 μg m^{-2} min^{-1}.

The range in potential N_2 efflux was calculated using the upper and lower values of these spatial and temporal ranges; calculations were performed at the time-step of water level measurement in each river. Previous research found that a 4.6 hr lag occurred between inundation of wetland sediments and an oxidation-reduction potential conducive to denitrification in the surficial sediments (Ensign et al. 2008). Since our objective was to examine the influence of riparian denitrification on nitrate concentration in river water advected into the wetland during high tide, we incorporated this 4.6 hr lag between inundation and the onset of N_2 efflux. Our calculations assume that denitrification within the surficial (>5 cm depth) reduced sediment layer utilizes NO_3^- from the overlying water; while denitrification likely occurs in sediments below 5 cm, we did not consider this N_2 production would directly affect the NO_3^- concentration in the water column. The sensitivity of the estimated N_2 efflux to variation in lag time was not examined, although a shorter lag time would result in greater N_2 efflux while a longer lag time would result in less N_2 efflux.

4.3. Results

4.3.1. Hydrology and floodplain topography

Temporal changes in water level in the four rivers were related to upstream discharge and tidal influence. Water level measurements in the Newport River were made during a period of high river discharge following a 4 cm rain event that occurred 25 Dec 2009 (Figure 4.2A). Tidal amplitude in the upper river diminished immediately after this rain event as water level rose, and slowly resumed a semi-diurnal frequency through the rest of the period as water level decreased. In the lower tidal river, the semi-diurnal tidal range was briefly suppressed by this event, but water level did not rise as it did upstream. The range in water level throughout the White Oak River was remarkably consistent throughout the period, indicating that any changes in upstream discharge that occurred did not influence water level in the river (Figure 4.2C). Changes in tidal amplitude and water level in the White Oak River corresponded with the spring-neap tidal sequence, with spring tides occurring 6 and 23 June, and neap tides occurring 15 June and 2 July. Water level in the upper New River reflected a small runoff event on 17 June, but this did not influence water level in the lower tidal river (Figure 4.2E). Water level in the upper Northeast Cape Fear River reflected the tail of a storm hydrograph and semi-diurnal tidal amplitude increased as and water level decreased (Figure 4.2G). The lower Northeast Cape Fear River tidal amplitude and water level reflected the neap tides on 22 March and 7 April and spring tides on 31 March and 15 April.

GIS analysis revealed a range of patterns in hypsometric curves between rivers. The Newport (Figure 4.2B) and White Oak Rivers (Figure 4.2D) demonstrated the greatest inundated area in the upper portion of the tidal river, while the Northeast Cape

Fear River (Figure 4.2H) had greatest inundation in the lower river. The New River showed greatest inundation downstream when water level was greater than 0.1 m (Figure 4.2F).

4.3.2. Floodplain inundation

We present the inundation data that reflect a 4.6 hr lag (as measured in Ensign et al. 2008) to more effectively compare and discuss the relative importance of inundation versus denitrification rate; consequently areas inundated for less than 4.6 hr are not shown in the graphs presented. The Newport River showed much greater inundation in the upper than lower river, and was continually inundated to some extent throughout the month of study (Figure 4.3A). The lower half of the Newport River drained completely on all but one day of the month (Figure 4.3B). A general decline in inundation occurred in the upper river that reflected the decrease in water level (Figure 4.3C).

The White Oak River displayed greater inundation in the upper than lower portion of the tidal river, despite nearly equal water level along the river (Figure 4.4A). The daily range of inundation in both the upper and lower river corresponded with the spring-neap tidal sequence (Figure 4.4B and 4.4C, Figure 4.2C). Complete drainage of the riparian zone occurred daily, and on days 9 and 26 the floodplain was inundated for less than 4.6 hr (as represented by gaps in inundation in Figure 4.4B and 4.4C).

The New River displayed greatest inundation in the middle portion of the tidal river (Figure 4.5A), contributing to a peak inundation occurring in the middle of the study period in the lower river (Figure 4.5B). Continual inundation of the upper river occurred throughout the study period (Figure 4.5C).

Inundation in the Northeast Cape Fear River was dominated by the lower half of the river (Figure 4.6A), despite the high water level upstream (Figure 4.2G). The lower half of the river drained completely almost every day (Figure 4.6B), while the upper half of the river was continually inundated to some extent throughout the study period (Figure 4.6C).

4.3.3. N_2 efflux

The predicted range in N_2 efflux reflected the temporal and spatial trends in floodplain inundation from which they were calculated. The majority of the N_2 efflux occurred in the upper portion (longitudinally) of all rivers (Figures 4.3-4.6), regardless of the discharge condition of the river (storm flow versus baseflow) and hypsometric curves (Figure 4.2). The lack of overlap in the range of potential N_2 efflux along this spatial gradient (e.g., the black bars representing N_2 efflux from a range of denitrification rates do not all overlap) indicated that N_2 efflux was more sensitive to variation in inundation along this spatial gradient (Figures 4.3A, 4.4A, 4.5A, and 4.6A). The range in potential N_2 efflux differed over time in the lower portion of all rivers (e.g., the black bars do not all overlap), indicating that differences in inundation over time had a greater effect on N_2 efflux than the temporal variability in denitrification rate (Figures 4.3B, 4.4B, 4.5B, and 4.6B). In contrast, the range in potential N_2 efflux in the upper Newport, New, and Northeast Cape Fear Rivers did not differ over time (e.g., the black bars all overlap), indicating that N_2 efflux was more sensitive to the temporal variation in denitrification rate than inundation (Figures 4.3C, 4.5C, and 4.6C). The White Oak River, the only river in which we assumed that upstream runoff did not affect tidal amplitude, showed similar

temporal variability upstream and downstream, and N_2 efflux was more influenced by inundation over time than variation in denitrification rate (Figure 4.4B and 4.4C).

4.4. Discussion

4.4.1. Two Modes of N_2 Efflux

The temporal contrasts in the range in potential N_2 efflux can be summarized as occurring in two dominant modes of emission (Figure 4.7). High river discharge caused continual inundation of the upper half of the tidal rivers regardless of their topography (as demonstrated by the opposite hypsometric curves in the Newport and Northeast Cape Fear Rivers (Figure 4.2B and 4.2H) but similar patterns in inundation (Figures 4.3C and 4.6C). During these periods of continual inundation, the variation in day-to-day N_2 efflux is highly sensitive to factors controlling biogeochemical rates (as indicated by the overlap in the potential N_2 efflux). We refer to these periods as exhibiting a biochemical mode of N_2 efflux since the temporal variation in biochemical rates most strongly affect N_2 efflux. In contrast, when river discharge was low and inundation was dictated by tides, the effect of daily hydrologic variation superseded the effect of temporal variability in denitrification rate; we refer to this period as a hydrologic mode. Biochemical mode was more common in the upper river, while hydrologic mode was most common in the lower tidal river.

Strong spatial gradients in N_2 efflux were observed, with higher N_2 efflux upstream than downstream due to patterns in hydrology and topography. In all rivers studied, the spatial gradient in the relationship between hydrology and topography resulted in much more area inundated in the upper river, and consequently higher N_2

efflux. These physical gradients had a greater influence on N_2 efflux than did the spatial variation in denitrification rate, as indicated by the lack of overlap in N_2 efflux along the length of the rivers. Overall, the upper half of all rivers was the major contributor of N_2 efflux due to their high inundation areas (Figure 4.7). However, these data represent only a one month period which was influenced by high river discharge in half of the rivers studied. The temporal constraints of our study lead to two issues which we address in the following section: What is the annual contribution of high versus low river flow regimes on inundation and subsequent N_2 efflux, and what is the corresponding mode of N_2 efflux over annual time scales?

Our model of TFW N_2 efflux was based on three assumptions which generated a characteristic response to variation in water level. First, N_2 efflux was not expected to occur until after a 4.6 hr lag time to account for the time necessary for the sediment water interface to become reduced and denitrification of NO_3^- in the overlying water to begin. Second, N_2 efflux occurring after this lag period was calculated directly from the TFW area inundated. Third, the maximum N_2 efflux was limited to a 20 hectare per river km area due to the boundaries of the LIDAR data analyzed. These assumptions lead to the expectation that N_2 efflux should scale as a sigmoid function of water level. This response is apparent from a plot of the daily mean water level from each river against the corresponding daily N_2 efflux per river km (Figure 4.8). The New River exhibited greater N_2 efflux per water level than the other rivers (Figure 4.8), perhaps because tidal amplitude was lower and therefore the daily draw-down of water at low tide was less severe than the other rivers.

4.4.2. Water level governs N_2 efflux in TFW

The strength of the relationship between daily N_2 efflux and mean daily water level is striking considering the inter- and intra-river variations in topography and hydrology. While some degree of auto-correlation is expected between model output (N_2 efflux) and a summary measure of the data input (water level), the strength of this regression indicates that much of the topographic and hydrologic complexity of our model can be simplified to a single three parameter, non-linear model:

$$N_2\ efflux = \frac{x}{(y \times exp^{-z})} \quad (4.1)$$

where *x* is the maximum amount of denitrification that could occur within a river reach and *y* is a fitted variable and *z* is the area inundated. Despite the different spatial patterns in topography among rivers and differences in their tidal and fluvial dynamics, water level alone explained a substantial part of their inundation dynamics.

The empirical relationship between N_2 efflux and mean water level allowed us to address the question of how river flow regime (e.g., baseflow versus stormflow) affects N_2 efflux over annual time scales (versus the one month period we observed). The occurrence of an ecosystem process, such as N_2 efflux, over long time periods in rivers can be calculated from the magnitude of the process and the corresponding frequency at which it occurs (sensu Doyle et al. 2005). We performed this magnitude-frequency analysis using the relationship between N_2 efflux and water level (Figure 4.8) in conjunction with the long-term distribution of water level at a tidal gaging station. The log-normal frequency distribution was computed for 10 years of mean daily water level at the USGS gaging station at Burgaw on the Northeast Cape Fear River (#02108566) and multiplied by the sigmoid function in Figure 4.8. The peak value from this calculation

(0.6 m) represents the water level where most N_2 efflux occurs in the upper Northeast Cape Fear River (Figure 4.9A). To put this water level in context with the flow regime of the river, we compared water level to discharge at this gaging station. A water level of 0.6 m occurred during low (baseflow) discharge periods (Figure 4.9B), indicating that high river discharge had a minimal effect on N_2 efflux over an annual period. Most N_2 efflux in the upper tidal river occurred when tides, not high river discharge, were the predominant influence on TFW inundation. Tides are even more influential in controlling inundation (and subsequent N_2 efflux) in the lower river, which is even less affected by river discharge.

4.4.3. Modeling denitrification in TFW

Accounting for the temporal and spatial variability in denitrification rate has been identified as the foremost challenge in denitrification modeling (Groffman et al. 2009), but our analysis suggests this issue may be of secondary importance in TFW. While the environmental factors (e.g.,, temperature, carbon substrate, nitrate concentration) regulating denitrification are of primary importance during the biochemical mode of N_2 efflux, they are equally or less important than inundation dynamics during the hydrologic mode. The frequency-magnitude analysis we performed indicates that most N_2 efflux occurs during the hydrologic mode over an annual period, and therefore accurate estimation of denitrification rate is of secondary importance. From a landscape-scale perspective, we suggest that equal, or greater, emphasis be given to characterizing the surface hydrology of a TFW relative to the biochemical mechanisms regulating denitrification rate.

A weakness in current models of riverine denitrification is the effect of riparian processes on downstream riverine nitrogen transport (Boyer et al. 2006). Our analysis revealed that water level fluctuation alone may be sufficient to link TFW riparian processes with riverine transport in a manner similar to other aquatic denitrification models (reviewed by Boyer et al. 2006). The daily nitrogen load exiting a river reach (N_{out}) is the difference between the daily load entering the reach (N_{in}) and the riparian processes contributing to denitrification:

$$N_{out} = N_{in} - \frac{a \times v_f \times C}{1+(y \times exp^{-z \times L})} \quad (4.2)$$

where a is the TFW area per river length, v_f is the denitrification mass-transfer coefficient, C is the NO_3^- concentration in the river, y and z are fitted constants, and L is the water level in the river. This equation reflects the combined influence of biochemical process (expressed as v_f and C) and the degree of hydrologic interaction between the river and TFW (expressed as a sigmoid function of L with the fitted constants y and z), thereby allowing specificity of model parameters . Representation of the in-channel denitrification would also need to be included by means of one of the many formulations already developed (Boyer et al. 2006). The results of the current study indicate that river water level is the most parsimonious single variable with which to couple downstream river nitrogen transport with denitrification in TFW.

4.4.4. Shifting landscapes and denitrification during sea level rise

The spatial patterns in TFW topography and hydrology in the NC rivers we studied were similar to other TFW. Floodplain elevation was lower upstream than downstream, a pattern similar to that observed in the Suwannee River, FL (Light et al.

2007) and Nanticoke River, MD (Baldwin 2007). Inundation extent was greater upstream than downstream, a pattern also seen in other TFW (Hackney et al. 2007). These spatial gradients along tidal rivers are the combined result of long-term temporal changes in topography and tidal amplitude as sea level rises. One explanation for the spatial gradient in inundation along tidal rivers is that sediment accretion is more rapid in the lower river's TFW (e.g., Darke and Megonigal 2003), but tidal amplitude increases faster in the upper river's TFW (see Pasternack 2009 for review of TFW evolution and Neubauer et al. 2002).

As sea level rises, the balance between TFW accretion and the simultaneous landward expansion of tidal influence govern the net change in N_2 efflux from tidal rivers. Our data indicate that most N_2 efflux occurs in the upper region of tidal rivers. Thus, if the rate of downstream accretion is proportionally faster than the expansion of tidal inundation upstream, total N_2 efflux from the tidal river may decline over time. Alternatively, if tidal inundation extends upstream faster than downstream habitats accrete, total N_2 efflux may increase as sea level rises. With a landward tidal migration rate of 30 m per decade, the net effect of these processes is conceivably detectable in multi-year study of a tidal river. Measuring these shifts in tidal inundation is an exciting prospect for long-term environmental monitoring, particularly since the rate of sea level rise may be increasing and accelerating these landscape-scale ecosystem processes.

Riparian forested TFW were the location of most N_2 efflux in this study. These habitats have received less attention than emergent tidal marshes with respect to nitrogen cycling and denitrification, yet appear to be crucial to the overall N_2 efflux in tidal rivers. Forested riparian wetlands in non-tidal rivers sequester nitrogen through both

denitrification (Brinson et al. 1984) and burial (Noe and Hupp 2005 and 2009), except during very short hydroperiods (Noe and Hupp 2007). Broad-scale comparisons have been made between tidal and non-tidal forested riparian habitats (Verhoeven et al. 2001), but how biogeochemistry of these habitats changes upon conversion to a tidal hydroperiod is unknown. These tidally-induced biogeochemical transformations in tidal forested wetlands are another topic in need of future research in the broader effort to understand nitrogen dynamics in tidal rivers.

4.5. Conclusions

Tidal rivers are the final hydrologic link connecting watersheds with estuaries. Biochemical processing of nitrogen within the TFW of these rivers significantly influences the delivery of nitrogen to the marine environment, but our ability to predict this process at the landscape-scale has been hindered by the hydrologic complexity of tidal rivers. This study revealed that this hydrologic complexity, particularly that which is due to tides, strongly affects TFW N_2 efflux. In fact, over annual time-scales this tidal hydrology is the dominant factor affecting N_2 efflux, exceeding the influence of river floods on TFW inundation. Not only do tides dominate TFW inundation, but they are as, or more important to consider when calculating landscape-scale N_2 efflux than the potential variability in denitrification rate.

Consistent spatial patterns in topography and hydrology occurred in three of the four rivers studied, and we discovered that the complexity of the topographic-hydrologic inundation model could be simplified to a 3 parameter regression model based on average daily water level. This simplified model was used to develop an equation for estimating

NO_3^- loss in TFW during riverine transport; elaboration of this equation in future research may provide an effective way of coupling riparian TFW processes with riverine transport. An exciting challenge for future TFW research is quantifying the rate of landward expansion in tides and the subsequent conversion of non-tidal to tidal biogeochemical regimes in tidal forests. Establishing how N_2 efflux from tidal rivers responds to the upstream addition of tidal forests with the simultaneous changes in TFW inundation is of particular interest given expectations of a future increase in the rate of sea level rise.

Table 4.1. River characteristics and riparian vegetation type from the NWI.

Rivers	Length studied (km)	Watershed area (km^2)	Vegetation type				
			Estuarine and marine wetland	Freshwater emergent wetland	Freshwater forested and shrub wetland	Riverine	Estuarine and marine deepwater
Newport	17	178	41%	0%	57%	1%	2%
White Oak	23	551	14%	14%	68%	3%	1%
New	12	431	0%	0%	98%	2%	0%
NE Cape Fear	64	4513	0%	0%	93%	7%	0%

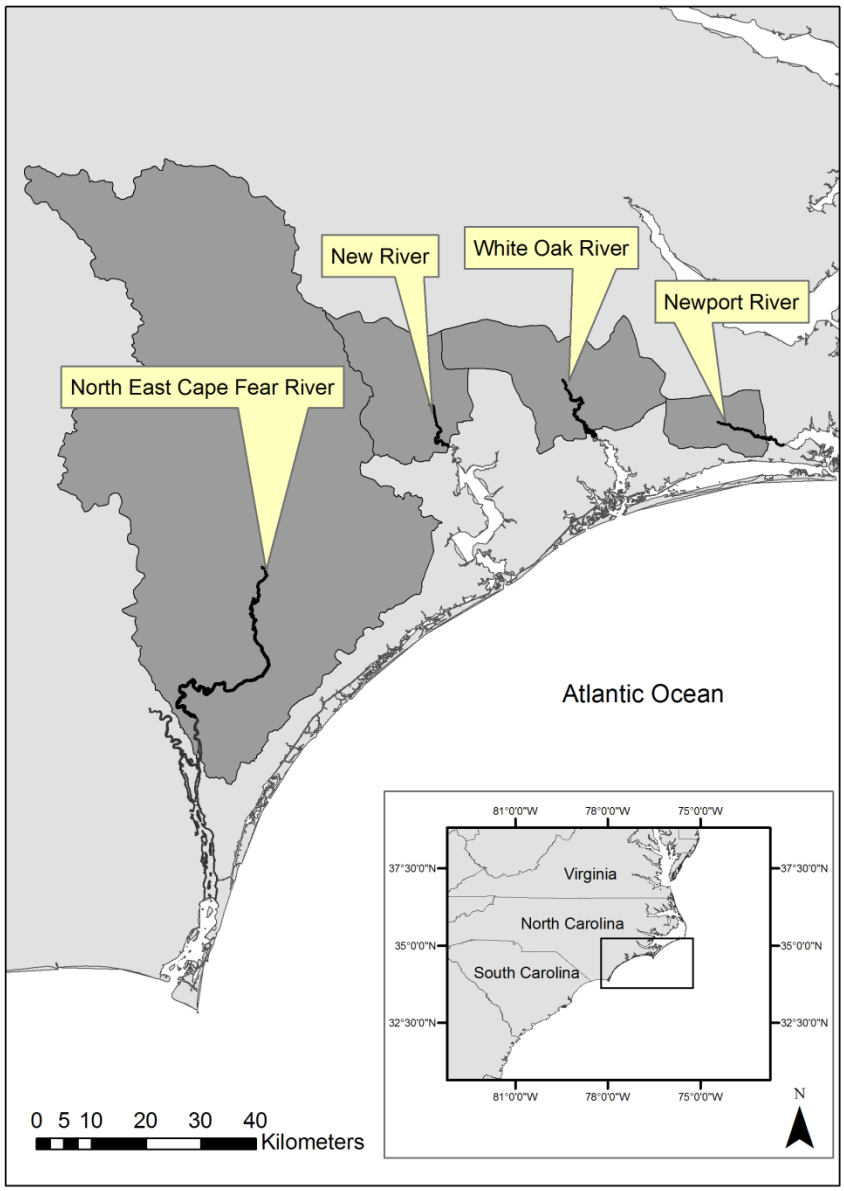

Figure 4.1 The location of the rivers studied in North Carolina. The thick black lines indicate the extent of the tidal freshwater zone, and the shaded gray indicates the extent of the watershed.

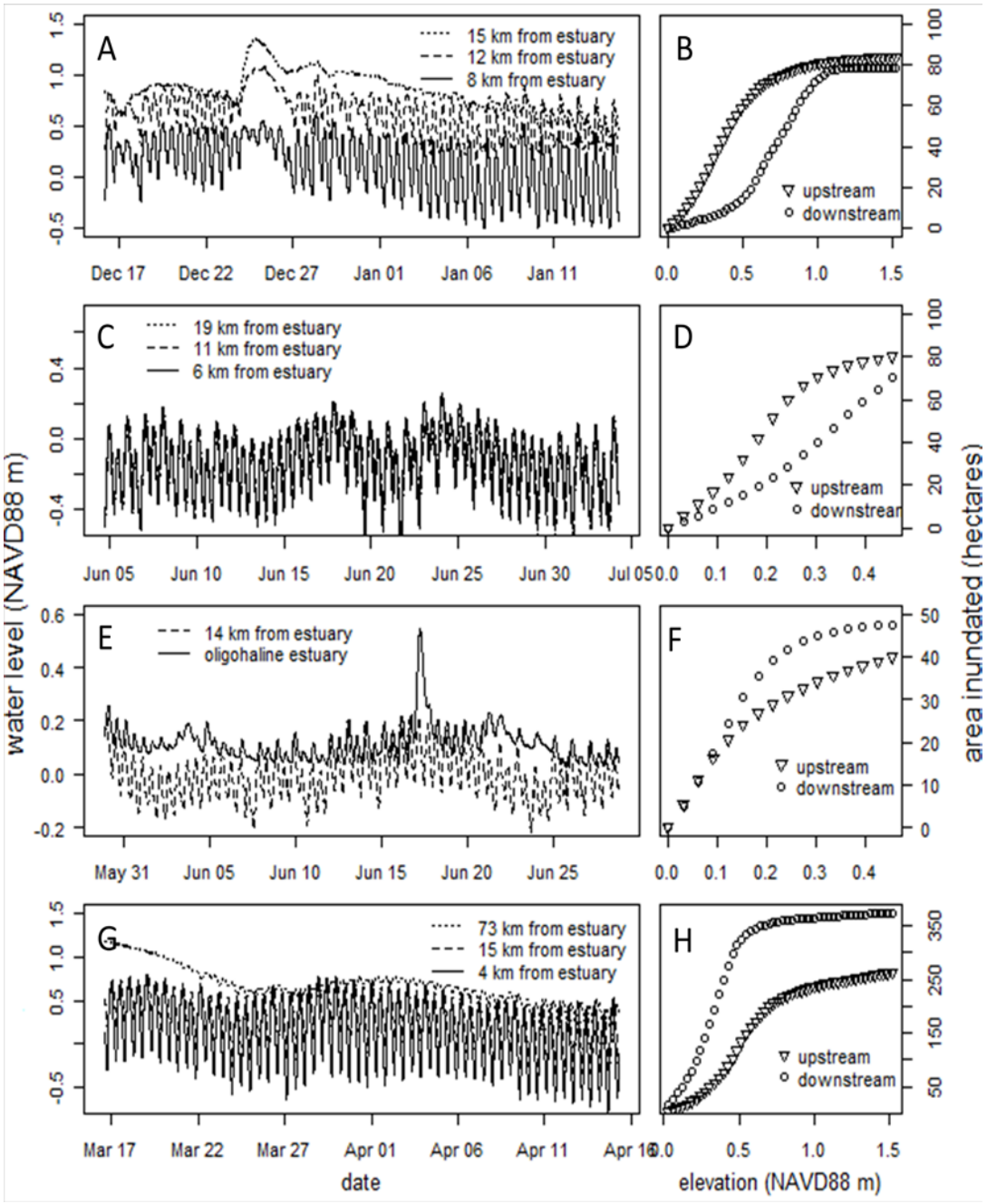

Figure 4.2 Water level and hypsometric curves in the Newport River (A and B), White Oak River (C and D), New River (E and F), and Northeast Cape Fear River (G and H).

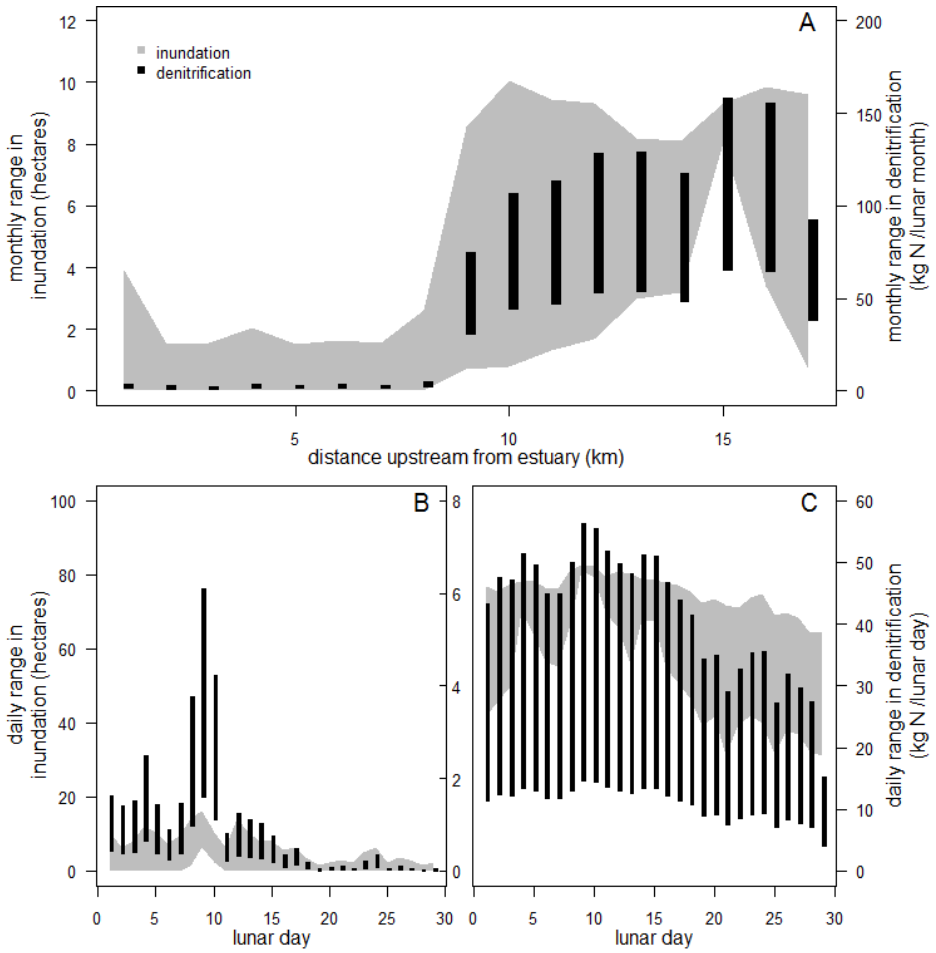

Figure 4.3 Range in inundation and N_2 efflux along the Newport River over a one month period (A), range in inundation and N_2 efflux each day in the lower (B) and upper (C) tidal river.

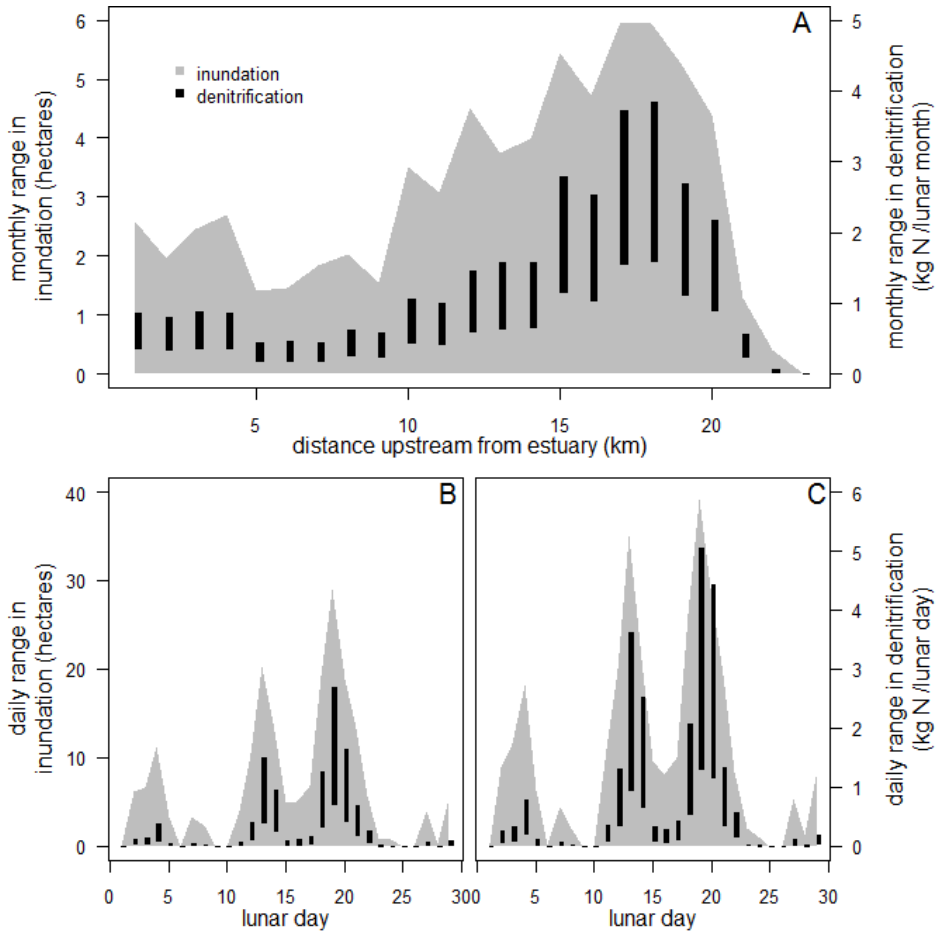

Figure 4.4 Range in inundation and N_2 efflux along the White Oak River over a one month period (A), range in inundation and N_2 efflux each day in the lower (B) and upper (C) tidal river.

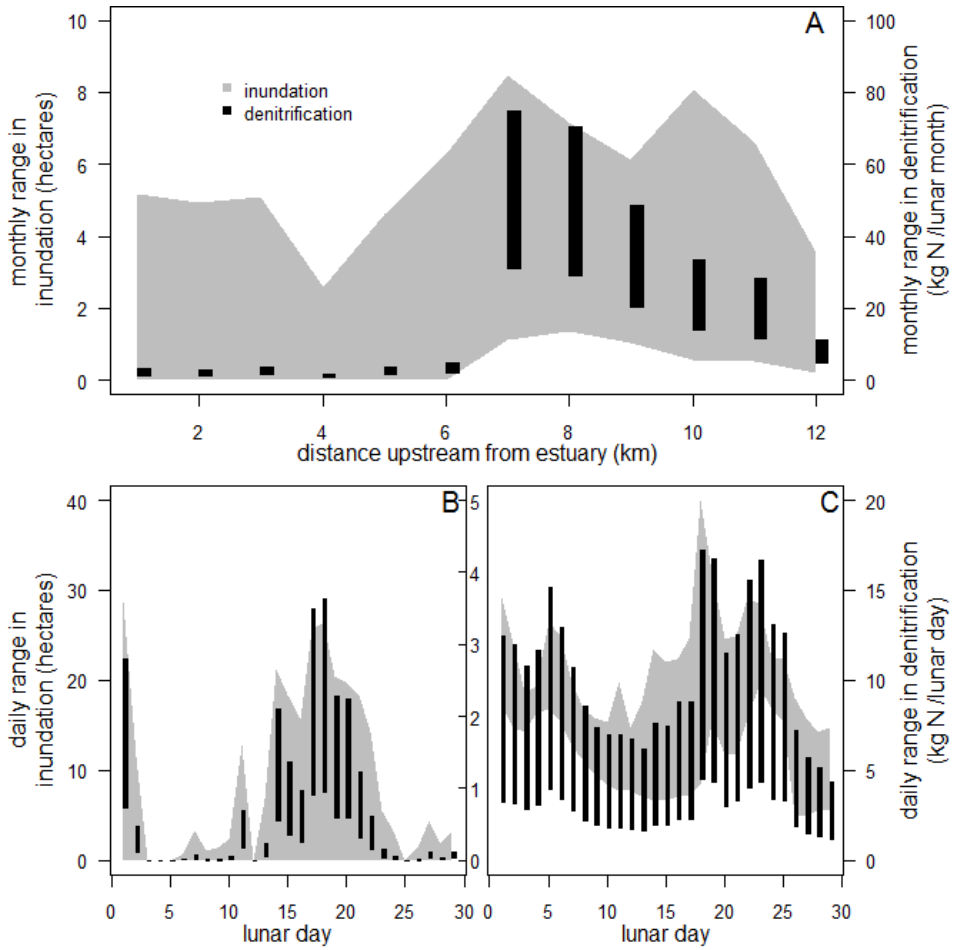

Figure 4.5 Range in inundation and N_2 efflux along the New River over a one month period (A), range in inundation and N_2 efflux each day in the lower (B) and upper (C) tidal river.

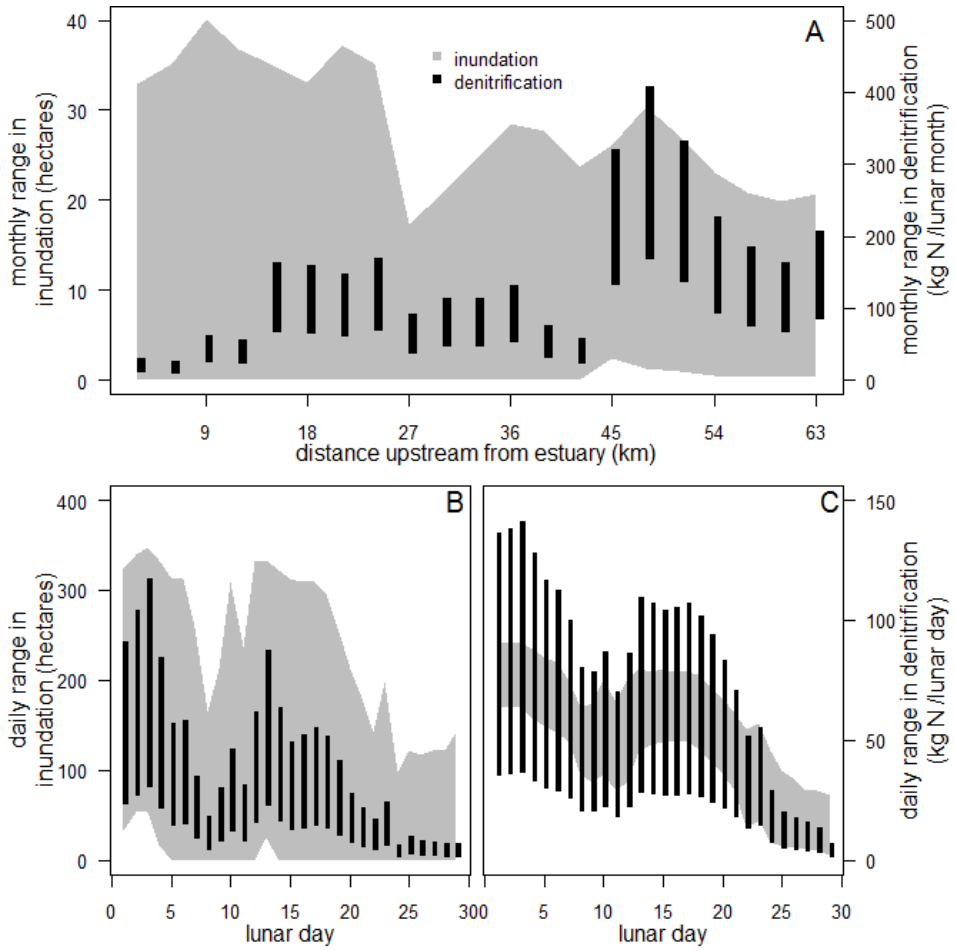

Figure 4.6 Range in inundation and N_2 efflux along the Northeast Cape Fear River over a one month period (A), range in inundation and N_2 efflux each day in the lower (B) and upper (C) tidal river.

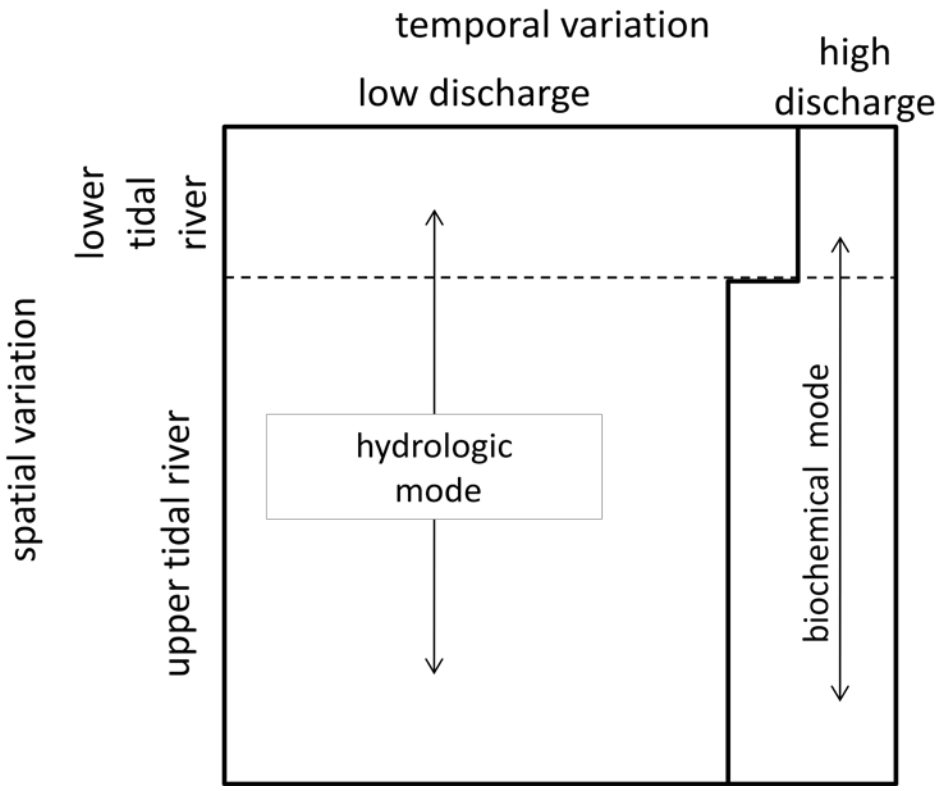

Figure 4.7 Generalized, qualitative model of the temporal and spatial variation in N_2 efflux in a tidal river showing the periods of hydrologic and biochemically-driven modes of N_2 efflux. The size of the four sections of the figure show the relative N_2 efflux over an annual period.

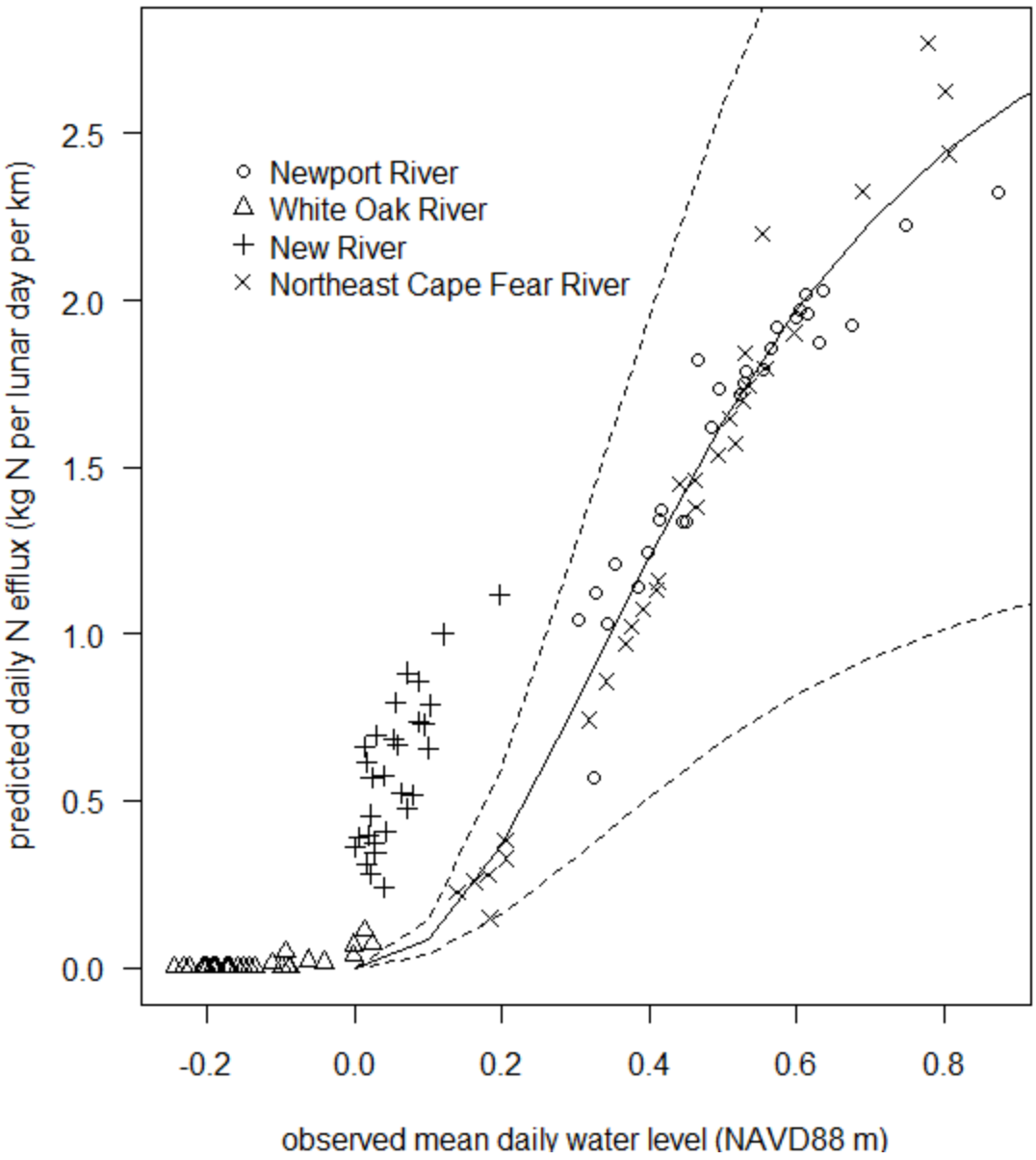

Figure 4.8 Predicted N_2 efflux versus the mean daily water level in each river over the month of study. Model predictions represented by symbols are for those calculated using the grand mean denitrification rate (29 μg m^{-2} min^{-1}). The solid line shows a three parameter logistic regression curve fit to all data except the New River. The dashed lines show this model fit to predictions of a maximum (36 μg m^{-2} min^{-1}) and minimum (22 μg m^{-2} min^{-1}) denitrification rate.

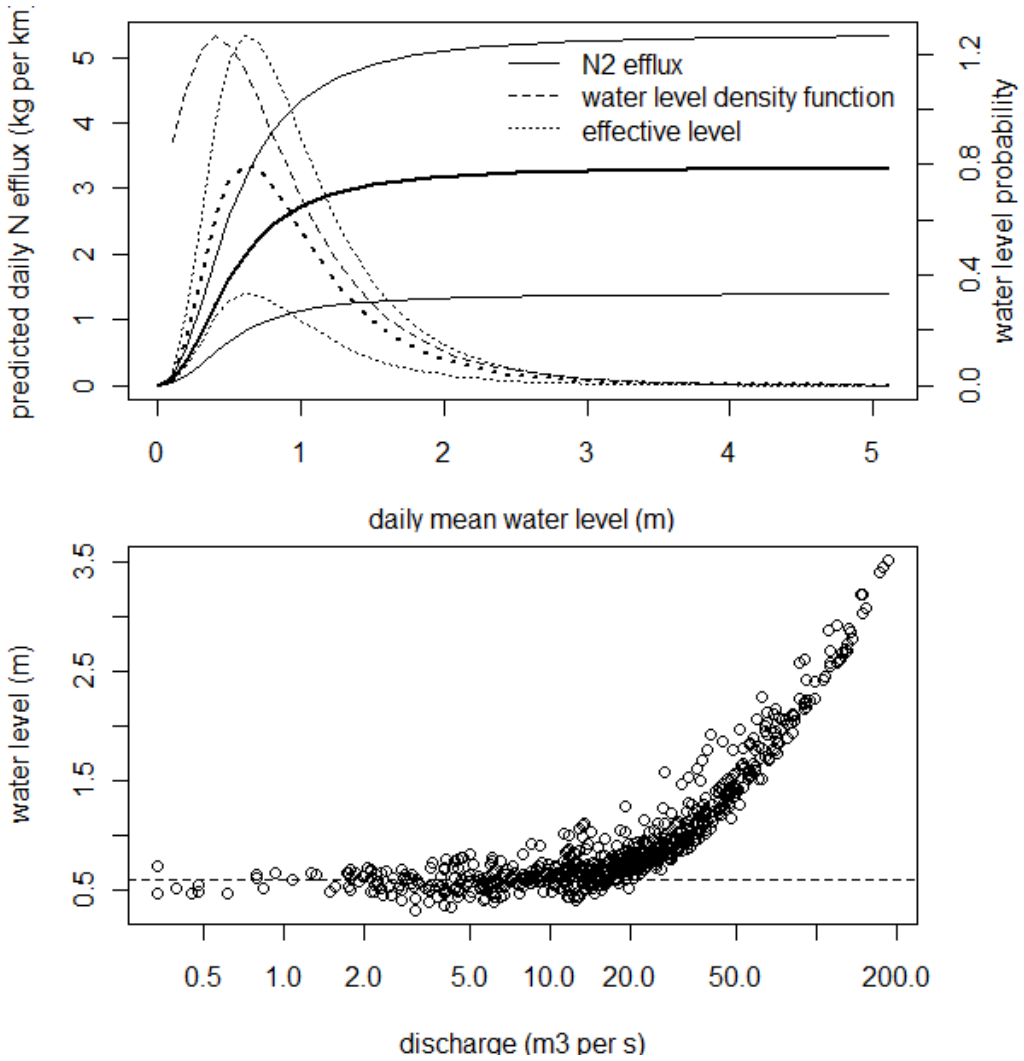

Figure 4.9 Frequency-magnitude plot of water level and N_2 efflux in the upper Northeast Cape Fear River (A), and the relationship between water level and discharge at this site (B). In panel A, the frequency of mean daily water level over a 10 year period is shown by the dashed line. The empirically-derived N_2 efflux is shown for the mean (solid bold line), maximum, and minimum (solid lines) presented in Figure 8. The dotted lines represent the product of the water level histogram with the corresponding empirical N_2 efflux model. The effective level (0.6 m) is the same for all N_2 efflux models, regardless of denitrification rate. In panel B the dashed line indicates the effective level of N_2 efflux.

5. THE END OF THE RIVER CONTINUUM: TIDES AND RIVER ECOSYSTEMS

5.1. Introduction

One premise of ecosystem ecology is that water flows down hill, exerting a uni-directional flux of water and material across the landscape. This hydrologic connectivity across landscapes has provided the foundation for broadly-influential concepts such as the watershed ecosystem concept (Bormann and Likens 1967) and the river continuum concept (Vannote et al., 1980). Recent concepts and theory regarding spatial patterns in ecological process (Fisher et al. 2004), community disturbance and succession (Power et al. 2008), and ecosystem nutrient cycling (Brookshire et al. 2009) highlight the importance of terrestrial processes upstream to rivers ecosystems downstream.

The corollary to the terrestrial-riverine view of stream ecosystems is the estuarine-riverine view at the end of the river continuum. Ocean tides propagate upstream through tidal rivers, affecting the flow of water, sediment, solutes, and organisms. Here, the normal conceptualization of streams as dependent on upstream forces is reversed: instead of watershed runoff shaping river hydrology and morphology, tidal rivers are dominated by the influence of tides (Ensign et al. in review). Tidal rivers are a nearly universal component of river networks, and more than half the length of coastal rivers are tidal freshwater.

Despite being a common phenomenon in river networks, tidal rivers are conspicuously omitted from the formative conceptualizations of rivers. The river

continuum concept (Vannote et al. 1980), hierarchical patch dynamics concept (Frisell et al. 1986), flood-pulse concept (Junk et al. 1989) and the nutrient spiraling concept (Webster and Patten 1979) did not include a tidal component nor have they been extended to the tidal zone in subsequent research. Tidal rivers are not explicitly discussed in any of the basic stream ecology texts, yet many of the ecological aspects of tidal rivers have been examined (primary production (e.g.,, Muylaert et al. 2000), secondary production (e.g.,, Findlay et al. 1996), and food webs (e.g.,, Strayer et al. 2008). Given this body of knowledge, why have tidal rivers been so ignored from synthesis efforts in stream ecology? We suspect that the answer is in part because concepts in stream ecology are largely premised on a hydrogeomorphic template, and too little is known about how tides affect this template and subsequent ecological process to allow integration of tidal rivers with broader conceptual understanding of river networks.

The goal of this study was to identify systematic changes in river hydrogeomorphology along a tidal river and quantify their influence on a fundamental biotic processes: phytoplankton growth. Based on the fact that tides affect channel width (Leopold et al. 1964) and hydrologic residence time (Pace et al. 1992), two a priori hypotheses can be proposed regarding tidal river phytoplankton. First, increased channel width in tidal rivers will increase irradiance and subsequently primary production; second, increased residence time should provide more time for plankton growth and biomass accumulation (Figure 5.1). We test the first prediction by characterizing temporal and spatial patterns in irradiance and phytoplankton biomass, and the second prediction using mesocosm experiments.

If phytoplankton growth in tidal rivers was predominantly influenced by irradiance and residence time, then biological production in tidal rivers could be predicted from hydrogeomorphic patterns. However, tidal hydrology and geomorphology may also affect other aspects of the river (e.g.,, water chemistry, community composition) which may subsequently influence phytoplankton (Figure 5.1). We conducted mesocosm experiments in a tidal river to test the null hypothesis that phytoplankton biomass and growth were governed solely by irradiance and residence time along the tidal continuum. Understanding the primacy of tidal forces versus biological processes on primary production in tidal rivers is a fundamental step towards integrating ecological patterns in tidal river with the rest of the river continuum.

5.2. Methods

5.2.1. Study sites

The Newport (34.8^{o}N 76.8^{o}W)and White Oak (34.8^{o}N 77.2^{o}W) Rivers in North Carolina are blackwater streams with relatively small drainage areas (150 km^2 and 200 km^2, respectively), low channel gradients, and extensive riparian wetlands. The transition from headwater stream, to tidal freshwater river, to estuary occurs over a relatively short distance (9 and 23 river km in the Newport and White Oak Rivers, respectively), making these rivers compact models for examining tidal effects on river ecosystems.

5.2.2. Channel morphology, irradiance, and phytoplankton biomass

Channel width was measured between the vegetated banks of both rivers in the field or using aerial photographs when widths exceeded 20 m. Sampling was conducted from the purely non-tidal upstream reach all the way through a continuum of increasingly tidally-influenced reaches, ultimately ending at the freshwater-saltwater interface. To compare actual dimensions to what would be expected in the absence of tides, we estimated non-tidal channel hydraulic geometry (width as function of drainage area) using relationships specific to non-tidal coastal plain streams in North Carolina (Sweet and Geratz 2003).

Average water column irradiance (photosynthetically active radiation, PAR) was calculated using the formula

$$I_x = \frac{I_0\left[1 - \exp(-kz)\right]}{kz} \quad (5.1)$$

where I_x is the average water column irradiance, I_0 is the surface irradiance, k is the water column attenuation coefficient, and z is water depth. Water column attenuation of PAR was measured using a 4-pi irradiance sensor and LI1400 display/logger (Li-Cor Environmental, Lincoln, NB). Depth was measured at 500 m intervals along the length of the tidal freshwater zone at mid-tide. Average daily solar irradiances for the study area were obtained from observations made by the North Carolina State Climate Office (http://www.nc-climate.ncsu.edu/) at 3 sites near the study area, and solar irradiance values were converted to PAR using a conversion factor of 2.04 (Meek et al. 1984). Canopy interception of irradiance was calculated from digitized hemispherical photographs of the tree canopy taken with a Nikon Coolpix 4500 camera with fisheye lense at 500 m (Newport River) and 1000 m (White Oak River) intervals during leaf-on and leaf-off conditions. The color photographs were digitized to black and white using

automatic threshold detection algorithms in SideLook 1.1.01 software (Nobis and Hunzicker, 2005), and the average daily irradiance to the river's surface after attenuation by the riparian tree canopy was calculated following the methods of Julian et al. (2008).

Phytoplankton biomass and water column light attenuation were measured bi-weekly at 5 sites on the Newport River in 2006-2007, and at 3 sites on the White Oak River on 4 occasions in 2009. Logistical constraints restricted sampling of the White Oak River, so sampling was focused around the period of maximum phytoplankton biomass observed in the Newport River. Water samples (50 mL) were filtered through a 0.7 μm glass fiber filters, and chlorophyll *a* (a proxy for phytoplankton biomass) was extracted for 24 hr in 90% acetone and analyzed on a Turner Trilogy fluorometer (Turner Designs, Inc, Sunnyvale, CA).

5.2.3. Photosynthetic response to irradiance along a tidal gradient

The photosynthetic response of the phytoplankton community to irradiance was measured in short-term ^{14}C uptake experiments with river water collected from the non-tidal, upper tidal, and lower tidal portions of the Newport and White Oak Rivers on 18 and 19 June 2009. Water samples (10 ml) were spiked with 1 μCi ml^{-1} of $H^{14}CO_3$ and incubated for 45 min at irradiances ranging from 23-1951 μM PAR m^{-2} s^{-1}. Uptake of ^{14}C into algal biomass was quantified using a LS6500 scintillation counter (Beckman Coulter, Inc., Brea, CA) after the un-incorporated $^{14}HCO_3$ was removed by acidification. Algal uptake of ^{14}C (P^B) was modeled as a function of irradiance (I) using the equation

$$P^B l = P_S^B \left[1 - exp\left(\frac{-\beta \times I}{P_S^B}\right)\right] \quad (5.2)$$

where P^B_S is the maximum photosynthetic rate normalized to chlorophyll *a*, and β is the slope of the curve as *I* goes to zero. Parameterization of this model and all statistical procedures described below were performed using R software (R Development Core Team 2010).

5.2.4. Mesocosm growth experiments in the Newport river

Mesocosm experiments were conducted to determine phytoplankton growth rates (a net measure of biomass accumulation implicitly accounting for primary production, respiration, and loss due to senescence and grazing). Experiments were performed in April, June, and October 2006 and March 2007 using river water from the Newport River's non-tidal, upper tidal, and lower tidal freshwater regions. Irradiance and temperature were equivalent for all mesocosms, thereby isolating the effects of water chemistry and zooplankton grazing on phytoplankton growth. Potential nutrient limitation of phytoplankton growth was evaluated by experimental addition of nitrogen and phosphorus.

River water (5 L) was incubated in 10 L polyethylene Cubitainers (Hedwin Corp., Baltimore, MD) in an outdoor pond at the nearby UNC Institute of Marine Science in Morehead City, NC. A control and a nutrient treatment were applied in 4 replicates; nutrient additions were +140 μg $N\text{-}NO_3$ L^{-1}, +140 μg $N\text{-}NH_4$ L^{-1}, and +155 μg $P\text{-}PO_4$ L^{-1} (expressed as the concentration increase over background). Irradiance was reduced to 66% of ambient conditions using black plastic window screen to replicate light attenuation in the water column. Phytoplankton growth rate was determined from the slope of mixed-effects linear models developed from log(chlorophyll *a*) values on days 1,

2 and 4 of each experiment, with fixed effects for site and nutrient treatment and random effects for each cubitainer over the course of the experiment. Model simplification was performed iteratively using likelihood ratio tests in an ANOVA to remove insignificant model terms ($p>0.05$) while following the principal of marginality.

Travel time of water flowing through the tidal freshwater zone of the Newport River was estimated using the modified tidal prism method (Dyer 1997) and direct measurements of discharge and channel bathymetry reported in a previous study (Ensign et al. 2008). Travel time in the absence of tides was estimated by dividing reach length by non-tidal flow velocity. Both methods are simple approximations of travel time in tidal and non-tidal rivers so we expect that comparison of their predictions should yield a relative measure of the difference in phytoplankton travel time in the river under tidal versus non-tidal conditions. Differences between chlorophyll *a* in non-tidal mesocosms after the predicted non-tidal travel time and chlorophyll a observed after the predicted tidal travel time to the estuary were evaluated with Walsh two sample t-tests ($p<0.05$).

5.3. Results

5.3.1. Channel morphology, irradiance, and phytoplankton biomass

The width of the tidal portion of both rivers was 3 times greater than would be expected in the absence of tides (Figure 5.2A and 5.2B). This increase in width corresponded with a dramatic increase in total irradiance at the river surface (Figure 5.2C and 5.2D). The highest water surface irradiances occurred in the lower tidal region of both rivers during April, corresponding with the peak above-canopy irradiance. Water surface irradiance during summer (May-September) was lower upstream due to the more

foliated tree canopy. Attenuation of irradiance within the river decreased the average water column irradiance; an increase in channel depth also reduced water column-averaged irradiance in the lower portion of both rivers (Figure 5.2E and 5.2F). Chlorophyll *a* peaked during April-May in the Newport River and June-July in the White Oak River, periods which corresponded with the peak in water column irradiance.

5.3.2. Photosynthetic response to irradiance

Primary productivity per unit of irradiance was greater in the tidal than non-tidal portion of the Newport and White Oak Rivers, although the tidal region where this increase occurred (i.e., upper vs. lower) differed between rivers. In the Newport River, the upper and lower tidal river had a greater maximum photosynthetic rate (P^S_B) than the non-tidal river (Figure 5.3A). The lower tidal White Oak River had a higher P^S_B than the upper tidal and non-tidal (Figure 5.3B). Similarly, the rate of increase in photosynthesis with irradiance (β) was greater in the Newport River's lower and upper tidal than the non-tidal (Figure 5.3A). In the White Oak River, β was greater in the lower tidal region than the upper and non-tidal regions (Figure 5.3B).

5.3.3. Mesocosm growth experiments

Tidal travel time for the Newport River ranged from 3.6-5.1 days, while the predicted travel time in the absence of tides ranged from 0.4-1.1 days (Figure 5.4A-D). In the non-tidal mesocosms, the extra travel time provided by tides allowed significantly more chlorophyll *a* to accumulate during March ($p<0.001$), April ($p<0.001$), and June

(p=0.003) when nutrients were added, but no increase was observed in October (p=0.09) (Figure 5.4A-D).

In March phytoplankton growth was significantly different between the non-tidal and tidal mesocosms, but the differences were alleviated by the addition of nutrients to the non-tidal mesocosms (Figure 5.4E). The difference between non-tidal and upper tidal mesocosms in April may have been a result of anomalously low chlorophyll on day 1 in the upper tidal mesocosms (Figure 5.4B), and no differences were apparent when nutrients were added (Figure 5.4F). In June growth in non-tidal mesocosms was slower than in the lower tidal mesocosms, but faster when nutrients were added to the non-tidal mesocosms (Figure 5.4G). No difference was observed between non-tidal and upper tidal mesocosms in June under ambient or nutrient enriched conditions. In October, no differences in growth rate were observed, and mixed effects modeling showed the nutrient term to not be significant (therefore separate slopes for the nutrient treatment are not shown in Figure 5.4H).

5.4. Discussion

The first objective of this study was to examine the hydrogeomorphic patterns affecting phytoplankton biomass and growth in tidal rivers. We found that tides tripled channel width and subsequently the irradiance to the river surface increased 6-fold. As predicted, these spatio-temporal patterns in irradiance corresponded with those of chlorophyll *a*, and mesocosm experiments demonstrated that the increased residence time provided by tides significantly increased phytoplankton biomass during most of the year. The contrast between the observed and predicted non-tidal channel width indicated that

tides had a more profound effect on channel morphology (and subsequently phytoplankton production) than the watershed flow regime.

The second objective was to determine if the spatio-temporal patterns in phytoplankton biomass we observed were due solely to changes in river hydrology and morphology. If the growth rate of phytoplankton along the tidal river continuum was the same, then hydrology and irradiance (a function of morphology) alone would control the accumulation of phytoplankton biomass (Figure 5.1, H_o). Alternatively, differences in phytoplankton growth rate would indicate that biologic characteristics affected phytoplankton biomass in addition to hydrogeomorphology (Figure 5.1, H_a). Mesocosm results were not consistent over time, instead demonstrating a period of tidal hydrogeomorphic control (April and October) and a second period when nutrient concentrations also affected growth (March and June). In April and October, no differences in phytoplankton growth were observed along the tidal river continuum (except for those resulting from anomalous data in April's upper tidal river mesocosm), and the null hypothesis of hydrogeomorphic forcing could not be rejected. During March and June phytoplankton growth rates in non-tidal mesocosms were lower than in the tidal mesocosms due to nutrient limitation, permitting rejection of the null hypothesis in favor of an additional factor (nutrients) affecting growth.

Nutrients not only stimulated non-tidal phytoplankton growth in June, but this growth rate exceeded that occurring in the lower tidal river. This was surprising given the much lower α and P^S_B measured in non-tidal river phytoplankton. In hindsight, we wondered if differences in zooplankton grazing may have suppressed phytoplankton growth in the tidal river but not in the non-tidal river. While we did not quantify

zooplankton during the experiment, we were able perform counts in water samples from the mesocosms preserved with Lugol's iodine intended for phytoplankton analysis. Based on counts from a relatively small volume (400 mL), zooplankton were much more numerous in the tidal versus non-tidal mesocosms at the end of the June experiment. Higher zooplankton abundance could have lead to a top-down suppression of phytoplankton growth rates that superseded the higher rate of primary production.

Phytoplankton biomass accumulation in the Newport River was dictated by the irradiance and residence time in April and October, and also by nutrients (and perhaps grazers) in March and June. General knowledge of the geomorphologic template of the tidal river and tidal influence on residence time would have been necessary to predict phytoplankton biomass in April and October. However, additional knowledge of resource limitation and grazer control would be necessary for prediction of phytoplankton biomass in March and June. Thus, a generalized understanding of tidal hydrogeomorphology in rivers may explain variations in phytoplankton biomass during some of the year, but higher-order affects of tides must sometimes be taken into account. The transition from resource limitation to grazer control of primary production along the tidal continuum may be an another indirect effect of tides; nitrogen cycling is profoundly affected by tides (Ensign et al. 2008) and the enhanced residence time in the tidal river may allow zooplankton communities to develop (Pace et al. 1992). Previous research has documented nutrient limitation in non-tidal blackwater streams similar to the Newport River (Mallin et al. 2004), and control by zooplankton grazing has been observed in tidal rivers (Kobayashi et al. 1996), but this study is the first to quantify their combined influence on phytoplankton along the non-tidal to tidal river continuum. This study is

also not the first to find differences in primary production and food web processes between non-tidal and tidal rivers (see Schuchardt et al. 1993), but it is the first to experimentally quantify the separate influence of hydrogeomorphic forces on production in tidal rivers.

Processes originating in the open ocean increased production in the tidal, freshwater region of the rivers we studied. Tides affected the hydrogeomorphic template much more profoundly than upstream watershed discharge would in the absence of tides. Since these abiotic factors were strong determinants of primary production during much of the year, understanding general patterns in how tides affect river morphology and hydrology may allow prediction of broader-scale ecological patterns. Research on the environmental (e.g.,, tidal regime and resultant nutrient cycling) and ecological (e.g.,, presence of zooplanktivorous anadromous fish) factors that alter the relative importance of bottom-up and top-down forces in tidal rivers is also critical to making conceptual linkages between tidal with non-tidal rivers

Tidal rivers exist at the intersection of riverine and estuarine forces, where flow regime is a combination of river discharge, lunar, and wind tides, all operating on disparate time-scales. As this study highlights, it is the convolution of these forces that dictate hydrologic residence time and the subsequent accumulation of biomass and associated trophic transfers within the food web. I believe that the time scale and variation in flow and residence time in tidal rivers may present unique opportunities for investigating environmental regulation of ecological processes (high frequency, low magnitude tides convoluted with low frequency, high magnitude floods), possibly using recently developed methods of time series analysis (Denny et al. 2009). I also suspect that

the combination of riverine hydrogeomorphology and food web connectivity with migratory marine species in tidal rivers may provide an opportunity to examine nascent concepts such as ecosystem boundaries (Post et al. 2007). Thus, tidal rivers provide an exciting venue for ecological research by embracing the end of the river continuum.

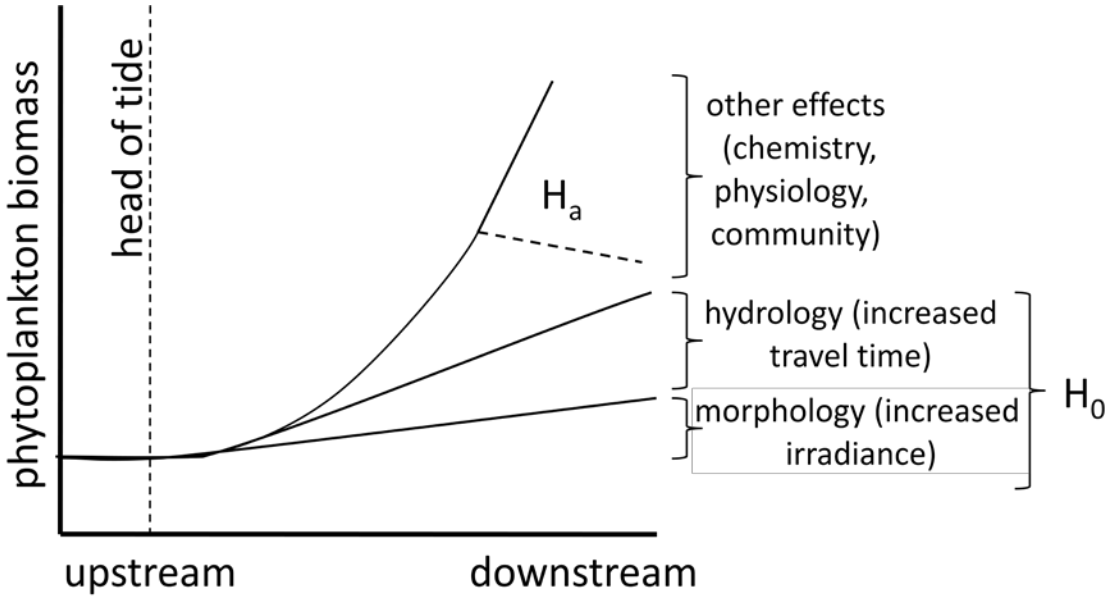

Figure 5.1 The a priori assumptions that residence time and channel width in the tidal freshwater river will affect phytoplankton (h_o). Alternatively, physiological adaptations, community-scale changes, and food web alterations may act in concert with hyrology and geomorphology to increase (or decrease) phytoplankton growth (h_a).

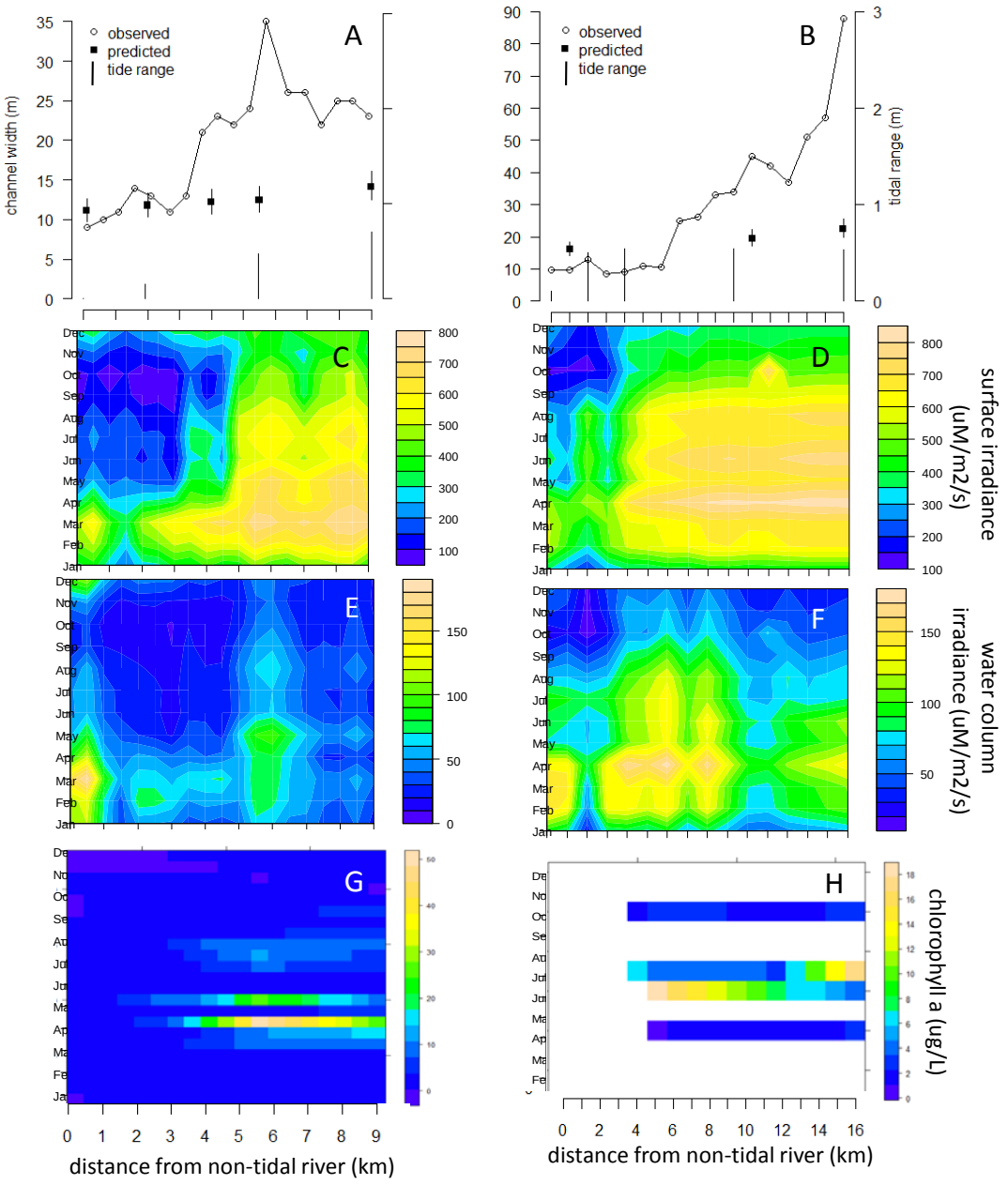

Figure 5.2 Tidal amplitude, observed width, and predicted width (in the absence of tides) of the Newport (A) and White Oak River (B); error bars on the predicted width indicate the 95% confidence interval of the model. Water surface PAR in the Newport (C) and White Oak River (D); average water column irradiance in the Newport (E) and White Oak River (F); chlorophyll a in the Newport (G) and White Oak River (H).

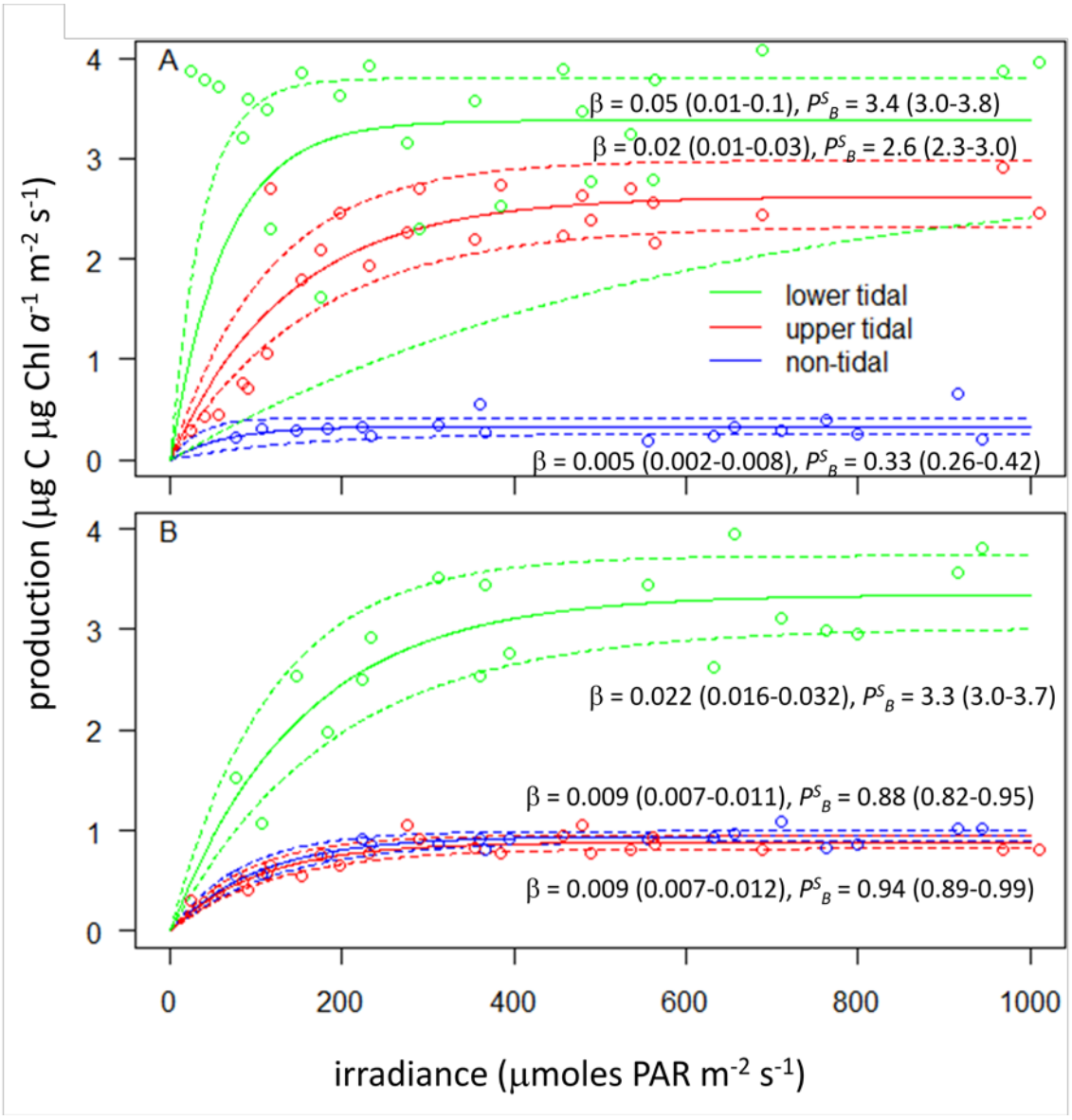

Figure 5.3 Modeled relationship between photosynthesis and irradiance in the Newport (A) and White Oak River (B). Dashed lines represent the 95% confidence interval of the model predictions. The three lowest productivity values at the lower tidal site in the Newport River were omitted from the regression analysis.

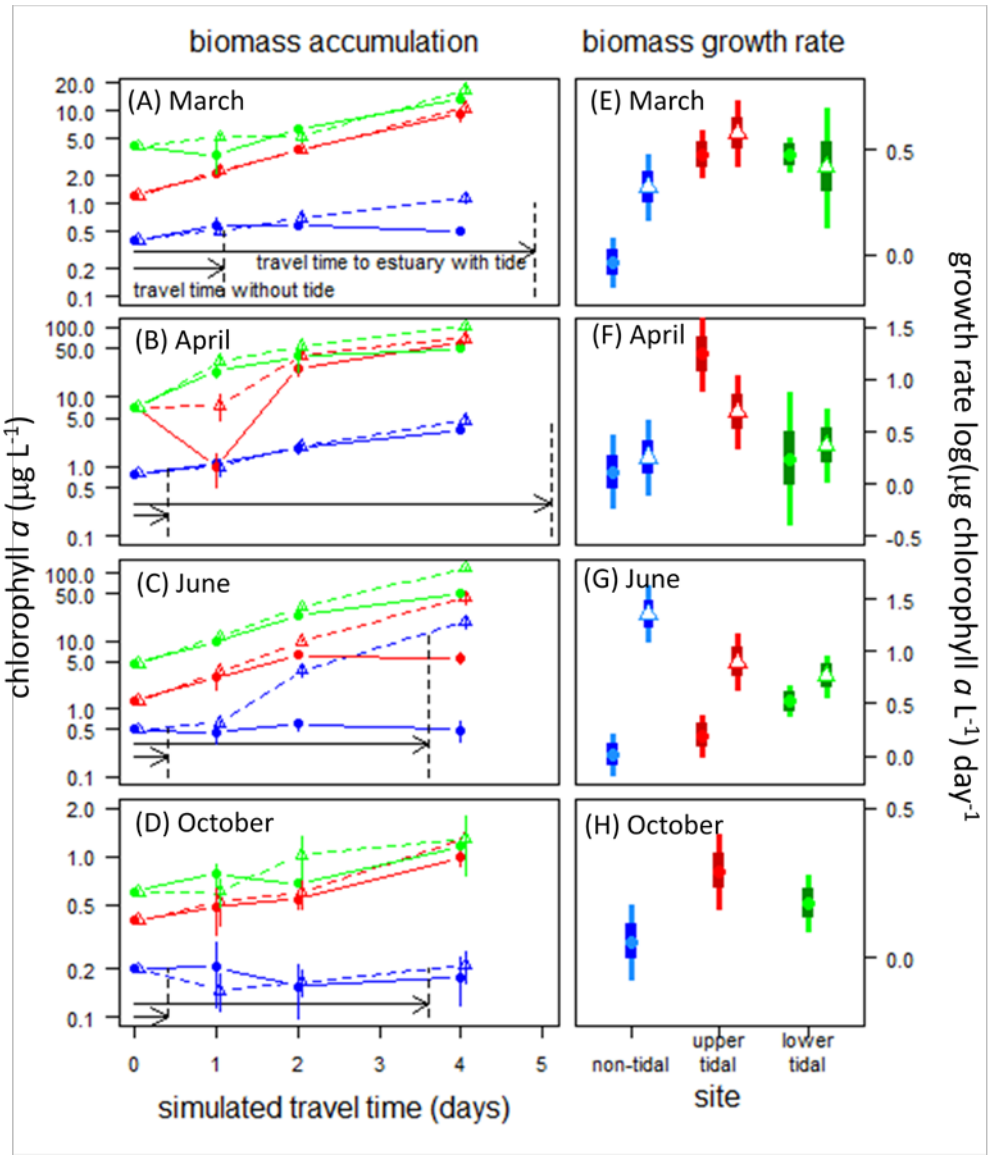

Figure 5.4 Chlorophyll *a* response in mesocosm experiments from the non-tidal, upper tidal, and lower tidal sections of the Newport River (A-D), and the rate of growth determined using linear, mixed effects modeling (E-H). Colors in A-D correspond with those in E-H; solid lines indicate control mesocosms and dashed lines indicate nutrient additions. In panels E-H, the darker, thicker bars represent the 50% confidence interval of the slope estimate, and the lighter, longer bars represent the 95% confidence interval of the slope estimate.

6. CONCLUSIONS

> Limnologists and oceanographers alike are comfortable thinking of copepods and clams and fish as highly transformed solar energy. And no one objects that the heat energy from the sun is important in regulating the speed of growth in plants and animals. It is more difficult, but no less real, to see the work of the wind in the rich catch of *Tilapia* from an African lake or the gentle pull of the moon made manifest in the great harvest from Georges Bank. –Scott W. Nixon, 1988

Nixon's contention that tides affect ecological process is supported by studies that have revealed how physical energy directly affects organisms (Denny 1994), communities (Leonard et al. 1998), and ecosystems function (Odum et al. 1995). The goal of this dissertation was to examine the effects of tides on physical and ecological process in tidal rivers. In the 5 years of research represented in this dissertation, I made many exciting discoveries, sharpened several into hypotheses for further study, and disposed of many less fruitful ideas in the trash. As a whole, the results of my research will provide a much-needed foundation for further study and synthesis of ecosystem processes in tidal rivers.

6.1. Hydrology and geomorphology

Tidal rivers have not been integrated with foundational concepts in fluvial geomorphology because the physical nature of tidal rivers was not well understood. Although the direction of flow may vary, the hydraulic mechanisms affecting channel morphology are the same: kinetic energy of flowing water is dissipated as heat and turbulence, a portion of which moves sediment. In Chapter 2, measurement of energy

dissipation proved to be useful metric for understanding how stream morphology changed with tidal influence. The important contribution of this research was discovery of the counter-intuitive process whereby tides suppress energy dissipation in the upper portion of tidal rivers as a result of slower flow velocity and larger channel area. Tides supplemented the fluvial energy dissipation in the lower portion of the tidal river which resulted in higher suspended sediment flux. The temporal adjustment in channel morphology to tidal influence was inferred from contemporary spatial patterns and suggested hypotheses for future research.

The hydrogeomorphic data in Chapter 2 provide a bridge between two disparate time scales at which coastal landform development is examined. Geologists use stratigraphic methods and facies models to examine riverine-estuarine transitions over Quaternary time-scales (Dalrymple et al. 1992; Schumm 1993; Blum and Tornqvist 2000). Fluvial and estuarine geomorphologists use experimental approaches to understand the mechanisms affecting sediment transport and deposition over contemporary time scales (e.g.,, Meade 1982; Friedrichs 1995). Conceptual models for the evolution of river-estuary systems during sea level rise have been provided, but the specific mechanisms, sequence, and time scale over which tides affect river morphology have not. The hydraulic mechanisms I identified will help link the contemporary processes in tidal rivers with longer-term geologic formations in coastal environments.

Understanding the hydraulic implications of tides on channel morphology will aid river restoration efforts. Engineers have known about the unique morphology of tidal rivers for at least 117 years (Wheeler 1893), yet there is currently no guidance for river restoration in tidal rivers (Bernhardt and Doyle, in press). The characterization of

discrete zones of tidal influence that are made in Chapter 2 are based on the simple variables of tidal amplitude and flow regime. These easily measured variables, and the corresponding channel morphology documented in Chapter 2 will provide a first step towards developing guidance for tidal channel restoration.

6.2. Biogeochemistry

Rivers and their floodplains are critical landscape features which attenuate nitrogen transport through the process of denitrification. The hydrologic connectivity between tidal rivers and their floodplains plays a particularly important role in affecting the downstream transport of nitrogen in tidal rivers. At the landscape-scale, it is the combination of denitrification rate and the area over which denitrification occurs that affects downstream transport of nitrogen. Previous research has focused on quantifying the factors that control the rate of denitrification in tidal river wetlands, but virtually no attention has been given to how tidal hydrology influences inundation and subsequent N_2 flux in tidal river wetlands.

In Chapter 3, denitrification rates were measured over an annual period in three tidal riparian habitat types of the Newport River. The temporal variation was greater than the spatial variation, but the short-term lag between inundation of the floodplain and the onset of denitrification was crucially important to extrapolating denitrification rates across the floodplain. Field and laboratory studies of oxidation-reduction potential provided similar estimates of this lag of approximately 4.5 hr. Incorporation of this riparian wetland denitrification with the expected in-channel denitrification led to a 38% increase in overall denitrification flux for this tidal river.

In Chapter 4, the relative role of denitrification rate versus inundation dynamics was examined using a landscape-scale model of inundation. General patterns emerged from four different tidal rivers in North Carolina. In the lower half of tidal rivers, hydrology exerted more influence on N_2 efflux than the rate of denitrification. In the upper tidal rivers, N_2 efflux was more sensitive to denitrification rate than tidal hydrology during high river discharge periods when the floodplain was continually inundated for weeks at a time. Over long time scales, however, baseflow periods (when tides drive water level variation) were more important to the N_2 efflux than storm events (causing sustained inundation of the floodplain). This study should bring increased attention to how tidal hydrology affects nitrogen efflux in tidal rivers. It also contributes fundamental information required to begin landscape-scale modeling of nitrogen efflux in tidal rivers through the development of a simple, three parameter empirical model of N_2 efflux as a function of water level in tidal rivers.

6.3. Biological Production

Formative concepts in stream ecology have excluded the tidal freshwater zone of rivers because not enough is known about how their hydrogeomorphic patterns affect ecological process. Chapters 2, 3, and 4, indicate consistent downstream trends in tidal river channel morphology. Relating these hydrogeomorphic patterns with their abiotic influence on biological production in rivers may open the door to integrating tidal rivers with existing theory and concept in stream ecology.

I examined the influence of water residence time and channel morphology on primary production in tidal rivers in Chapter 5. The systematic influence of tides on river

morphology (and subsequently irradiance) contributed to an increase in phytoplankton biomass along the tidal river continuum. Tides also increased hydrologic residence time, which lead to more phytoplankton biomass than would have occurred without tidal action. Phytoplankton growth was more than simply the additive effect of irradiance and residence time, and reflected higher-order affects of tide on nutrient chemistry and food webs. Differences in phytoplankton growth rates between the non-tidal and tidal river were alleviated under nutrient replete conditions, despite a greater photosynthetic efficiency for the tidal phytoplankton community. The data suggested a transition from nutrient limitation to grazer suppression of phytoplankton along the tidal river continuum, highlighting how hydrogeomorphic trends led to fundamental changes in food web structure.

Tidal rivers constitute a hybrid of other aquatic ecosystems. Lakes, rivers, and estuaries provide an end-member condition for two of three conditions: geomorphology, hydrology, and food web structure (Figure 6.1). River morphology and ecosystem function are dependent on watershed discharge, while their food webs lie in between the open nature of estuaries and insular nature of lakes. Lake ecosystem functions are semi-dependent on watershed processes, although they are not prone to hydrologic disturbance like rivers; their food webs are closed with respect to migratory species (except for some coastal lakes reached by anadromous species). Estuarine morphology is independent of watershed runoff and their communities are not prone to hydrologic disturbance, but their food webs have high temporal variability due to migratory species. Tidal rivers occupy a central position in this triumvariate of ecosystem types because their hydrologic,

geomorphologic, and ecologic characteristics are intermediate between the end-member ecosystems.

The combination of physical and ecological attributes of rivers, lakes, and estuaries has facilitated investigation of particular ecological phenomena. The hydrologically-dynamic and terrestrially-dominated nature of rivers has facilitated our understanding of succession and disturbance (Fisher et al. 1982). The hydrologically-static and organismally-closed nature of lakes has contributed to understanding of top-down and bottom-up processes (Carpenter and Kitchell 1993; Sheffer 1998). The organismally-open, marine morphology of estuaries has contributed to understanding of dispersal (Levin 1984) and community structure (Leonard et al. 1998).

It remains to be seen what ecological processes may be resolved by studying tidal rivers. Perhaps their unique combination of attributes will offer insight into ecological disturbance and succession in aquatic ecosystems when colonization can occur from two directions. Maybe their hydrologic and geomorphic-independence from watershed runoff will provide new opportunities to examine the influence of hydrology and stochasticity in aquatic communities (sensu Sabo and Post 2008). Or maybe the migratory nature of animals in their food webs together with their physically constrained morphology will allow unique ways to examine the boundaries of aquatic ecosystems (sensu Post et al. 2007).

Tidal river ecosystems are a final frontier for research along the river continuum, and will likely yield many exciting discoveries. The research presented in this dissertation is a significant contribution to this burgeoning field of research, and I hope the ideas contained herein may provide some guidance for further explorations.

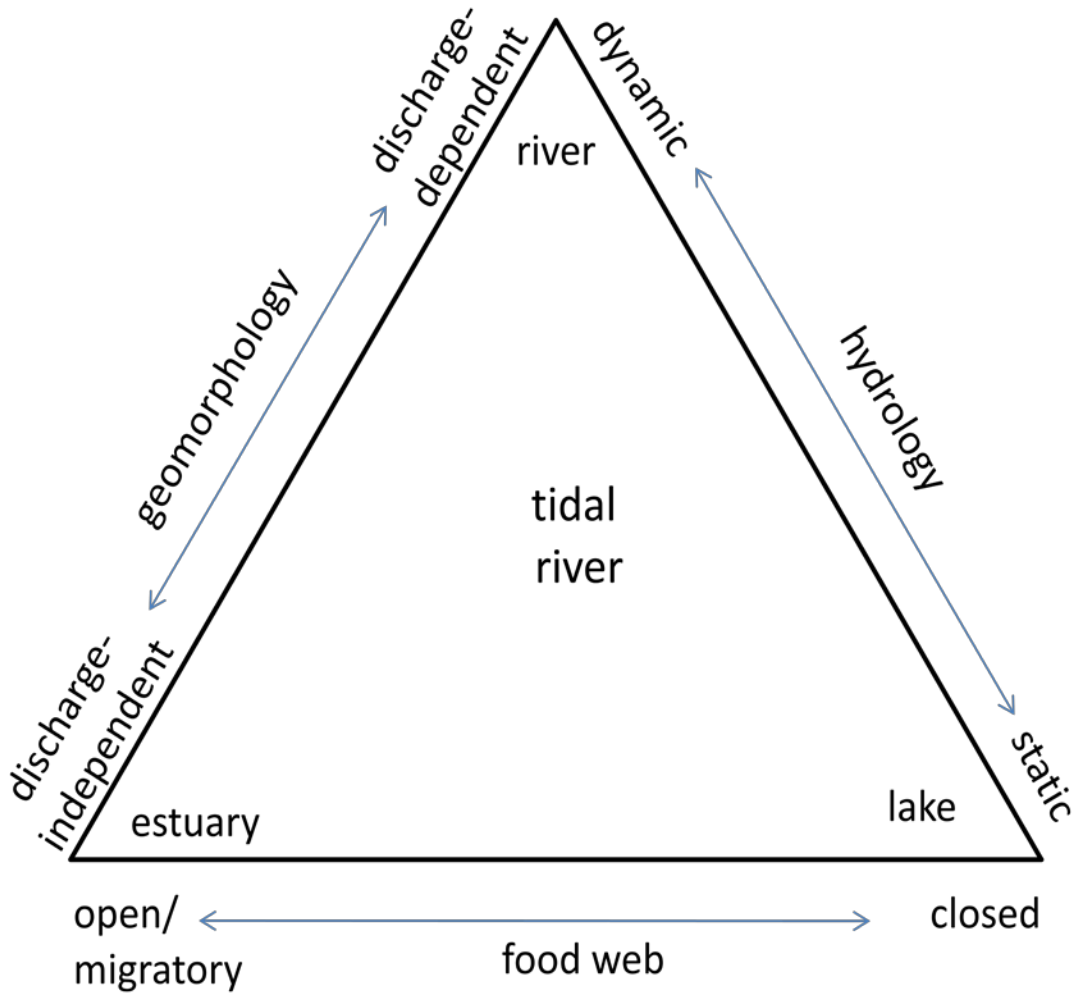

Figure 6.1 Trichotomy of river, lake, and estuarine ecosystems on the basis of their geomorphology, hydrology, and food web characteristics, with tidal rivers occupying a central condition with respect the three characteristics on the sides of the triangle.

REFERENCES

Amphlett, M. B., and T. E. Brabben. 1991. Measuring fresh water flows in large tidal rivers. In:Water management of the Amazon Basin. Braga, B. P. F., and C. A. Fernandez-Jauregui. Manaus, 5-9 August 1990. UNESCO Montevideo pp. 179-190.

Anderson, G. F. 1986. Silica, diatoms and a freshwater productivity maximum in Atlantic coastal plain estuaries. Chesapeake Bay: Estuarine, Coastal and Shelf Science **22**:183-197.

Ashley, G.M. 1980. Channel morphology and sediment movement in a tidal river, Pitt River, British Columbia. Earth Surface Processes and Landforms. **5**:347-368.

Bacon, E. M. 1906. The Connecticut River and the valley of the Connecticut. G. P. Putnam's and Sons, New York.

Baldwin, A. H. 2007. Vegetation and seed bank studies of salt-pulsed swamps of the Nanticoke River, Chesapeake Bay. In Ecology of Tidal Freshwater Forested Wetlands of the Southeastern United States, Connor, W. H., Doyle, T. W., Krauss, K.W. (eds). Springer: Netherlands; 139-160.

Bennett, J., J. Woodward, and D. Shultz. 1986. Effect of discharge on the chlorophyll a distribution in the tidally-influenced Potomac River. Estuaries and Coasts **9**:250-260.

van den Berg, J. H. 1987. Bedform migration and bed-load transport in some rivers and tidal environments. Sedimentology **34**:681-698.

Blum, M.D., and T. E. Törnqvist. 2000. Fluvial responses to climate and sea-level change: a review and look forward. Sedimentology **47**:2-48.

van Bochove E., S. Beauchemin, and G. Theriault. 2002. Continuous multiple measurement of soil oxidation-reduction potential using platinum microelectrodes. Soil Science Society of America Journal **66**:1813-1820.

Bormann, F. H. and G. E. Likens. 1967. Nutrient cycling. Science **155**:424-429.

Brookshire, E. N. J., H. M. Valett, and S. Gerber. 2009. Maintenance of terrestrial nutrient loss signatures during in-stream transport. Ecology **90**:293–299.

Bowden, W.B., C. J. Vörösmarty, J. T. Morris, B. J. Peterson, J. E. Hobbie, P. A. Steudler, and B. Moore. 1991. Transport and processing of nitrogen in a tidal freshwater wetland. Water Resources Research **27**:389-408.

Boyer, E. W., R. B. Alexander, W. J. Parton, C. Li, K. Butterbach-Bahl, S. D. Donner, R. W. Skaggs, and S. J. Del Grosso. 2006. Modeling denitrification in terrestrial and aquatic ecosystems at regional scales. Ecological Applications **16**:2123-2142.

Brinson, M.M., R.R. Christian, and L. K. Blum. 1995. Multiple states in the sea-level induced transition from terrestrial forest to estuary. Estuaries. **18**:648-659.

Buschman, F.A., A. J. F. Hoitink, M. van der Vegt, and P. Hoekstra. 2009. Subtidal water level variation controlled by river flow and tides. Water Resources Research **45**:W10420.

Carlough, L. A. 1994. Origins, structure, and trophic significance of amorphous seston in a blackwater river. Freshwater Biology **31**:227-237.

Carpenter, S. R., and J. F. Kitchell (eds.). 1993. The trophic cascade in lakes. Cambridge University Press, Cambridge, England.

Chen, Y-H., P-T. Shaw, and T. G. Wolcott. 1997. Enhancing estuarine retention of planktonic larvae by tidal currents. Estuarine, Coastal and Shelf Science **45**:525-533.

Chen, Y-C., and C-L. Chiu. 2002. An efficient method of discharge measurement in tidal streams. Journal of Hydrology **265**:212-224.

Chen, M.S., S. Wartel, B. Van Eck, and D. Van Maldegem. 2005. Suspended matter in the Scheldt estuary. Hydrobiologia **540**:79-104.

Cornwell, J. C., W. M. Kemp, and T. M. Kana. 1999. Denitrification in coastal ecosystems: methods, environmental controls, and ecosystem level controls, a review. Aquatic Ecology **33**:41-54.

Cowardin, L. M., V. Carter, F. C. Golet, and E. T. LaRoe. 1979. Classification of wetlands and deepwater habitats of the United States. U. S. Department of the Interior, Fish and Wildlife Service. Washington, D.C. FWS/OBS-79/31.

Craft, C., J. Clough, J. Ehman, S. Joye, R. Park, S. Pennings, H. Guo, and M. Machmuller. 2009. Forecasting the effects of accelerated sea-level rise on tidal marsh ecosystem services. Frontiers in Ecology and the Environment **7**:73-78.

Dalrymple, R. W., B. A. Zaitlin, and R. Boyd. 1992. Estuarine facies models: conceptual basis and stratigraphic implications: Journal of Sedimentary Petrology **62**:1130-1146.

Dame, R., D. Childers, and E. Koepfler. 1992. A geohydrologic continuum theory for the spatial and temporal evolution of marsh-estuarine ecosystems. Netherlands Journal of Sea Research **30**:63-72.

Darke, A. K., and J. P. Megonigal. 2003. Control of sediment deposition rates in two mid-Atlantic Coast tidal freshwater wetlands. Estuarine Coast and Shelf Science **57**:255-268.

Davidson, E. A., and S. Seitzinger. 2006. The enigma of progress in denitrification research. Ecological Applications **16**: 2057-2063

Denny, M. 1994. Extreme drag forces and the survival of wind- and water-swept organisms. Journal of Experimental Biology **194**:97-115.

Denny, M. W., L. J. H. Hunt, L. P. Miller, and C. D. G. Harley. 2009. On the prediction of extreme ecological events. Ecological Monographs **79**:397-421.

Destouni, G., F. Hannerz, C. Prieto, J. Jarsjö, and Y. Shibuo. 2008. Small unmonitored near-coastal catchment areas yielding large mass loading to the sea. Global Biogeochemical Cycles **22**:GB4003.

Diefenderfer, H., A. Coleman, A. Borde, and I. Sinks. 2008. Hydraulic geometry and microtopography of tidal freshwater forested wetlands and implications for restoration, Columbia River, U. S. A. Ecohydrology and Hydrobiology **8**:339-361.

Doyle, M. W., and E. S. Bernhardt. What is a stream? Environmental Science and Technology, in press.

Doyle, M. W., E. H. Stanley, D. L. Strayer, R. B. Jacobson, and J. C. Schmidt. 2005. Effective discharge analysis of ecological processes in streams. Water Resources Research **41**:W11411.

Dyer, K. R. 1997. Estuaries: a physical introduction. New York, John Wiley and Sons.

Dyer, K.R. 1995. Sediment transport processes in estuaries. In Geomorphology and Sedimentology of Estuaries, Perillo, G.M.E. (ed). Elsevier: London; 423-449.

Eisma, D. 1986. Flocculation and de-flocculation of suspended matter in estuaries. Netherlands Journal of Sea Research. **20**:183-199.

Ensign, S. H., M. F. Piehler, M. W. Doyle, and A. R. Smyth. 2007. Effects of tidal flow on riparian zone hydraulics and nitrogen dynamics: Implications for nutrient management in coastal creeks. Water Resources Research Institute of the University of North Carolina: Raleigh

Ensign, S. H., M. F. Piehler, and M. W. Doyle. 2008. Riparian zone denitrification affects nitrogen flux through a tidal freshwater river. Biogeochemistry. **91**:133-150.

Eyre, B.D., S. Rysgaard, T. Dalsgaard, and P. B. Christensen. 2002. Comparison of isotope pairing and N2:Ar methods for measuring sediment denitrification – Assumptions, modifications, and implications. Estuaries **25**:1077-1087.

Fagherazzi, S., M. Marani, and L. K. Blum. 2004. The ecogeomorphology of tidal marshes. American Geophysical Union: Washington, D.C.

Faulkner, S. P., and W. H. Patrick. 1992. Redox processes and diagnostic wetland soil indicators in bottomland hardwood forest. Soil Science Society of America Journal **56**:856-865.

Fear, J. M., S. P. Thompson, T. E. Gallo, and H. W. Paerl. 2005. Denitrification rates measured along a salinity gradient in the eutrophic Neuse River Estuary, North Carolina, USA. Estuaries **28**:608-619.

Findlay, S., M. Pace, and D. Fischer. 1996. Spatial and temporal variability in the lower food web of the tidal freshwater Hudson River. Estuaries and Coasts **19**:866-873.

Fisher, S. G., L. J. Gray, N. B. Grimm, and D. E. Busch. 1982. Temporal Succession in a Desert Stream Ecosystem Following Flash Flooding. Ecological Monographs **52**:93-110.

Fisher, S. G., R. A. Sponseller, and J. B. Heffernan. 2004. Horizons in stream biogeochemistry: flowpaths to progress. Ecology **85**:2369-2379.

Forshay, K. J., and E. H. Stanley. 2005. Rapid nitrate loss and denitrification in a temperate river floodplain. Biogeochemistry **75**:43-64.

Friedrichs, C. T. 1995. Stability shear stress and equilibrium cross-sectional geometry of sheltered tidal channels. Journal of Coastal Research **11**:1062-1074.

Friedrichs, C. T., and D. G. Aubrey DG. 1988. Non-linear tidal distortion in shallow well-mixed estuaries: a synthesis. Estuarine, Coastal, and Shelf Science **27**:521-545.

Frissell, C. A., W. J. Liss, C. E. Warren, and M. D. Hurley. 1986. A hierarchical framework for stream habitat classification: Viewing streams in a watershed context. Environmental Management **10**:199-214.

Fry, V. A., and D. G. Aubrey. 1990. Tidal velocity asymmetries and bedload transport in shallow embayments. Estuarine, Coastal, and Shelf Science **30**:453-473.

Garcia-Ruiz. R., S. N. Pattinson, and B. A. Whitton. 1998. Kinetic parameters of denitrification in a river continuum. Applied and Environmental Microbiology **64**:2533-2538.

Gardner, L. R., and M. Bohn. 1980. Geomorphic and hydraulic evolution of tidal creeks on a subsiding beach ridge plain, North Inlet, S.C. Marine Geology **34**:M91-M97.

Gordon, N. D., T. A. McMahon, B. L. Finlayson, and C. J. Gippel. 2004. Stream Hydrology: An Introduction for Ecologists: Wiley:West Sussex, England.

Green, P.A., C. J. Vörösmarty, M. Meybeck, J. N. Galloway, B. J. Peterson, and E. W. Boyer. 2004. Pre-industrial and contemporary fluxes of nitrogen through rivers: a global assessment based on typology. Biogeochemistry **68**:71-105.

Gribsholt, B., H. T. S. Boschker, E. Struyf, M. Andersson, A. Tramper, L. De Brabandere, S. van Damme, N. Brion, P. Meire, F. Dehairs, J. J. Middleburg, and C. H. R. Heip. 2005. Nitrogen processing in a tidal freshwater marsh: A whole-ecosystem 15N labeling study. Limnology and Oceanography **50**:1945-1959.

Gribsholt, B., E. Struyf, A. Tramper, M. G. I. Andersson, N. Brion, L. De Brabandere, S. van Damme, P. Meire, J. J. Middelburg, F. Dehairs, and H. T. S. Boschker. 2006. Ammonium transformation in a nitrogen-rich tidal freshwater marsh. Biogeochemistry **80**:289-298.

Gribsholt, B., E. Struyf, A. Tramper, L. De Brabandere, N. Brion, S. van Damme, P. Meire, F. Dehairs, J. J. Middelburg, and H. T. S. Boschker. 2007. Nitrogen assimilation and short term retention in a nutrient-rich tidal freshwater marsh - a whole ecosystem 15N enrichment study. Biogeosciences **4**:11-26.

Groffman, P. M., M. A. Altabet, J. K. Bohlke, K. Butterback-Bahl, M. B. David, M. K. Firestone, A. E. Giblin, T. M. Kana, L. P. Nielsen, and M. A.Voytek. 2006. Methods for measuring denitrification: Diverse approaches to a difficult problem. Ecological Applications **16**:2091-2122.

Groffman, P. M., K. Butterbach-Bahl, R. W. Fulweiler, A. J. Gold, J. L. Morse, E. K. Stander, C. Tague, C. Tonitto, and P. Vidon. 2009. Challenges to incorporating spatially and temporally explicit phenomena (hotspots and hot moments) in denitrification models. Biogeochemistry **93**:49-77.

Guézennec, L., R. Lafite, J. P. Dupont, R. Meyer, and D. Boust. 1999. Hydrodynamics of suspended particulate matter in the tidal freshwater zone of a macrotidal estuary. Estuaries. **22**:717-727.

Gurnell, A. M. 1997. Adjustments in river channel geometry associated with hydraulic discontinuities across the fluvial-tidal transition of a regulated river. Earth Surface Processes and Landforms. **22**:967-985.

Hackney, C.T., G. B. Avery, L. A. Leonard, M. Posey, and T. Alphin. 2007. Biological, chemical, and physical characteristics of tidal freshwater swamp forests of the Lower Cape Fear River/Estuary, North Carolina. . In Ecology of Tidal Freshwater

Forested Wetlands of the Southeastern United States, Connor, W. H., T. W. Doyle, K. W. Krauss (eds). Springer: Netherlands; 183-221.

Hoitink, A. J. F., F. A. Buschman, B. Vermeulen. 2009. Continuous measurements of discharge from a horizontal acoustic Doppler current profiler in a tidal river. Water Resources Research **45**:W11406.

Hopfensperger, K. N., S. S. Kaushal, S. E. Findlay, and J. C. Cornwell. 2009. Influence of Plant Communities on Denitrification in a Tidal Freshwater Marsh of the Potomac River, United States. Journal of Environmental Quality **38**:618-626.

Horton, B., W. Peltier, S. Culver, R. Drummond, S. Engelhart, A. Kemp, D. Mallinson, E. Thieler, S. Riggs, D. Ames, and K. Thomson. 2009. Holocene sea-level changes along the North Carolina Coastline and their implications for glacial isostatic adjustment models. Quaternary Science Reviews **28**:1725-1736.

Howarth, R. W., and R. Marino. 2006. Nitrogen as the limiting nutrient for eutrophication in coastal marine ecosystems: Evolving views over three decades. Limnology and Oceanography **51**:364–376.

Hupp, C.R. 2000. Hydrology, geomorphology and vegetation of Coastal Plain rivers in the south-eastern USA. Hydrological Processes **14**:2991-3010.

Julian, J. P., E. H. Stanley, and M. W. Doyle. 2008. Basin-Scale Consequences of Agricultural Land Use on Benthic Light Availability and Primary Production Along a Sixth-Order Temperate River. Ecosystems **11**:1091-1105.

Junk, W., P. Bayley, and R. Sparks. 1989. The flood pulse concept in river-floodplain systems. *in* D. P. Dodge [ed.] Proceedings of the International Large River Symposium. Can. Spec. Publ. Fish. Aquat. Sci. 106.

Kana, T., C. Darkangelo, D. Hunt, J. Oldham, G. Bennet, and J. Cornwell. 1994. Membrane inlet mass spectrometer for rapid high-precision determination of N_2, O_2, and Ar in environmental water samples. Analytical Chemistry **66**:4166-4170.

Kana, T., and D. L. Weiss. 2004. Comment on "Comparison of isotope pairing and N2:Ar methods for measuring sediment denitrification" by BD Eyre, S Rysgaard, T Dalsgaard, and PB Christensen (2002) Estuaries 25:1077-1087. Estuaries **27**:173-176.

Kerner, M., H. Kausch, and G. Miehlich. 1990. The effect of tidal action on the transformations of nitrogen in freshwater tidal flat sediments. Archive fur Hydrobiology Supplement **75**:251-271.

Knighton, A. D. 1999. Downstream variation in stream power. Geomorphology **29**:293-306.

Kobayashi, T., P. Gibbs, P. Dixon, and R. Shiel. 1996. Grazing by a river zooplankton community: Importance of microzooplankton. Marine and Freshwater Research. **47**:1025-1036.

Kroes, D. E., C. R. Hupp, and G. B. Noe. 2007. Sediment, nutrient, and vegetation trends along the tidal, forested Pocomoke River, Maryland. In Ecology of Tidal Freshwater Forested Wetlands of the Southeastern United States, Connor, W. H., T. W. Doyle, and K. W. Krauss (eds). Springer: Netherlands; 113-137.

Kulkarni, M. V., P. M. Groffman, and J. B. Yavitt. 2008. Solving the global nitrogen problem: it's a gas! Frontiers in Ecology and the Environment **6**:199-206.

Lampman, G., N. Caraco, and J. Cole. 1999. Spatial and temporal patterns of nutrient concentration and export in the tidal Hudson River. Estuaries and Coasts **22**:285-296.

Langbein, W. B. 1963. The hydraulic geometry of a shallow estuary. Bulletin of the International Association of Scientific Hydrology **8**:84-94.

Lehman, P. 2007. The influence of phytoplankton community composition on primary productivity along the riverine to freshwater tidal continuum in the San Joaquin River, California. Estuaries and Coasts **30**:82-93.

Leonard, G. H., J. M. Levine, P. R. Schmidt, and M. D. Bertness. 1998. Flow-driven variation in intertidal community structure in a Maine estuary. Ecology **79**:1395–1411.

Leopold, L. B., and T. Maddock. 1953. The hydraulic geometry of stream channels and some physiographic implications. U.S. Geological Survey Professional Paper 252.

Leopold, L. B., M. G. Wolman, and J. P. Miller. 1964. Fluvial processes in Geomorphology. WH Freeman, San Francisco.

Levin, L. A. 1984. Life History and Dispersal Patterns in a Dense Infaunal Polychaete Assemblage: Community Structure and Response to Disturbance. Ecology **65**:1185-1200.

Lide, D. R. 2004. Handbook of chemistry and physics. CRC

Light, H. M., M. R. Darst, and R. A. Mattson. 2007. Ecological characteristics of tidal freshwater forests along the lower Suwannee River, Florida. In Ecology of Tidal Freshwater Forested Wetlands of the Southeastern United States, Connor, W. H., T. W. Doyle, and K. W. Krauss (eds). Springer: Netherlands; 291-320.

Likens, G. E., F. H. Bormann, N. M. Johnson, D. W. Fisher, and R. S. Pierce. 1970. Effects of Forest Cutting and Herbicide Treatment on Nutrient Budgets in the Hubbard Brook Watershed-Ecosystem. Ecological Monographs **40**:23-47.

Lindau, C.W., R. D. DeLaune, and J. H. Pardue. 1994. Inorganic nitrogen processing and assimilation in a forested wetland. Hydrobiologia **277**:171-178.

Machefert, S. E., and N. B. Dise. 2004. Hydrological controls on denitrification in riparian ecosystems. Hydrology and Earth System Science **8**:686-694.

Mallin, M. A., M. R. McIver, S. H. Ensign, and L. B. Cahoon. 2004. Photosynthetic and heterotrophic impacts of nutrient loading to blackwater streams. Ecological Applications **14**:823-838.

Mattheus, C. R., A. B. Rodriguez, and B. A. McKee. 2009. Direct connectivity between upstream and downstream promotes rapid response of lower coastal-plain rivers to land-use change. Geophysical Research Letters **36**:L20401.

McCarthy, M. J., P. J. Lavrentyev, L. Yang, L. Zhang, Y. Chen, B. Qin, and W. S. Gardner. 2007. Nitrogen dynamics and microbial food web structure during a summer cyanobacterial bloom in a subtropical, shallow, well-mixed, eutrophic lake (Lake Taihu, China). Hydrobiologia **581**:195-207.

Meade, R. H. 1969. Landward transport of bottom sediments in estuaries of the Atlantic coastal plain. Journal of Sedimentary Petrology. **39**:222-234.

Meade, R. H. 1982. Sources, Sinks, and Storage of River Sediment in the Atlantic Drainage of the United States. The Journal of Geology **90**:235-252.

Meek, D. W., J. L. Hatfield, T. A. Howell, S. B. Idso, and R. J. Reginato. 1984. A Generalized Relationship between Photosynthetically Active Radiation and Solar Radiation. Agronomy Journal **76**:939-945.

Megonigal, J. P., and S. C. Neubauer. 2009. Biogeochemistry of tidal freshwater wetlands. Coastal Wetlands: An Integrated Ecosystem Approach. Elsevier Science, Amsterdam, pp. 535–562.

Meyer, J. L. 1990. A blackwater perspective on riverine ecosystems. Bioscience **40**:643-651.

Molnár, P., and J. A. Ramírez. 1998. An analysis of energy expenditure in Goodwin Creek. Water Resources Research **34**:1819-1829.

Muylaert, K., K. Sabbe, and W. Vyverman. 2000. Spatial and Temporal Dynamics of Phytoplankton Communities in a Freshwater Tidal Estuary (Schelde, Belgium). Estuarine, Coastal and Shelf Science **50**:673-687.

Muylaert, K., M. Tackx, and W. Vyverman. 2005. Phytoplankton growth rates in the freshwater tidal reaches of the Schelde estuary (Belgium) estimated using a simple light-limited primary production model. Hydrobiologia **540**:127-140.

Myrick, R., and L. Leopold. 1963. Hydraulic geometry of a small tidal estuary. USGS professional paper 422:1-18.

National Oceanic and Atmospheric Administration. 200. North Carolina bathymetry /topography sea level rise project: determination of sea level trends: NOAA Technical Report NOS CO-OPS 041, Silver Spring MD.

Neubauer, S. C. 2008. Contributions of mineral and organic components to tidal freshwater marsh accretion. Estuarine, Coastal and Shelf Science **78**:78-88

Neubauer, S. C., I. C. Anderson, J. A. Constantine, and S. A. Kuehl. 2002. Sediment deposition and accretion in a mid-Atlantic (U.S.A.) tidal freshwater marsh. Estuarine, Coastal and Shelf Science **54**:713-727.

Neubauer, S. C. 2008. Contributions of mineral and organic components to tidal freshwater marsh accretion. Estuarine, Coastal and Shelf Science **78**:78-88.

Neubauer, S. C., I. C. Anderson, and B. B. Neikirk. 2005. Nitrogen cycling and ecosystem exchanges in a Virginia tidal freshwater marsh. Estuaries **28**:909-922.

Nixon, S. W. 1988. Physical Energy Inputs and the Comparative Ecology of Lake and Marine Ecosystems. Limnology and Oceanography **33**:1005-1025.

Nobis, M., and U. Hunziker. 2005. Automatic thresholding for hemispherical canopy-photographs based on edge detection. Agricultural and Forest Meteorology **128**:243-250.

Noe, G. B., and C. R. Hupp. 2005. Carbon, nitrogen, and phosphorus accumulation in floodplains of atlantic coastal plain rivers, USA. Ecological Applications **15**:1178-1190.

Noe, G. B., and C. R. Hupp. 2007. Seasonal variation in nutrient retention during inundation of a short-hydroperiod floodplain. River Research and Applications **23**:1088-1101.

Noe, G. B., and C. R. Hupp. 2009. Retention of riverine sediment and nutrient loads by coastal plain floodplains. Ecosystems **12**:728-746.

North Carolina Division of Emergency Management. 2002. NC Floodplain Mapping: White Oak Basin; LIDAR Bare Earth Mass Points, Jan-Mar 2001. EarthData International of North Carolina.

North Carolina Division of Emergency Management. 2004a. NC NC Floodplain Mapping: New River Basin; LIDAR Bare Earth Mass Points, Feb-Apr and Dec 2003. EarthData International of North Carolina.

North Carolina Division of Emergency Management. 2004b. Cape Fear Basin NC, Bare Earth Lidar Data, 2004. EarthData International of North Carolina.

Odum, W. E., E. P. Odum, and H. T. Odum. 1995. Nature's Pulsing Paradigm. Estuaries **18**:547-555.

Orr, C. H., E. H. Stanley, K. A. Wilson, J. C. Finlay. 2007. Effects of restoration and reflooding on soil denitrification in a leveed Midwestern floodplain. Ecological Applications **17**:2365-2376.

Pace, M. L., Findlay S, and D. Lints. 1992. Zooplankton in advective environments: the Hudson River community and a comparative analysis. Canadian Journal of Fisheries and Aquatic Sciences **49**:1060-1069.

Paine, A. D. M. 1985. 'Ergodic' reasoning in geomorphology: time for a review of the term? Progress in Physical Geography **9**:1-15.

Parillo, G. M. E., E. Wolanski, D. R. Cahoon, and M. M. Brinson, eds. 2009. Coastal wetlands, an integrated ecosystem approach. Elsevier, New York.

Parker, G., T. Muto, Y. Akamatsu, W. Ditrich, and W. Lauer. 2008. Unravelling the conundrum of river response to rising sea-level from laboratory to field. Part I: Laboratory experiments. Sedimentology **55**:1643-1655.

Pasternack, G. B., and G. S. Brush. 2002. Biogeomorphic controls on sedimentation and substrate on a vegetated tidal freshwater delta in upper Chesapeake Bay. Geomorphology **43**:293-311.

Pasternack, G. 2009. hydogeomorphology and sedimentation in tidal freshwater wetlands, p. 31-40. *In* Tidal Freshwater Wetlands. Backhuys.

Phillips, J. D. 1997a. Human agency, Holocene sea level, and floodplain accretion in coastal plain rivers. Journal of Coastal Research **13**:854-866.

Phillips, J. D. 1997b. A short history of a flat place: Three centuries of geomorphic change in the Croatan National Forest. Annals of the Association of American Geographers **87**:197-216.

Phillips, J. D., and M. C. Slattery. 2006. Sediment storage, sea level, and sediment delivery to the ocean by coastal rivers. Progress in Physical Geography **30**:513-530.

Phillips, J. D., and M. C. Slattery. 2007. Downstream trends in discharge, slope, and stream power in a lower coastal plain river. Journal of Hydrology **334** : 290-303.

Phlips, E. J., M. Cichra, F. J. Aldridge, J. Jembeck, J. Hendrickson, and R. Brody. 2000. Light Availability and Variations in Phytoplankton Standing Crops in a Nutrient-Rich Blackwater River. Limnology and Oceanography **45**:916-929.

Pinay, G., C. Ruffinoni, and A. Fabre. 1995. Nitrogen cycling in two riparian forest soils under different geomorphic conditions. Biogeochemistry **30**:9-29.

Pinay, G., V. J. Black, A. M. Planty-Tabacchi, B. Gumiero, H. DéCamps. 2000. Geomorphic control of denitrification in large floodplain soils. Biogeochemistry **50**:163-182.

Pinay, G., B. Gumiero, E. Tabacchi, O. Gimenez, A. M. Tabacchi-Planty, M. M. Hefting, T. P. Burt, V. A. Black, C. Nilsson, V. Iordache, F. Bureau, L. Vought, G. E. Petts, and H. DéCamps. 2007. Patterns of denitrification rates in European alluvial soils under various hydrological regimes. Freshwater Biology **52**:252-266.

Post, D. M., M. W. Doyle, J. L. Sabo, and J. C. Finlay. 2007. The problem of boundaries in defining ecosystems: A potential landmine for uniting geomorphology and ecology. Geomorphology **89**:111-126.

Power, M. E., M. S. Parker, and W. E. Dietrich. 2008. Seasonal reassembly of a river food web: Floods, droughts, and impacts of fish. Ecological Monographs **78**:263-282.

R Development Core Team. 2009. R: A language and environment for statistical computing. R Foundation for Statistical Computing, Vienna, Austria. ISBN 3-900051-07-0.

Rayburg, S., M. Thoms, and M. Neave. 2009. A comparison of digital elevation models generated from different data sources. Geomorphology **106**:261-270.

Reinfields, I., T. Cohen, P. Batten, and G. J. Brierly. 2004. Assessment of downstream trends in channel gradient, total, and specific stream power: a GIS approach. Geomorphology **60**:403-416.

Rhoads, B. L. 1987. Stream power terminology. Professional Geographer **39**:189-195.

Riley, S. J. 1972. A comparison of morphometric measures of bank full. Journal of Hydrology. **17**:23-31.

Runge, J. 2007. The Congo River, Central Africa. in Large Rivers: Geomorphology and Management, Gupta A. (ed). John Wiley and Sons.

Sabo, J. L., and D. M. Post. 2008. Quantifying periodic, stochastic, and catastrophic environmental variation. Ecological Monographs **78**:19-40.

Schuchardt, B., and M. Schirmer. 1991. Phytoplankton maxima in the tidal freshwater reaches of two coastal plain estuaries. Estuarine, Coastal and Shelf Science **32**:187-206.

Schuchardt, B., U. Haesloop, and M. Schirmer. 1993. The tidal freshwater reach of the Weser Estuary: riverine or estuarine? Netherlands Journal of Aquatic Ecology **27**:215-226.

Schumm, S. A. 1993. River response to baselevel change: implications for sequence stratigraphy. Journal of Geology **101**:279-294.

Seitzinger, S. P. 1988. Denitrification in freshwater and coastal marine ecosystems: ecological and geochemical significance. Limnology and Oceanography **33**:702–724.

Seitzinger, S., J. A. Harrison, J. K. Bohlke, A. F. Bouwman, R. Lowrance, B. Peterson, C. Tobias, and G. Van Drecht. 2006. Denitrification across landscapes and waterscapes: A synthesis. Ecological Applications **16**:2064-2090.

Seybold, C. A., W. Mersie, J. Y. Huang, and C. McNamee. 2002. Soil oxidation-reduction potential, pH, temperature, and water-table patterns of a freshwater tidal wetland. Wetlands **22**:149-158.

Sheffer, M. 1998. Ecology of shallow lakes. Kluwer, The Netherlands.

Simmons, C. E. 1988. Sediment characteristics of streams in North Carolina, 1970-79. U.S. Geological Survey Open-File Report 87-701.

Simpson, M. R,, and R. Bland. 2000. Methods for accurate estimation of net discharge in a tidal channel. IEEE Journal of Oceanic Engineering **25**:437-445.

Singh, I. B. 2007. The Ganga River, in Large Rivers; Geomorphology and Management, Gupta, A., (ed). pp 375-368.

Singh, V. P. 2003. On the theories of hydraulic geometry. International Journal of Sediment Research **18**:196-218.

Smith, V. H., G. D. Tilman, and J. C. Nekola. 1999. Eutrophication: Impacts of excess nutient inputs on freshwater, marine, and terrestrial ecosystems. Environmental Pollution **100**:179-196.

Soil Conservation Service. 1987. Soil survey of Carteret County, North Carolina. United States Department of Agriculture: Washington

Strayer, D. L., M. L. Pace, N. F. Caraco, J. J. Cole, and S. E. G. Findlay. 2008. Hydrology and grazing jointly control a large-river food web. Ecology **89**:12-18.

Sweet, W. V., and J. W. Geratz. 2003. Bankfull hydraulic geometry relationships and recurrence intervals for North Carolina's coastal plain. Journal of the American Water Resources Association **39**:861-871.

Thorp, J. H., M. C. Thoms, and M. D. Delong. 2008. The riverine ecosystem synthesis. Elsevier, New York. 208 p.

Tockner, K., D. Pennetzdofer, N. Reiner, F. Schiemer, and J. V. Ward. 1999. Hydrological connectivity, and the exchange of organic matter and nutrients in a dynamic river-floodplain system (Danube, Austria). Freshwater Biology **41**:521-535.

U.S. Fish and Wildlife Service. 2010. National Wetlands Inventory. Washington, D.C.

Valett, H. M., M. A. Baker, J. A. Morrice, C. S. Crawford, M. C. Molles, C. N. Dahm, D. L. Moyer, J. R. Thibault, and L. M. Ellis. 2005. Biogeochemical and metabolic responses to the flood pulse in a semiarid floodplain. Ecology **86**:220-234.

Van Damme, S., E. Struyf, T. Maris, T. Cox, and P. Meire. 2009. Characteristic aspects of the tidal freshwater zone that affect aquatic primary production. Tidal Freshwater Wetlands, pp. 123-136. Backhuys Publishers, Leiden, The Netherlands.

Vannote, R. L., G. W. Minshall, K. W. Cummins, J. R. Sedell, and C. E. Cushing. 1980. The River Continuum Concept. Canadian Journal of Fisheries and Aquatic Sciences **37**:130-137.

Verhoeven, J. T. A., D. F. Whigham, R. van Logtestijn, and J. O'Neill. 2001. A comparitive study of nitrogen and phosphorus cycling in tidal and non-tidal riverine wetlands. Wetlands **2**:210-222.

Villard, P., and M. Church. 2003. Dunes and associated sand transport in a tidally influenced sand-bed channel: Fraser River, British Columbia. Canadian Journal of Earth Sciences **40**:115-130.

Vitousek, P. M., J. D. Aber, R. W. Howarth, G. E. Likens, P. A. Matson, D. W. Schindler, W. H. Schlesinger, and D. G. Tilman. 1997. Human alteration of the global nitrogen cycle: sources and consequences. Ecological Applications **7**:737-750.

Vörösmarty, C., and T. Loder. 1994. Spring-neap tidal contrasts and nutrient dynamics in a marsh-dominated estuary. Estuaries and Coasts **17**:537-551.

Wall, G., E. Nystrom, and S. Litten. 2008. Suspended Sediment Transport in the Freshwater Reach of the Hudson River Estuary in Eastern New York. Estuaries and Coasts **31**:542-553.

Webster, J., and B. Patten. 1979. Effects of watershed perturbation on stream potassium and calcium dynamics. Ecological Monographs **49**:51-72.

Wells, J. T. 1995. Tide-dominated estuaries and tidal rivers, In Geomorphology and Sedimentology of Estuaries, Perillo, G. M. E. (ed). Elsevier: London; 179-205.

van der Wegen, M., Z. B. Wang, H. H. G. Savenije, and J. A. Roelvink. 2008. Long-term morphodynamic evolution and energy dissipation in a coastal plain, tidal embayment. Journal of Geophysical Research **113**:F03001.

Wheeler, W. H. 1893. Tidal rivers. Longmans, Green, and Co., London.

Williams, P. B., M. K. Orr, and N. J. Garrity. 2002. Hydraulic geometry: A geomorphic design tool for tidal marsh channel evolution in wetland restoration projects. Restoration Ecology **10**:577-590.

Wright, S. A., and D. H. Schoellhamer. 2005. Estimating sediment budgets at the interface between rivers and estuaries with application to the Sacramento-San Joaguin River delta. Water Resources Research **41**:W09428.

Wollheim, W. M., C. J. Vörösmarty, B. J. Peterson, S. P. Seitzinger, and C. S. Hopkinson. 2006. Relationship between river size and nutrient removal. Geophysical Research Letters **33**:L06410.

Wollheim, W. M., C. J. Vörösmarty, A. F. Bouwman, P. Green, J. Harrison, E. Linder, B. J. Peterson, S. P. Seitzinger, and J. P. M. Syvitski. 2008. Global N removal by freshwater aquatic systems using a spatially distributed, within-basin approach. Global Biogeochemical Cycles **22**:GB2026.

Wolman, M. G., J. P. Miller. 1960. Magnitude and frequency of forces in geomorphic processes. Journal of Geology **68**:54-74.